

HIGH ENERGY ELECTRON LINACS:
APPLICATIONS TO STORAGE RING RF SYSTEMS AND LINEAR COLLIDERS*

Perry B. Wilson
Stanford Linear Accelerator Center
Stanford University, Stanford, California 94309

ABSTRACT

The theory of electron linacs in their conventional form is well covered in the existing literature. A few topics, such as the design of standing-wave rf structures, beam loading and beam breakup, are reviewed here for completeness. In recent years, however, an important application of electron linacs has been to serve as rf cavities in high energy electron-positron storage rings. The theory underlying this application is developed, with particular attention to the problems of transient beam loading and energy loss to higher-order cavity modes. Still more recently, electron linacs have been viewed in a potential role as high-gradient linear colliders. The theory of beam loading for intense single bunches in a collider structure is developed. As background for this theory, the properties of the impedance function in the frequency domain and the wake potential in the time domain, together with the transform relations connecting the frequency and time domains, are reviewed.

Throughout these notes the application of basic physical principles such as energy conservation, superposition and causality is emphasized, both to provide insight and to simplify certain derivations. Phasor diagrams are liberally used to present the analysis of complex beam loading effects, in particular transient beam loading, in a visual form which can be readily grasped by the reader.

Based on Lectures given in the 1981 Summer School on
High Energy Particle Accelerators,
Fermi National Accelerator Laboratory,
July 13-24, 1981

* Work supported by the Department of Energy, contract DE-AC03-76SF00515.

PREFACE TO SLAC-PUB-2884 (REVISED)

The original SLAC-PUB-2884 was based on lectures presented at the 1981 Summer School on High Energy Particle Accelerators, held at Fermilab July 13-24, 1981. It was published in AIP Conference Proceedings No. 87 (American Institute of Physics, New York, 1982) pp. 550-563. The present revision updates the original document in several ways. First, all of the sections on linear collider design and on high peak power rf sources has been eliminated. The material in these sections is by now completely out of date. These two areas (linear colliders and high power rf sources) have experienced almost exponential growth since 1981, and the reader must look to more modern references (probably many of them). This leaves the core of the original publication, which deals primarily with the interaction between electron beams and rf structures. This material has aged reasonably well in the past ten years, and has not required major revisions to bring it up to date. Typos and other minor errors have of course been corrected. Of more consequence, one section and two appendices have been added for completeness. Section 10.5 treats the long-range wake potentials, multi-bunch beam loading and beam breakup for short bunch trains. Appendix A* gives the details of the derivation of the expression for beam loading in a constant gradient structure. This was passed off as problem 5.2 in the original text, moreover with an incorrect suggestion for a starting point. Appendix B* gives a short summary of beam loading in non-synchronous structures. Finally, in Section 9.2 the definition of the Fourier transform has been changed by a factor of π to bring it in line with more generally accepted usage.

Perry B. Wilson

November 1991

* Not included.

CONTENTS

1.	INTRODUCTION	1
2.	BASIC CONCEPTS	2
2.1	Phasors	2
2.2	The "Big Four" Basic Principles	3
2.3	Differential Superposition	4
3.	STANDING-WAVE LINACS	5
3.1	Shunt Impedance	5
3.2	Transit-Time Factor	7
3.3	Bunch Form Factor	9
3.4	Standing-Wave Structures	10
3.5	Equivalent Circuit for a Cavity with Beam Loading	17
4.	APPLICATION TO STORAGE RING RF SYSTEMS	23
4.1	Beam Loading in Storage Ring RF Systems	23
4.2	Phase Stability and Robinson Damping	24
5.	TRAVELING-WAVE LINACS	28
5.1	Basic Principles	28
5.2	Structure Parameters	30
5.3	Energy Gain and Beam Loading	32
5.4	Non-Synchronous Operation	34
6.	SINGLE-BUNCH BEAM LOADING	35
6.1	The Fundamental Theorem of Beam Loading	35
6.2	Higher-Order Cavity Modes and the Loss Impedance	38
6.3	Efficiency for Energy Extraction from a Cavity	40
6.4	Beam Loading by a Bunch Train with $T_b \sim T_f$	41
6.5	The Resonance Function	44
7.	TRANSIENT BEAM LOADING	46
7.1	Transient Response of a Resonant Cavity	46
7.2	Transient Variation of Cavity Voltage and Reflected Power Between Bunches	48
7.3	Transient Beam Loading in Traveling-Wave Linacs	51
8.	BEAM BREAKUP	53
8.1	Resonant ^{Regenerative} Beam Breakup	53
8.2	Cumulative Beam Breakup	55
9.	IMPEDANCES AND WAKES	57
9.1	Longitudinal Impedance Function and Wake Potential	57
9.2	Transform Relations	57

9.3	Properties of the Impedance Function	60
9.4	Application to Resonant Modes	64
9.5	The Transverse Wake	68
9.6	The Quadrupole Wake	72
9.7	Scaling of the Wake with Frequency and Structure Parameter	73
10.	SOME APPLICATIONS OF WAKE POTENTIALS	74
10.1	Single Bunch Acceleration	74
10.2	Single Bunch Beam Loading for a Gaussian Bunch	77
10.3	Two-Particle Model for Transverse Emittance Growth	84
10.4	Strong Head-Tail Instability in a Storage Ring	87
10.5	The Long Range Wake and Multibunch Acceleration	88
APPENDICES		
A.	Beam Loading in Constant Gradient Structures	*
B.	Non-Synchronous Beam Loading	
ACKNOWLEDGEMENTS		89
REFERENCES		89
LIST OF SYMBOLS		92

* See Sec. 7.2.2 in: P. B. Wilson, "Application of High Power Microwave Sources to TeV Linear Colliders"; Chapter 7 of Applications of High-Power Microwaves, A. Gaponov-Grekhov and V. Ginzburg eds., Artech House, Boston, 1994

Also: Z. D. Fortkos and P. B. Wilson, "Rampin Profile for Exact Beam Loading Energy Compens in the NLC Detuned Structure", NLC-Note 40 SLAC, December, 1994

HIGH ENERGY ELECTRON LINACS: APPLICATION TO
STORAGE RING RF SYSTEMS AND LINEAR COLLIDERS

Perry B. Wilson
Stanford Linear Accelerator Center
Stanford University, Stanford, California 95305

1. INTRODUCTION

The theory of electron linacs will be developed with two particular applications in mind: the use of standing-wave linacs as rf accelerating structures in high energy electron-positron storage rings, and the application of traveling-wave linacs to the acceleration of intense single bunches in very high gradient linear colliders. These topics are of special interest for the future of high energy particle accelerators, and in addition they are not covered in a coherent manner in the existing literature. Excellent and complete references to the theory of conventional high energy traveling-wave linacs, such as the SLAC two-mile accelerator, do of course exist. In Refs. 1 and 2, for example, topics such as structure design, particle dynamics and beam break-up in traveling-wave electron linacs are given extensive treatment. Although we cannot hope to duplicate the completeness of the coverage in these references, some of the main features of the theory will be summarized here. Hopefully these lecture notes will complement this previous work, especially in the area of beam loading by single bunches of charge.

Because of the broad scope of the material being covered, the treatment of some topics (for example, standing-wave rf structure design) must remain superficial. However, an attempt will be made to present a thorough and comprehensive treatment of the general problem of beam-structure interactions; that is, the problem of beam loading in all of its many manifestations. The interaction of intense single bunches with longitudinal and transverse modes in the rf structure sets fundamental limits on the performance of both linear colliders and electron storage rings, and will be given particular attention.

It is in principle possible to solve many beam-structure interaction problems by simply setting up an appropriate differential equation and turning the mathematical crank. In these notes we prefer to take a more visual approach, using the principle of superposition and the geometry of phasor diagrams to analyze rather complex multiple-bunch beam loading problems under transient conditions. In the case of single-bunch beam loading, we are able to bypass some messy details in the direct solution of Maxwell's equations by a careful application of basic principles such as superposition, conservation of energy and causality. These concepts are useful not only as aids in developing physical thinking; they also provide techniques for solving important real-world problems in a relatively simple way.

The initial charge for this particular set of lectures was to cover both linacs and rf power sources. We have already chosen to limit the discussion of linacs to high energy electron linacs, and in fact to only a portion of this subject area. The theory and design

of rf power sources, usually klystrons, for conventional cw and pulsed electron linacs is a separable subject that will not be treated here. The reader is referred to Refs. 3 and 4 for an introduction to klystron theory and design. Ref. 46 gives a recent (1991) survey of the status of R&D on high peak power klystrons for linear colliders. Also, in recent years rf pulse compression has assumed increasing importance as a means of boosting the peak power of existing sources. The SLED pulse compression scheme is described in Ref. 47, binary rf pulse compression is described in Ref. 48, and the SLED-II method in Ref. 49.

2. BASIC CONCEPTS

2.1 Phasors

Fields and voltages in standing-wave rf structures are taken to be complex (phasor) quantities, written with a tilde. For example,

$$\tilde{V} = V e^{j\omega t} \quad (2.1)$$

where $V = |\tilde{V}|$ is the absolute value of \tilde{V} . Here \tilde{V} might represent the voltage gain for a particle crossing a cavity driven at rf angular frequency ω . In this case eV is the maximum energy that can be gained by a non-perturbing charge traversing the cavity; that is, the charge is assumed to be sufficiently small so that the beam-induced voltage is negligible compared to the rf driving voltage. The trajectory of a particle or bunch of particles is usually taken to be the axis of symmetry of a cavity or structure, except when considering dipole (deflecting) modes. In that case the trajectory is assumed to be displaced from, but parallel to, the axis. The real part of \tilde{V} , $\text{Re } \tilde{V} = V \cos\theta$ where $\theta = \tan^{-1}[\text{Im } \tilde{V}/\text{Re } \tilde{V}]$, gives the energy gain for a charge crossing the cavity or structure at an arbitrary phase with respect to the cavity field. The position of a charge at time t can be written $z = z_0 + ct$. The position z_0 at time $t = 0$ for a point charge which receives the maximum possible energy gain defines a reference position or plane inside the cavity. It is often useful to take this reference plane as the origin for the axial coordinate z .

For problems concerning resonant cavities driven by an external generator, it is useful to view the phasor in a frame of reference rotating at the driving frequency ω . Thus if the phase of the rf voltage is varying with time as $\theta = \omega t + \theta_0$, the phasor is written in this reference frame as

$$\tilde{V} = V e^{j\theta_0} \quad (2.2)$$

The importance of choosing a reference frame determined by the external generator will become apparent in the discussion of the longitudinal stability of the beam in a storage ring against phase oscillations.

Phasors are manipulated using the usual rules of complex algebra. In particular, it is useful to recall that multiplying a phasor by $e^{j\psi}$ rotates the phasor through angle ψ without changing its magnitude.

2.2 The "Big Four" Basic Principles

Four basic principles that will often be of use in the development to follow are: superposition, conservation of energy, orthogonality of modes and causality. Superposition will be called upon most frequently. As a typical example, consider a standing-wave resonant cavity driven by an external rf generator and loaded by a beam current. The total cavity voltage \tilde{V}_c can be considered to be the superposition of a voltage component \tilde{V}_g produced by the rf generator acting alone (beam current off), and a component \tilde{V}_b due to the beam (generator off):

$$\tilde{V}_c = \tilde{V}_g + \tilde{V}_b \quad . \quad (2.3)$$

Conservation of energy will be called upon to establish some basic theorems concerning beam loading. Conservation of total energy is straightforward. If a charge q with energy U_i enters a cavity with no initial stored energy, and if after the charge leaves the cavity the stored energy is W_c , then clearly

$$W_c = U_i - U_f \quad , \quad (2.4)$$

where U_f is the final energy of the charge. Conservation of energy can also be applied to differential energy exchanges. Suppose, for example, that a charge q at position $z = z'$ moves a distance dz' along a trajectory (taken to be the z coordinate axis) such that the electric field for a given mode has a z component $E_z(z')$. The change in the energy stored in the mode is then

$$dW = -qE_z(z') dz' \quad . \quad (2.5)$$

The field at position \vec{r} for the mode in question is related to the energy W stored in the mode by $E^2(\vec{r}) = f(\vec{r})W$, where the function $f(\vec{r})$ depends on the cavity geometry. Thus we have on the cavity axis

$$f(z) dW = 2 E_z(z) dE_z \quad . \quad (2.6)$$

From these two expressions, together with the fact that time is related to the position of the charge through $ct' = z'$, an expression is obtained for dE_z as a function of z at time t' . Treated as a phasor, the field element dE_z at some later time t will be described by

$$d\tilde{E}_z(z, t) = d\tilde{E}_z(z, t') e^{j\omega_0(t - t')} \quad (2.7)$$

where ω_0 is the resonant frequency of the mode. Using the concept of differential superposition, the total beam-induced cavity field at any position z and time t can now be obtained by adding up all the differential field elements induced at previous times through an integration which takes proper account of the phase relationships

between elements. But as will be seen later, one more ingredient - causality - must be added to complete the picture.

Implicit in the foregoing analysis is the concept of normal modes. It is assumed that each mode in the cavity can be treated independently in computing the fields induced by a charge crossing the cavity. The total stored energy is taken as the sum of the energies in the separate modes. The total field is the vector (phasor) sum of all the individual mode fields at any instant.

Causality is a somewhat more subtle principle that must also be taken into account in computing the field induced by a charge passing through an rf cavity or structure. By causality we mean simply that there can be no disturbance ahead of a charge moving at the velocity of light. Thus, in a mode analysis of the growth of the beam-induced field, the field must vanish ahead of the moving charge for each mode. As we will see in more detail in Sec. 9.3, this is accomplished if the charge also induces imaginary differential field components in addition to the real field components as obtained from the energy interchange described by Eqs. (2.5) and (2.6). These imaginary components, which lie at $\pm 90^\circ$ with respect to the real component at time $t = t'$, must have an amplitude distribution as a function of frequency such that they add up, when integrated over frequency, to cancel the real induced components ahead of the charge ($t < t'$) and to double the real components behind the charge ($t > t'$).

Real high energy electrons and positrons move at velocities which are close to, but not exactly equal to, the velocity of light. Subtle questions arise as to how close is close enough so that the $v \approx c$ approximation is sufficiently accurate in any given situation. There will not be space here to go into this problem in detail; in fact, some aspects of the causality problem are still controversial and have not yet been adequately resolved to everyone's satisfaction. For our purposes here, we will assume that causality is absolute for point charges moving through rf cavities and traveling-wave structure

2.3 Differential Superposition

Because of the importance of the concept of differential superposition, let us use it here to compute the answer to a practical question: what is the voltage induced in a cavity by a Gaussian charge distribution with total charge q , if the voltage induced by a point charge q is V_0 ? A charge element dq will induce a voltage $dV = V_0(dq/q)$. Assume that the charge element dq crosses the cavity reference plane at time t_0 . At some other time t the voltage induced by this charge element will be

$$d\tilde{V} = \frac{V_0}{q} e^{j\omega(t-t_0)} dq(t_0) \quad (2.8)$$

For a Gaussian charge distribution

$$dq(t_0) = I(t_0)dt_0 = \frac{q}{\sqrt{2\pi\sigma}} e^{-t_0^2/2\sigma^2} dt_0 \quad (2.9)$$

and therefore

$$d\tilde{V} = \frac{V_o}{\sqrt{2\pi\sigma}} e^{j\omega_o t} e^{-t_o^2/2\sigma^2} (\cos\omega_o t_o - j \sin\omega_o t_o) dt_o \quad (2.10)$$

We invoke differential superposition and integrate over all arrival times t_o , noting that the integral of the second term in the preceding expression vanishes by symmetry. The result is

$$\tilde{V} = V_o e^{j\omega_o t} e^{-\omega_o^2 \sigma^2 / 2} \quad (2.11)$$

where $V_o e^{j\omega_o t}$ is just the voltage induced by a point charge. Thus for a Gaussian charge distribution,

$$V = V_o e^{-\omega_o^2 \sigma^2 / 2} \quad (2.12)$$

Since bunch distributions in storage rings and linacs are usually Gaussian, or nearly so, the result given by Eq. (2.12) is of broad applicability.

3. STANDING WAVE LINACS

3.1 Shunt Impedance

The shunt impedance R_a for an rf cavity is a figure of merit which relates the accelerating voltage V to the power P dissipated in the cavity walls through the expression $V = (R_a P)^{1/2}$. For a mode with stored energy W , both the power dissipation $P = \omega W/Q$ and the longitudinal electric field on the cavity axis $E_z(z) = [f(z)W]^{1/2}$ are specified in terms of the geometry-dependent factors Q and $f(z)$. Assuming that these factors are known, it remains to compute V in terms of $E_z(z)$.

Assume that the path of an electron (positron) lies along the z coordinate in an arbitrary standing wave structure driven by an external generator at frequency ω . The z component of the electric field along the axis is then

$$E_z(z, t) = E(z) e^{j\omega t} \quad (3.1)$$

Assume that a positive E_z produces an accelerating force on the particle in question, and that the particle velocity is $v_e \approx c$. The particle position at time t is

$$z_e = c(t - t_o) \quad (3.2)$$

where $z_e = 0$ at $t = t_o$. The accelerating field seen in a reference frame moving with the particle (the co-moving frame) is then

$$\begin{aligned}
 E_z(\text{cmf}) &= E(z) e^{j\omega(t_0 + z/c)} \\
 &= E(z) e^{j\omega t_0} e^{jkz}
 \end{aligned}
 \tag{3.3}$$

where $k \equiv \omega/c$. The voltage gained by the particle in moving from $z = z_1$ to $z = z_2$ (z_1 and z_2 would normally be at the cavity entrance and exit) is

$$\begin{aligned}
 \tilde{V} &= \int_{z_1}^{z_2} E_z(\text{cmf}) dz = e^{j\omega t_0} \int_{z_1}^{z_2} E(z) e^{jkz} dz \\
 &= e^{j\omega t_0} [C + jS]
 \end{aligned}
 \tag{3.4}$$

Here C and S are the cosine and sine integrals

$$C = \int_{z_1}^{z_2} E(z) \cos kz \, dz \tag{3.5a}$$

$$S = \int_{z_1}^{z_2} E(z) \sin kz \, dz \tag{3.5b}$$

We then have

$$\tilde{V} = V e^{j(\omega t_0 + \theta)} \tag{3.6}$$

where

$$V = |\tilde{V}| = \left| \int_{z_1}^{z_2} E(z) e^{jkz} dz \right| = (C^2 + S^2)^{1/2} \tag{3.7a}$$

$$\theta = \tan^{-1}(S/C) \tag{3.7b}$$

If $E(z)$ is symmetric about a point on the z axis, the S integral in Eq. (3.5b) will vanish if the symmetry point is chosen to be the origin $z = 0$. Even if the structure is not symmetric, we can make the transformations

$$\begin{aligned}
 \omega t_0' &= \omega t_0 + \theta \\
 kz' &= kz - \theta
 \end{aligned}
 \tag{3.8}$$

where $z' = c(t - t_0')$ is the position of the charge with respect to the new coordinate origin. Then $\tilde{V} = V e^{j\omega t_0'}$ and the point $z' = 0$ defines the reference plane for the cavity. The shunt impedance is now defined as

$$R_a = \frac{V^2}{P} \quad , \quad (3.9)$$

where

$$P = \frac{1}{2} R_s \int_{\text{cavity surface}} H^2 dA \quad . \quad (3.10)$$

Here

$$R_s = (\omega\mu/2\sigma)^{1/2} = \pi Z_0 (\delta/\lambda) \quad (3.11)$$

is the surface resistance, μ the permeability, σ the dc conductivity, δ the skin depth, Z_0 the impedance of free space and $\lambda = 2\pi c/\omega$.

The above definition of shunt impedance, R_a , is the so-called accelerator definition, which is used in most of the modern literature on linac structure design. The shunt impedance is, however, occasionally defined with a factor of 2 in the denominator as $R = V^2/2P$. The reader should be aware of this potential source of confusion.

3.2 Transit-Time Factor

An "uncorrected" shunt impedance R_u is sometimes defined in terms of a voltage V_u , the integral of the electric field along the cavity axis:

$$R_u = \frac{V_u^2}{P} \quad (3.12a)$$

$$V_u = \int E(z) dz \quad . \quad (3.12b)$$

The shunt impedance defined in this way does not take into account the variation in the field during the time it takes a particle to cross an accelerating gap or pass through an rf cavity; that is, the effect of transit time is ignored. To obtain the true shunt impedance, a transit-time factor T is applied to the uncorrected shunt impedance so that*

$$R_a = R_u T^2 \quad , \quad (3.13a)$$

* In the literature Eq. (3.13) is often written $Z_{sh} = ZT^2$. In these notes we reserve Z for the rf impedance.

where

$$T = \frac{V}{V_u} = \frac{\left| \int E(z) e^{jkz} dz \right|}{\int E(z) dz} \quad (3.13b)$$

Problem 3.1: Show that the transit-time factor for a gap of length L with a uniform field E_z along the particle trajectory is

$$T = \frac{\sin(\theta/2)}{\theta/2} \quad (3.14)$$

where $\theta = kL = 2\pi L/\lambda$ is the transit angle. Use the definition in Eq. (3.13b) and compute the transit-time factor in two ways: with the origin $z = 0$ at the center of the gap, and with the origin such that the gap extends from $z = 0$ to $z = L$.

The transit-time factor is introduced here for historical reasons and because it is often found in the literature. Since the voltage V as given by Eq. (3.7a) has to be computed in any case, the attentive reader might wonder why the shunt impedance is not computed directly using Eq. (3.9), rather than through the circular process of Eqs. (3.12a), (3.13a) and (3.13b). Indeed, the transit-time factor does not need to be calculated to obtain the shunt impedance, and it is sometimes even misleading. Consider, for example, a cavity of length L operating in a mode such that the axial field is

$$E(z,t) = E_0 \cos kz \cos \omega t \quad (3.15)$$

If the cavity is exactly one-half wavelength long, then $kL = \pi$ and

$$V_u = E_0 \int_0^L \cos kz \, dz = 0$$

$$R_u = 0 \quad (3.16)$$

The axial field for such a cavity is shown by the solid curves in Fig. 3.1 at time $t = 0$ and $t = L/c$. (Can this cavity be a cylindrical "pillbox" cavity of finite radius? Why not?) On the other hand, the field in a co-moving frame ($kz = \omega t$) for a particle which enters the cavity at $t = 0$ varies as

$$E(\text{cmf}) = E_0 \cos^2 kz \quad (3.17)$$

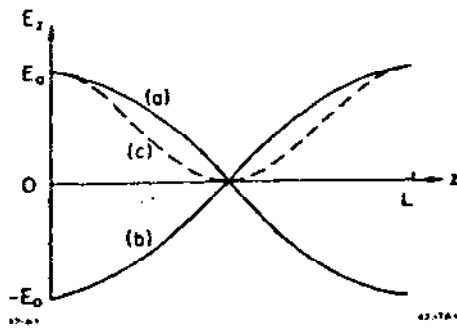


Fig. 3.1. Axial electric field in a TM_{011} -mode cavity one-half free-space wavelength long; (a) at $t = 0$, (b) at $t = L/c$ and (c) in a co-moving frame for a particle with $v \approx c$.

The field seen in such a frame moving with a relativistic particle is shown by the dashed line in Fig. 3.1. The voltage gained by the particle is

$$V = E_0 \int_0^L \cos^2 kz \, dz = E_0 L/2 \quad (3.18)$$

and

$$T = V/V_u = \infty \quad (3.19)$$

$$R_a = R_u T^2 = (0)(\infty) \quad .$$

In this case, it is meaningless to define the shunt impedance through Eq. (3.13a). Although the concept of a transit-time factor breaks down in this case, it is sometimes helpful in giving a better physical feeling for the process of optimizing the shunt impedance of accelerating cavities (see Sec. 3.4).

3.3 Bunch Form Factor

Real bunches in real accelerators and storage rings are not point bunches, but extend over some finite length. It is clear for this case that not all particles in the bunch can achieve the maximum energy gain, but that some particles must cross the cavity reference plane earlier or later than the time for peak gain. Suppose the current in the bunch flowing past a fixed point is $I(t)$, and that the total charge in the bunch is

$$\int_{-\infty}^{\infty} I(t) dt = q \quad (3.20)$$

Suppose also that a reference plane is again chosen such that the maximum voltage V_0 is gained by a particle which crosses the plane at $t = 0$. Then the average voltage gained by all the charge elements $dq = I(t)dt$ is

$$\bar{V}_a = \frac{\int_{-\infty}^{\infty} V_0 e^{j\omega t} \cdot I(t) dt}{\int_{-\infty}^{\infty} I(t) dt} = V_0 (C' + jS') \quad (3.21)$$

where C' and S' are the cosine and sine integrals

$$C' = \frac{1}{q} \int_{-\infty}^{\infty} I(t) \cos \omega t \, dt \quad (3.22a)$$

$$S' = \frac{1}{q} \int_{-\infty}^{\infty} I(t) \sin \omega t \, dt \quad (3.22b)$$

The magnitude of the average voltage gain is

$$V_a = |\tilde{V}_a| = F V_0 \quad (3.23)$$

where F is the bunch form factor,

$$F = (C'^2 + S'^2)^{1/2} \quad (3.24)$$

For a Gaussian bunch with rms bunch length σ_z and for a uniform bunch of time length t_b we have

$$F(\text{Gaussian}) = e^{-\frac{1}{2} \omega^2 \sigma_z^2} \quad (3.25a)$$

$$F(\text{rectangular}) = \frac{\sin\left(\frac{1}{2} \omega t_b\right)}{\frac{1}{2} \omega t_b} \quad (3.25b)$$

For $F = 0.9$, we have $\sigma_z/\lambda = 0.073$ and $t_b/\lambda = 0.25$, where $\sigma_z = c\sigma_t$ and $t_b = ct_b$. Note that the form factor for the case of a Gaussian bunch is the same as obtained previously in Sec. 2.3, where the voltage induced in a cavity by such a bunch was calculated using the principle of differential superposition.

3.4 Standing-Wave Structures

The longitudinal and transverse modes in a chain of cylindrical "pillbox" cavities provide an approximate yet often surprisingly accurate model for the accelerating and deflecting fields in more realistic accelerating structures. The properties of a single cylindrical resonator are simple to treat analytically, and will serve as a starting point for a discussion of standing-wave accelerating structures.

Consider a pillbox cavity with radius b and axial length L . The axial electric and azimuthal magnetic field components for the lowest-order accelerating mode (TM_{010} mode) are

$$E_z = E_0 J_0(kr) \cos \omega t \quad (3.26)$$

$$H_\phi = -\frac{E_0}{Z_0} J_1(kr) \sin \omega t$$

where $Z_0 = 377$ ohms, $k = 2\pi/\lambda = p_{01}/b$ and $p_{01} = 2.405$ is the first root of J_0 . The stored energy and power dissipation are computed to be

$$W = \frac{\epsilon_0}{2} \int_V E_z^2 dv = \frac{\pi}{2} \epsilon_0 b^2 L E_0^2 J_1^2(p_{01}) \quad (3.27)$$

$$P = \frac{R_s}{2} \int_A H_\phi^2 dA = \frac{\pi b R_s E_0^2}{Z_0^2} (b+L) J_1^2(p_{01})$$

The accelerator parameters of interest are

$$Q = \frac{\omega W}{P} = \frac{G_1}{R_s} \sim \omega^{-1/2} \quad (3.28a)$$

$$\frac{r}{Q} = \frac{V^2}{\omega W L} = \frac{G_2 T^2}{\lambda} \sim \omega \quad (3.28b)$$

$$r = \frac{V^2}{P L} = \frac{G_1 G_2 T^2}{\lambda R_s} \sim \omega^{1/2} \quad (3.28c)$$

Here $r \equiv R_s/L$ is the shunt impedance per unit length, $R_s = (\omega \mu_0 / 2\sigma)^{1/2}$ is the surface resistance, T is the transit angle factor and G_1 and G_2 are two constants, independent of frequency and cavity material, given by

$$G_1 = \frac{P_{01}}{2} \left(\frac{L}{b+L} \right) Z_0 = 453 \left(\frac{L}{b+L} \right) \text{ ohms} \quad (3.29a)$$

$$G_2 = \frac{4 Z_0}{2 P_{01} J_1^2(p_{01})} = 967 \text{ ohms} \quad (3.29b)$$

$$T = \frac{\sin(\pi L/\lambda)}{(\pi L/\lambda)} \quad (3.29c)$$

Problem 3.2: Show that the shunt impedance per unit length r for a pillbox cavity is maximum at $L/b = 0.75$, and that the total shunt impedance rL is maximum at $L/b = 1.15$. What are the corresponding values of r , rL and Q in these two cases for a room-temperature copper cavity at 500 MHz?

Designers of accelerating structures have been working for many years to increase the shunt impedance as much as possible beyond that which can be obtained from a chain of simple pillbox cavities. Initially this was accomplished by a combination of intuition and laborious rf measurements in the laboratory. In more recent years,

powerful computer programs have greatly facilitated the process of optimizing the design of standing-wave accelerating structures. The first of these codes, LALA,⁵ was developed at the Los Alamos Scientific Laboratory to aid in the design of structures for high-energy proton linacs. A more recent and more powerful code, SUPERFISH,⁶ is now available at many accelerator laboratories. SUPERFISH can calculate higher-order cavity modes as well as the lowest frequency accelerating mode, although both programs are limited to axially-symmetric modes in axially-symmetric structures. However, a new program, ULTRAFISH,⁷ is now under development which can compute the frequencies and fields of modes which vary as $\cos m\phi$ (where ϕ is the azimuthal angle and $m > 0$) in axially-symmetric structures. Modes with $m > 0$ can cause deflection and defocusing of bunches and trains of bunches in an accelerating structure, leading to emittance growth and to beam breakup.

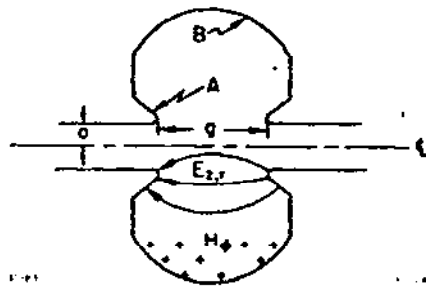


Fig. 3.2. Single Cell of a m -mode accelerating structure.

Figure 3.2 illustrates some of the factors entering into the design of a single cell of a standing-wave accelerating structure. The most characteristic features are the so-called "nose cones," as shown at A. For a given stored energy, the nose cones help to concentrate the electric field in the region of the beam, thus increasing the factor $R_a/Q = V^2/\omega W$. The gap length g between nose cones is adjusted for maximum R_a/Q . As g is decreased, the transit time factor T increases, but the integral of the axial field,

Eq. (3.12b), decreases for a given stored energy. After the R_a/Q factor has been optimized by shaping the nose cones and adjusting the gap length, the shunt impedance can be increased further by maximizing the Q . The Q is controlled largely by losses at the outer surfaces of the cavity, shown at B in Fig. 3.2, where the magnetic field is greatest. The highest Q is obtained if this part of the cavity surface can be made approximately spherical in shape. This, however, increases the complexity in manufacturing the cavity. It is often a reasonable trade-off to keep a cylindrical outer boundary with a consequent 10% or so reduction in shunt impedance.

It is usually awkward to feed each cavity separately with rf in a long linac structure. Thus a number of cavities, or cells, are usually coupled together to form a coupled-cavity structure with a single rf feed point. Such a structure is shown schematically in Fig. 3.3. A structure consisting of N coupled cells (resonators) will have N normal modes, as shown in the dispersion diagram of Fig. 3.4. The frequencies of the normal modes can be obtained by solving an equivalent circuit^{8,9} consisting of a chain of coupled LRC resonators as shown in Fig. 3.5. For a structure with weak magnetic cell-to-cell coupling and vanishingly small losses, the normal mode frequencies are given by

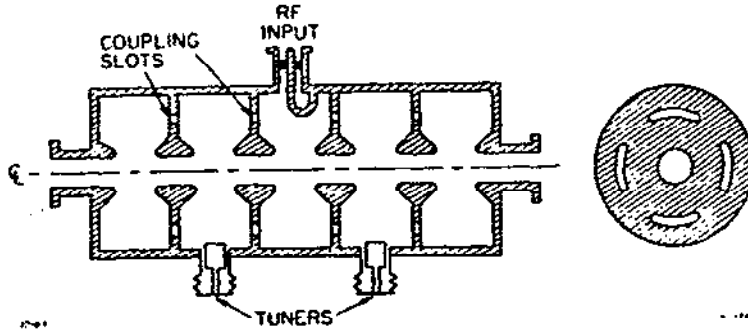


Fig. 3.3. Diagram showing the important features of a five-cell w -mode structure with magnetic field coupling.

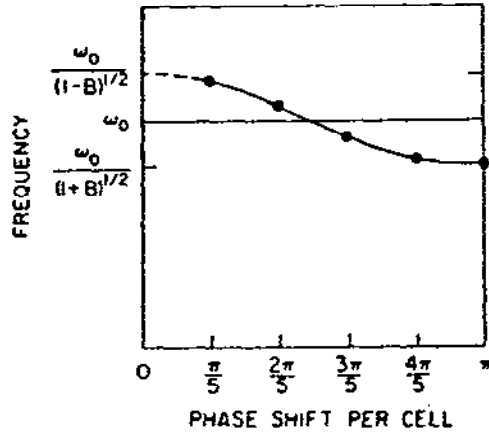
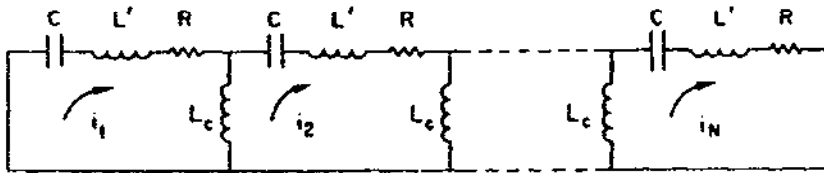


Fig. 3.4. Dispersion diagram for a five-cell structure with "flat" w -mode.



12-81

4237A8

Fig. 3.5. Equivalent circuit representation for a chain of coupled resonant cavities. For a flat w -mode, $L' = L + 2L_c$ and there is then no mode with zero phase shift per cell.

$$\omega(m) = \frac{\omega_0}{(1 - B \cos m\pi/N)^{1/2}} \approx \omega_0 \left(1 + \frac{B}{2} \cos m\pi/N\right) \quad (3.30)$$

where B is the bandwidth of the structure, m is the mode number (m = 1, 2, -- N for a structure with full-length end cells) and mπ/N is the phase shift per period.

RF structures for storage rings usually operate in the π mode (m = N). In order to obtain a "flat" π-mode (field amplitude equal in all N cells) in a structure with full-length end cells, the two end cells must be tuned lower in frequency (for magnetic-field coupling) by an amount δω/ω ≈ B/2. The field amplitude in the nth cell for the mth normal mode is for this case

$$E_n = A_m \sin [m\pi(2n-1)/2N] \quad , \quad (3.31)$$

where n = 1, 2, -- N.

Problem 3.3: Draw the equivalent circuit for a chain of N coupled resonators with half-length end cells (metal boundaries at the planes of symmetry in each end cell). Show that the normal-mode frequencies are given by $\omega(m) = \omega_0 [1 - B \cos m\pi/(N-1)]^{-1/2}$ and the corresponding field amplitudes by $E_n = A_m \cos [m\pi(n-1)/(N-1)]$, where n = 1, 2, -- N and m = 0, 1, -- (N-1). The π/2 mode is obtained for m = (N-1)/2. Compare the field amplitudes E_n for this case with the π/2-mode fields given by Eq. (3.31) with m = N/2.

It is important to know the sensitivity of the field amplitudes in the individual cells to errors in tuning, due either to unwanted perturbations or to the presence of tuners. It is usually not practical to put a remotely-controlled tuner in each cell of a multicell structure. If, for example, we attempt to adjust the frequency of a multicell structure with a single tuner in one cell, an error in field flatness will be introduced. A mathematically elegant approach to this problem is given by the application of perturbation theory to the equivalent circuit representation.¹⁰ The problem can also be treated in certain simple cases by considering the multiple reflections of a wave traveling on a finite-length chain of coupled resonators.¹¹ Suppose we have a chain of N π-mode cells with both the rf feed point and a single tuner located in the center cell in a structure with an odd number of cells. If f(n) is the flatness function defined as the ratio of the perturbed field amplitude to the unperturbed field along the structure, then the maximum deviation from flatness is given by

$$\delta f \approx \frac{(N-1)^2}{2B} \cdot \left(\frac{\delta\omega}{\omega}\right) \quad , \quad (3.32)$$

where $\delta\omega$ is the change in structure resonant frequency produced by the tuner, and $N = 3, 5, 7$ etc. We see that for the π mode the sensitivity of the field flatness to tuning varies quadratically with the number of cells, and is inversely proportional to the bandwidth. A similar analysis for the $\pi/2$ mode shows that the field flatness is less sensitive to tuning errors. The deviation from flatness varies as

$$\delta f \approx \frac{(N-1)^2}{2B^2} \cdot \left(\frac{\delta\omega}{\omega}\right)^2 \quad (3.33)$$

where $N = 5, 9, 13$ etc. As shown in Fig. 3.6a, every other cell in an unperturbed $\pi/2$ mode is unexcited for a lossless structure.* The main effect of a detuning error is to introduce a field in the nominally unexcited cells. The maximum value of this field is in the two cells adjacent to the center cell with tuner and is given by

$$\delta f \approx \frac{(N-3)}{B} \cdot \left(\frac{\delta\omega}{\omega}\right) \quad (3.34)$$

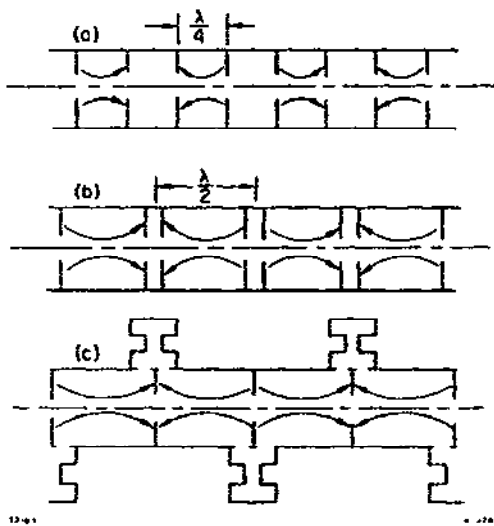


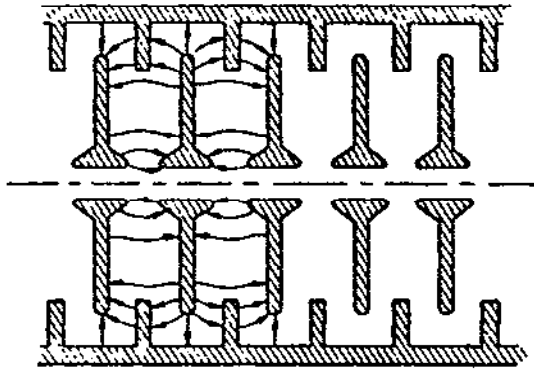
Fig. 3.6. (a) Simple $\pi/2$ -mode structure; (b) bi-periodic structure; (c) side-coupled structure.

A comparison of Eqs. (3.33) and (3.34) with Eq. (3.32) shows the superiority of the $\pi/2$ mode against tuning perturbations. However, from Fig. 3.6(a) it is apparent that the shunt impedance of the $\pi/2$ mode will be poor, since every other cavity is unexcited and will not contribute to the acceleration of particles. One solution is to shrink down the length of the unexcited cavities, as shown in Fig. 3.6(b), resulting in a so-called bi-periodic structure. A more elegant solution is to remove the unexcited cavities from the beam line entirely, as shown in Fig. 3.6(c). This results in the side-coupled structure, exploited extensively at Los Alamos.⁹ The field on the axis looks like that for a π -mode, but the structure

has the good stability against perturbations of the $\pi/2$ mode. Recently a new type of standing-wave structure with good shunt impedance and large bandwidth has been under development, particularly at

* This is true for a structure terminated in half-length end cells (see problem 3.3). Full-length end cells can also be used if they are properly detuned.

Los Alamos.^{12,13} This is the disk and washer (DAW) structure, shown schematically in Fig. 3.7. The r/Q of this structure is less than that of a chain π -mode cells with nose cones, but the Q is significantly higher. The reason for this is that the structure has evolved



from a chain of pillbox cavities operating in the next higher-order radial mode. The stored energy is therefore higher for a given field on the axis, leading to a lower r/Q . However, the current tends to flow as a lossless displacement current between the disks and the washers, rather than as a physical current in the surface at the outer boundary. This leads to a much greater value for Q . Like the side-coupled structure, the DAW structure works in a π -like mode, but with resonant coupling in the region of the disks. The coupling is very heavy, giving the structure a large bandwidth and

Fig. 3.7. Disk and Washer (DAW) structure with sketch of electric field lines.

great stability against perturbations.

Properties of several structures operating at 350 MHz are compared in the table below: the DAW structure just described, a π -mode structure proposed for the rf system for the LEP storage ring at CERN,¹⁴ and for comparison a chain of pillbox cavities $\lambda/2$ in length. The DAW and LEP structures have beam aperture radii of 5 cm, while the pillbox cavity, of course, has no beam opening. This brings up a very important point: structures should always be compared at the same value of beam hole radius, since the shunt impedance is a strong function of the size of the beam aperture. Figure 3.8 shows the variation in shunt impedance per unit length as a function of beam-hole radius a for a simple disk-loaded structure and for a shaped π -mode cell with nose cones. Note that the shunt impedance for these structures is reduced by a factor of two at a $\approx 0.15 \lambda$.

Table 3.1 A Comparison of Several Copper Structures at 350 MHz

	r/Q (Ω/m)	Q	r ($M\Omega/m$)	B
LEP ¹⁴	635	49,000*	31*	≈ 0.01
DAW ¹³	325	130,000*	42*	≈ 0.5
Pillbox	465	52,000	24	--

*These Q and r values should be reduced by about 15% for a practical structure to take into account losses due to washer supports (DAW), coupling slots (LEP), and imperfect surfaces.

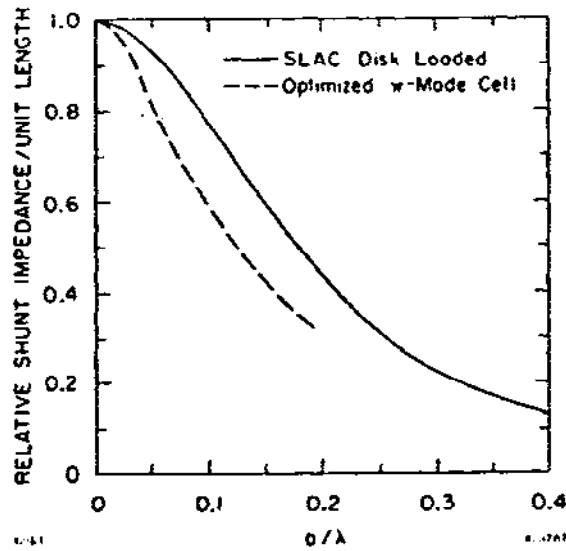


Fig. 3.8. Variation in shunt impedance per unit length as a function of beam-hole radius for two typical structures.

3.5 Equivalent Circuit for a Cavity with Beam Loading

Figure 3.9(a) shows the equivalent circuit for an rf source (usually a klystron) connected to a linac or storage ring cavity by a transmission line. Since such equivalent circuits are basic to the analysis of rf system design and performance, several comments are in order. First, note that the rf cavity and the klystron output cavity are represented by resonant LRC circuits. While this circuit representation may be intuitively obvious, a rigorous justification of the use of lumped-element circuits to model resonant modes in metal cavities is given in Ref. 15. Second, note that the beam in the rf cavity is represented by a current generator. This is an excellent representation for a relativistic beam, since the velocity of the particles passing through the cavity is independent of the cavity voltage. The situation is different for the case of the klystron output cavity. The velocities of the electrons as they pass through the gap of the output cavity can change in response to the cavity fields, and as a consequence a current-dependent beam loading admittance, Y_{bk} , is needed in the equivalent circuit (see, for example, Ref. 3). Third, note that the transmission line connecting cavity and klystron has both forward and backward traveling waves. These waves must satisfy the boundary condition $V_k^+ + V_k^- = V_k/a_k$ at the klystron, and a similar condition at the cavity. Since there may be a number of transmission line elements between A and B, each with reflection, phase shift and possibly loss, the solution of the general problem can be quite complex.¹⁶ For our purposes here, we can simplify the problem considerably by assuming that there is an isolator or circulator just before the cavity. Thus, any power which is reflected from the cavity and which travels back toward the klystron will be

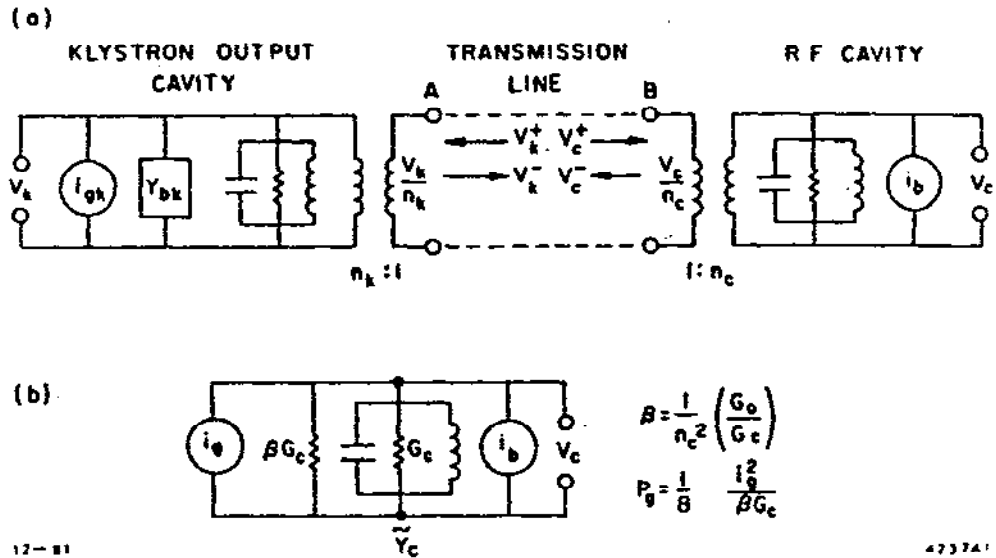


Fig. 3.9. (a) Equivalent circuit for a beam-loaded cavity couple to a klystron; (b) simplified circuit assuming a matched RF source

absorbed. The simplified equivalent circuit in Fig. 3.9(b), in which the transmission line impedance G_0 and the current generator representing the rf source are transformed to the cavity side of the transformer representing the transmission-line-to-cavity coupling network can now be used. Here β is termed the cavity coupling coefficient. If the source generator is off and the cavity is excited internally by the beam, β is then seen to be the ratio of the power radiated out of the cavity through the coupling loop or aperture to the power dissipated in the cavity walls.

In using the simplified equivalent circuit, the available power from the generator, P_g , is to be identified with the incident klystron power. Also watch out for factors of two. In terms of the accelerator definition of shunt impedance introduced previously, and the dc current I_0 , we have

$$G_c = \frac{2}{R_a}$$

$$P_c = \frac{1}{2} G_c V_c^2 = \frac{V_c^2}{R_a} \tag{3.3}$$

$$i_b = 2 I_0 e^{-\omega_{\sigma}^2 t / 2} \approx 2 I_0$$

Assuming short bunches ($\omega_0 \sigma_c \ll 1$), we have from Fig. 3.9(b) that the voltages at resonance produced by the beam and the rf source, if each one acts independently on the circuit, are

$$V_{gr} = \frac{i_g}{G_c(1+\beta)} = \frac{2\sqrt{\beta}}{1+\beta} \cdot \sqrt{R_a P_g} \quad (3.35a)$$

$$V_{br} = \frac{i_b}{G_c(1+\beta)} = \frac{I_o R_a}{1+\beta} \quad (3.35b)$$

It is instructive to consider the accelerating voltage V_a , the power dissipated the cavity walls P_c , the efficiency η for the conversion of generator power into beam power, and the reflected power P_r for the case of a linac operating on resonance and in phase (bunches receive maximum acceleration such that $V_a = V_c$). In terms of a beam-loading parameter $K = (I_o/2)(R_a/P_g)^{1/2}$, these quantities are:

$$V_a = \sqrt{R_a P_g} \left\{ \frac{2\sqrt{\beta}}{1+\beta} \left(1 - \frac{K}{\sqrt{\beta}} \right) \right\} = \sqrt{R_a P_c} \quad (3.36a)$$

$$\eta = \frac{I_o V_a}{P_g} = \frac{2\sqrt{\beta}}{1+\beta} \left[2K \left(1 - \frac{K}{\sqrt{\beta}} \right) \right] \quad (3.36b)$$

$$\frac{P_r}{P_g} = \frac{[(\beta-1) - 2K\sqrt{\beta}]^2}{(\beta+1)^2} \quad (3.36c)$$

Problem 3.4: Show that Eq. (3.36c) follows from conservation of energy: $P_r = P_g - \eta P_g - P_c$.

The important feature of Eq. (3.36a) is that the accelerating voltage decreases linearly with increasing current. These "load lines" are shown in Fig. 3.10 for various values of β . For a given beam current, the maximum accelerating voltage is determined by the condition $\partial V_a / \partial \beta = 0$ at $K_m = (\beta-1)/(2\sqrt{\beta})$. The conversion efficiency, shown in Fig. 3.11 with β as a parameter, is seen to vary parabolically as a function of beam current, reaching a maximum at $K_m = \sqrt{\beta}/2$. The beam voltage is then one-half of the voltage at zero current. From Eq. (3.36c), note that the condition for zero reflected power is given by $K = (\beta-1)/(2\sqrt{\beta})$, but that this is not the condition for optimum efficiency as a function of beam current.

Problem 3.5: What is the condition for optimum efficiency at a fixed current as a function of β ? Why is this different than the condition for maximum efficiency at fixed β as a function of beam current? What would a contour plot showing lines of constant efficiency in the $K - \beta$ plane look like? (See Ref. 16a.) Show also that for $P_r = 0$ the coupling coefficient is $\beta = 1 + P_b/P_c$, and $P_g = \beta P_c$.

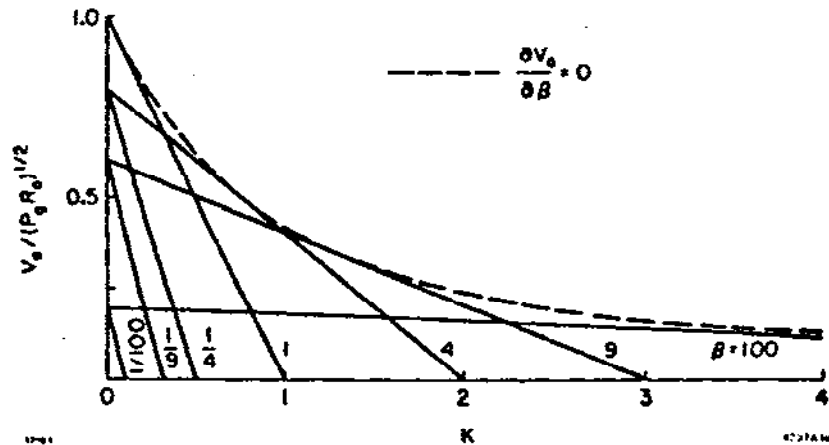


Fig. 3.10. Normalized energy gain as a function of the beam-loading parameter for various values of the coupling coefficient.

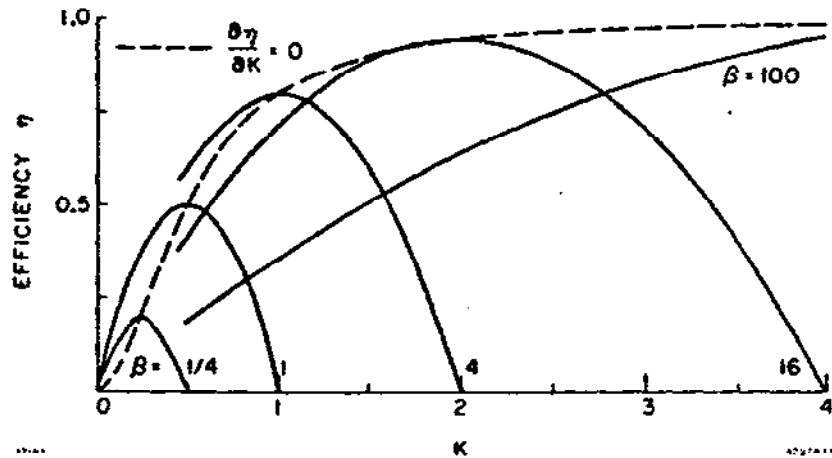


Fig. 3.11. Conversion efficiency as a function of the beam-loading parameter for various values of the coupling coefficient.

We next consider beam loading in a standing-wave structure which is tuned to be off resonance. The admittance of the parallel resonant circuit representing the cavity without coupling (\tilde{Y}_c in Fig. 3.9(b)) is

$$\tilde{Y}_c = G_c \left[1 + jQ_o \left(\frac{\omega}{\omega_o} - \frac{\omega_o}{\omega} \right) \right] \quad (3.37)$$

where $\omega_o = 1/\sqrt{LC}$ is the resonant frequency, $W = 1/2 CV_o^2$ is the stored energy, and $Q_o \equiv \omega_o W/P_c = \omega_o C/G_c$. We limit the following discussion to the case of a high Q cavity such that $\delta \equiv (\omega - \omega_o)/\omega_o \ll 1$. Introducing δ , Eq. (3.37) becomes

$$\tilde{Y}_c \approx G_c(1 + j 2 Q_o \delta) \quad (3.38)$$

The total admittance seen by the beam must include the loading by the coupled admittance of the input transmission line. This external admittance is taken into account by adding βG_c to the preceding expression to obtain the loaded cavity impedance

$$\tilde{Z}_L = \frac{1}{\tilde{Y}_L} = \frac{R_o}{1 + j 2 Q_L \delta} \quad (3.39)$$

where $R_o = [G_c(1 + \beta)]^{-1}$ is the loaded impedance at resonance and $Q_L = Q_o/(1 + \beta)$ is the loaded Q.

We now define a quantity ψ , termed the tuning angle for reasons that will be clear shortly, by

$$\tan \psi \equiv -2 Q_L \delta \quad (3.40)$$

A simple manipulation of Eq. (3.39) gives

$$\tilde{Z}_L = R_o (\cos^2 \psi)(1 + j \tan \psi) = R_o \cos \psi e^{j\psi} \quad (3.41)$$

In terms of the beam-loading voltage and the generator voltage at resonance, given by Eqs. (3.35), we have

$$\tilde{V}_g = i_g \tilde{Z}_L = V_{gr} \cos \psi e^{j\psi} \quad (3.42a)$$

$$\tilde{V}_b = i_b \tilde{Z}_L = V_{br} \cos \psi e^{j\psi} \quad (3.42b)$$

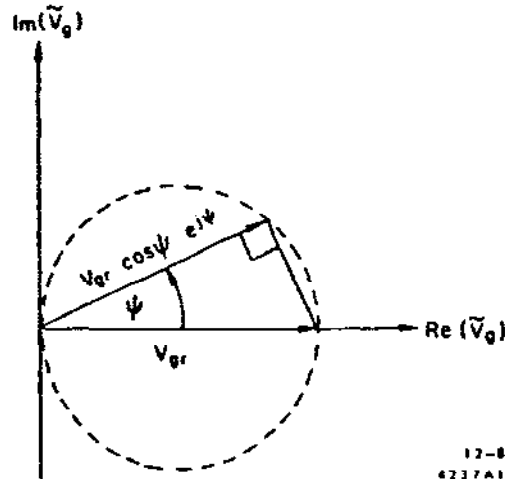


Fig. 3.12. Diagram showing how both generator and beam-loading voltages vary in the complex plane as a function of the tuning angle.

Thus, as the tuning angle increases from zero, the magnitudes of both \tilde{V}_g and \tilde{V}_b decrease as $\cos\psi$, and the phases rotate through angle ψ . This is illustrated in Fig. 3.12. Note especially that the tip of the phasor \tilde{V}_g or \tilde{V}_b traces out a circle in the complex plane as the tuning angle ψ is varied.

We are now ready to consider the superposition of the generator and beam-loading voltages to obtain the net cavity voltage. For convenience, the reference phase (positive real axis) is taken in the direction of $-i_b$. The accelerating voltage V_a is then simply the real component of the net cavity voltage. The superposition $\tilde{V}_c = \tilde{V}_g + \tilde{V}_b$ in this reference frame is shown in Fig. 3.13. Note that two additional important angles have been defined: the phase angle ϕ between \tilde{V}_c and $-i_b$, and the angle θ between \tilde{i}_g and $-i_b$. In storage ring applications, ϕ is termed the synchronous phase angle. In a linac ϕ is the angle between the current bunches and the crest of the rf voltage wave. The angle θ is under external control in an rf linac; it can be adjusted by means of a phase shifter in the input drive to a klystron feeding a cavity or group of cavities. In a storage ring θ is determined if the beam-current (or V_{br}), the cavity voltage V_c , the voltage gain per turn V_a and the tuning angle ψ are specified.

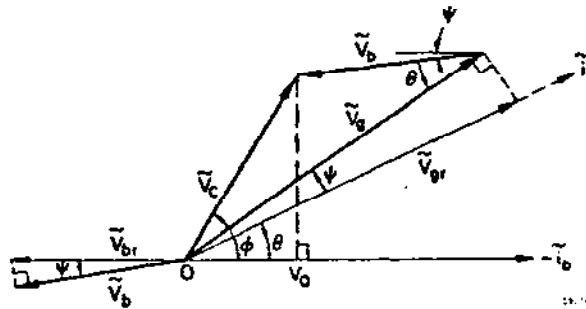


Fig. 3.13. Diagram showing the vector addition of generator and beam-loading voltages in an RF cavity.

A thorough understanding of the vector diagram in Fig. 3.13 is the key to steady-state beam loading calculations. The diagram will be exploited in the following section to compute, as an example, the optimum tuning and coupling for a storage-ring rf cavity. Before proceeding, however, we should recall what is meant by "steady-state". First of all, it is assumed that both the beam current and the rf generator have been turned on for a time which is long compared to the cavity filling time, which is given by

$$T_f = \frac{2 Q_L}{\omega_0} = \frac{2 Q_0}{\omega_0 (1 + \beta)} \quad (3.4)$$

If the beam current is turned on at $t = 0$, then for t less than several filling times the cavity fields are in a transient state.

However, another type of transient behavior is also possible. Suppose the bunches in either a linac or storage ring are spaced apart by time T_b . In this section we have implicitly assumed that all bunches contain equal charge, and that $T_b \ll T_f$. The case where T_b is comparable to T_f will be dealt with in a later section.

4. APPLICATION TO STORAGE RING RF SYSTEMS

4.1 Beam Loading in Storage Ring RF Systems

In high energy electron linacs, bunches are accelerated at the peak of the rf voltage wave in order to achieve the maximum possible energy gain. On the other hand, in an electron-positron storage ring it is necessary to operate off the crest of the accelerating voltage waveform in order to insure stability against phase oscillations, and to contain the energy fluctuations due to the quantum nature of synchrotron radiation. The rf cavities must as a consequence be detuned off resonance in order to minimize the reflected power and the required generator power.

Let us compute first the generator power required if the cavity shunt impedance R_a , the coupling coefficient β , the beam current I_0 , the cavity tuning angle ψ , the accelerating voltage $V_a = V_c \cos\phi$, and the desired synchronous phase angle ϕ are specified. From Fig. 3.13,

$$V_a = V_c \cos\phi = V_{gr} \cos\psi \cos(\theta + \psi) - V_{br} \cos^2\psi \quad (4.1a)$$

$$V_c \sin\phi = V_{gr} \cos\psi \sin(\theta + \psi) - V_{br} \cos\psi \sin\psi \quad (4.1b)$$

Eliminate $(\theta + \psi)$ from these two equations, and rewrite the result using Eqs. (3.35) to obtain

$$P_g = \frac{V_c^2}{R_a} \cdot \frac{(1+\beta)^2}{4\beta} \cdot \frac{1}{\cos^2\psi} \left\{ \left[\cos\phi + \frac{I_0 R_a}{V_c (1+\beta)} \cos^2\psi \right]^2 + \left[\sin\phi + \frac{I_0 R_a}{V_c (1+\beta)} \cos\psi \sin\psi \right]^2 \right\} \quad (4.2)$$

By choosing the tuning angle ψ correctly, we can make the cavity voltage look "real"; that is, just as is the case at resonance with no beam current, the net cavity voltage \tilde{V}_c must have the same phase as i_g . From Fig. 3.13 this implies that

$$\theta = \phi \quad (4.3)$$

Using the law of sines on the vector triangle in Fig. 3.13, we have

$$\frac{V_{br} \cos \psi}{V_c} = \frac{\sin(\phi - \theta - \psi)}{\sin \theta} = - \frac{\sin \psi}{\sin \phi}$$

$$\tan \phi = \frac{-I_o R_a}{V_c (1 + \beta)} \sin \phi \quad (4.4)$$

Problem 4.1: Show that the condition in Eq. (4.4) is also obtained by minimizing the generator power with respect to the tuning angle; that is, take $\partial P_g / \partial \psi = 0$ using Eq. (4.2).

Using Eq. (4.4) in Eq. (4.2), the generator power at optimum tuning is

$$P_g = \frac{(1 + \beta)^2}{4\beta} \cdot \frac{(V_c + V_{br} \cos \phi)^2}{R_a} \quad (4.5)$$

By differentiating this expression with respect to β (don't forget that V_{br} is also a function of β), the minimum generator power at $\beta = \beta_o$ is found to be

$$\beta_o = 1 + \frac{I_o R_a \cos \phi}{V_c} = 1 + \frac{P_b}{P_c} \quad (4.6a)$$

$$P_{go} = \frac{V_c^2 \beta_o}{R_a} = P_c \beta_o = P_c + P_b \quad (4.6b)$$

Here $P_b = I_o V_a = I_o V_c \cos \phi$ is the power transferred to the beam, and $P_c = V_c^2 / R_a$ is the power dissipated in the cavity walls. By conservation of energy, the reflected power is $P_r = P_g - P_c - P_b$. From the above expression for P_{go} , we see that the reflected power is zero when both ψ and β are set to their optimum values. At optimum coupling, Eq. (4.4) becomes

$$\tan \psi_o = - \frac{\beta_o - 1}{\beta_o + 1} \tan \phi \quad (4.7)$$

4.2 Phase Stability and Robinson Damping

As shown in E. Courant's lecture (see also Ref. 17, Ch.3), there is an effective restoring force in a storage ring for deviations in the energy or phase of a particle away from the synchronous energy or phase. A non-synchronous particle undergoes harmonic oscillations at the synchrotron frequency given by (for small amplitude oscillations)

$$\omega_s = \left[\frac{\alpha |dv_a/dt|}{V_o T_o} \right]^{1/2} \quad (4.8)$$

Here α is the momentum compaction factor, $U_0 = eV_0$ is the particle energy, T_0 is the revolution time and dV_a is the change in accelerating voltage per turn for a particle which is delayed by time dt per turn with respect to a synchronous particle. Above transition (always the case for high-energy electron storage rings), a particle with too much energy will follow a longer path compared to a synchronous particle, and will therefore return to a given point in the ring at a later time after one revolution. For stability, such a particle must gain less energy than a synchronous particle, or $dV_a/dt < 0$. In the absence of beam loading, this condition leads to

$$\frac{dV_a}{dt} = -\omega V_c \sin\phi < 0 \quad (4.9)$$

or $\phi > 0$ for stability. That is, the synchronous phase is on the time-falling side of the rf cavity voltage. However, at high currents where the beam-induced voltage component is large, the situation is more complicated. As the arrival time varies due to phase oscillations, the beam-induced voltage component moves with the bunch and hence cannot contribute to phase stability; only the generator voltage component can provide an effective restoring force against phase perturbations. From Fig. 3.13, recalling that the phasors rotate counterclockwise with angular velocity ω , the condition $dV_g/dt < 0$ implies

$$0 < (\theta + \psi) < \pi \quad (4.10)$$

An equivalent way to obtain this same condition is to compute $dV_g/d\theta$ directly from Eq. (4.1a), recognizing that t must be measured by an external clock which is independent of phase oscillations, and that the phase θ of the external rf generator \tilde{I}_g provides such a clock.

Problem 4.2: Draw a phasor diagram, similar to that in Fig. 3.13, with a large beam voltage component, with $\phi > 0$ and with $(\theta + \psi) < 0$. Show from the geometry of the figure that a positive Δt in arrival time results in a positive ΔV_a .

From Eq. (4.1b), using the condition in Eq. (4.10) that $\sin(\theta + \psi)$ is positive, we obtain

$$2V_c \sin\phi + V_{br} \sin 2\psi > 0 \quad (4.11)$$

This is the condition for the high-current limit on phase stability first derived by Robinson.¹⁸ Robinson's derivation involves setting up a set of linear equations in terms of perturbations to the variables of the system. He then applies Routh's criterion to the determinant of the coefficients to test for solutions which grow exponentially. However, it is well to remember that the result is completely equivalent to the simple condition in Eq. (4.10), which is almost immediately obvious from a carefully constructed phasor diagram.

If the cavity tuning is adjusted to make the beam-cavity impedance look "real" according to Eq. (4.4), then the condition for phase stability reduces to

$$V_{br} \cos\phi < V_c \quad (4.12)$$

Problem 4.3: If the cavity coupling is also optimized according to Eq. (4.6a), show that the condition in Eq. (4.12) is met for any value of beam current.

We next want to compute the damping time for phase oscillations (sometimes termed Robinson damping). A derivation in the frequency domain of the damping time is given in Ref. 19. Some interesting physics, however, is highlighted in a time-domain analysis.²⁰ Assume a beam current with phase modulation of the form $i_b = i_0 (1 + jA \cos\omega_s t)$ where $A \ll 1$. The response of a parallel resonant circuit to this driving current is

$$\tilde{V}_b(t) = R_0 \tilde{i}_0 \left\{ \frac{1}{1 + j\xi} + \frac{jA}{2} \left[\frac{e^{j\omega_s t}}{1 + j(\xi + \eta)} + \frac{e^{-j\omega_s t}}{1 + j(\xi - \eta)} \right] \right\} \quad (4.13)$$

where $\xi = -\tan\psi = (\omega - \omega_0)T_f$ and $\eta = \omega_s T_f$. The terms in $e^{\pm j\omega_s t}$ represent two counter-rotating vectors with origins at the tip of the steady-state beam loading vector $\tilde{V}_0 = R_0 \tilde{i}_0 \cos\psi e^{j\psi}$ where $R_0 i_0 = V_{br}$.

Problem 4.4: Show that the resultant of the two vectors is a vector whose tip moves on an ellipse in the complex plane with semi-major axes

$$a = (A/2) \left\{ [1 + (\xi + \eta)^2]^{-1/2} + [1 + (\xi - \eta)^2]^{-1/2} \right\} V_{br} \quad (4.14)$$

$$b = (A/2) \left\{ [1 + (\xi + \eta)^2]^{-1/2} - [1 + (\xi - \eta)^2]^{-1/2} \right\} V_{br}$$

Show further that the angle γ in Fig. 4.1 is given by $\gamma = \pi/2 + (\psi_+ + \psi_-)/2$, where $\tan\psi_+ = -(\xi + \eta)$ and $\tan\psi_- = -(\xi - \eta)$.

The phasor diagram in Fig. 4.1 illustrates the response $V_b(t)$ to a driving current resulting from a phase oscillation of the bunch center of charge. Note from the result of Problem 4.4 that as ω_s approaches zero the ellipse collapses to a line perpendicular to \tilde{V}_0 , while for $\omega_s T_f \gg 1$ it collapses to a point at the tip of \tilde{V}_0 .

The ellipse in Fig. 4.1 is quite suggestive. In analogy with similar diagrams in the force-displacement plane, or the pressure-volume plane in thermodynamics, we conjecture that the area of the ellipse is proportional to the power transfer to or from the oscillation. The conjugate coordinates in the present case are voltage and charge, given by $\delta V = (dV/d\phi)\delta\phi = (V_c \sin\phi)(A \cos\omega_s t)$ and

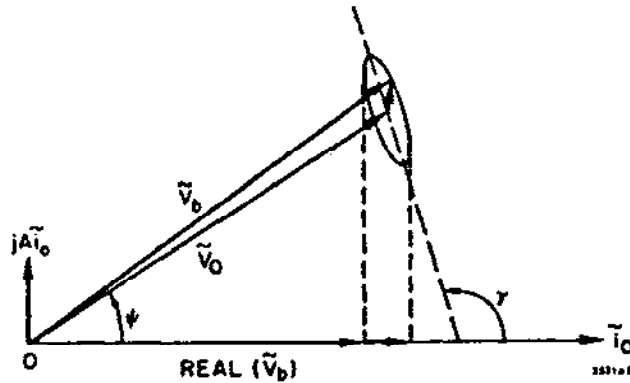


Fig. 4.1. Response of a resonant circuit to a phase-modulated driving current.

$\delta q = (\pi A i_0 / \omega_s) \cos \omega_s t$ (the relation between charge and current is given in Sec. 9.1). Assume small damping and integrate $\delta V dq = \delta V [d/dt(\delta q)] dt$ to obtain the energy in the oscillation,

$$\delta W = \frac{\pi A^2 i_0 V_c \sin \phi}{2 \omega_B}$$

Likewise, the average power transfer to the oscillation can be shown to be $\bar{P} = (i_0 / V_{br})$ times the area πab of the ellipse, where a and b are given by Eqs. (4.14).

Problem 4.5: Show that $\bar{P} = \pi i_0 ab / V_{br}$ using the following procedure. First, take the real part of Eq. (4.13) to find $\delta V_b(t)$. Then $P(t) = \delta q [d/dt(\delta V_b)]$ is the instantaneous power transfer during the oscillation. Average over one cycle of $\omega_s t$ to find \bar{P} .

The damping time is now obtained from

$$\frac{1}{\tau_d} = \frac{1}{2} \frac{\bar{P}}{\delta W} = \frac{V_{br} \omega_s}{V_c \sin \phi} \cdot \frac{-\xi \eta}{[1 + (\xi + \eta)^2][1 + (\xi - \eta)^2]} \quad (4.15)$$

Here a negative τ_d implies damping, and a positive τ_d growth of the phase oscillation. Whether there is growth or damping of the oscillation depends on the direction that the ellipse in Fig. 4.1 is followed with time, and in turn this depends on the sign of ξ . Positive ξ (or negative tuning angle) gives damping. The origin of the damping can be traced to the inertia of the stored energy in the rf cavities. Because of the finite filling time, the beam-induced voltage cannot follow changes in beam current instantaneously. A phase difference between the induced voltage and driving current appears, which in turn leads to an energy interchange between the oscillation and the cavity fields.

A somewhat different derivation of Eq. (4.15) is given in Ref. 20. It is also shown there that the synchrotron oscillation frequency is shifted as the beam loading increases. The limit of zero frequency is just the stability limit in Eq. (4.11). The condition $\xi > 0$ is the dynamic stability condition, also derived by Robinson.¹⁸ It is worth noting that the dynamic condition $\xi > 0$ and the "static" condition in Eq. (4.11) have analogs in any high frequency resonant system in which the stored energy is modulated by a low frequency parametric variation. For example, Ceperly²¹ has analyzed the electromechanical oscillations which result from the modulation of the resonant frequency of a cavity by mechanical vibrations. In this case, the mechanical oscillation is coupled to the rf stored energy through the force exerted by the rf fields on the cavity walls. Ceperly concludes that in this case the oscillations are antidamped for $\omega > \omega_0$, and that for $\omega < \omega_0$ a static instability occurs as the cavity fields increase and the modulation frequency goes to zero, corresponding to the limit in Eq. (4.11).

As a final comment, we note that Robinson damping operates only on the center of charge of the bunch as a whole. Radiation damping, on the other hand, acts on the incoherent synchrotron oscillations of the individual particles within the bunch.

5. TRAVELING-WAVE LINACS

5.1 Basic Principles

Consider a traveling wave for a given mode of propagation in a structure of arbitrary cross section with periodic length p along the z axis. By Floquet's theorem,²² at a given frequency the fields at one cross section differ from those one period away only by a complex constant. Thus

$$\vec{E}(r, \phi, z, t) = \vec{E}_p(r, \phi, z) e^{-\gamma z} e^{j\omega t}, \quad (5.1)$$

where $\gamma = j\beta_0 + \alpha$ is the propagation constant and $\vec{E}_p(r, \phi, z)$ is periodic in z with period p . Expanding $\vec{E}_p(r, \phi, z)$ in a Fourier series,

$$\vec{E}(r, \phi, z, t) = \sum_{n=-\infty}^{\infty} \vec{E}_n(r, \phi) e^{j(\omega t - \beta_n z)} e^{-\alpha z}, \quad (5.2)$$

where

$$\beta_n = \beta_0 + \frac{2\pi n}{p} \quad (5.3)$$

and

$$\vec{E}_n(r, \phi) = \frac{1}{p} \int_z^{z+p} \vec{E}_p(r, \phi, z) e^{j(2\pi n/p)z} dz \quad (5.4)$$

Thus the total traveling-wave field has been expanded in a series of space harmonics, each with its own propagation constant β_n and phase velocity $v_{pn} = \omega/\beta_n$, but with all space harmonics having the same group velocity $v_g = d\omega/d\beta$. These relationships are illustrated by the dispersion curve (also called a Brillouin diagram or $\omega - \beta$ diagram) in Fig. 5.1.

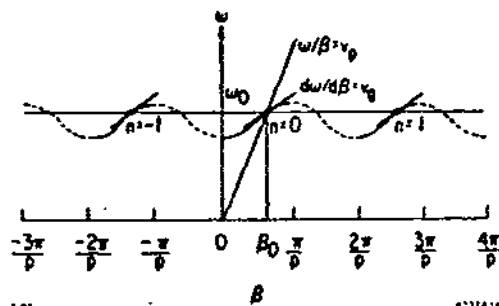


Fig. 5.1. Dispersion diagram for a periodic accelerating structure.

Consider the specific case of a cylindrically symmetric structure. In the neighborhood of the axis, the accelerating field component for a given propagating mode in a lossless structure has the form (see for example Ref. 23),

$$E_z(r, \phi, z, t) = \cos m\phi \sum_{n=-\infty}^{\infty} A_n J_m(X_n r) e^{j(\omega t - \beta_n z)} \quad (5.5)$$

where

$$X_n^2 = (\omega/c)^2 - \beta_n^2 \quad (5.6)$$

For a space harmonic component which is synchronous with a velocity of light particle, $\beta_n = \omega/c$ and $E_z \sim r^m$ in the region of the beam aperture.²³ Thus for a synchronous wave in the accelerating mode ($m = 0$), the accelerating field is independent of transverse position within the beam aperture. The structure design problem now consists of several parts. First, at the operating frequency the transverse dimensions of the structure are adjusted to obtain synchronism with the fundamental space harmonic component ($n = 0$). Second, the geometry of the structure is chosen, in so far as possible, to reduce the amplitudes of the non-synchronous space harmonic components. These components carry energy which can play no part in the acceleration of particles. Third, the geometry is adjusted to reduce the stored energy per unit length for a given synchronous accelerating field. Finally, the Q of the structure is maximized by choosing a structure material, usually copper, with good conductivity. As in the case of standing wave cavities, the Q of the structure does not depend very strongly on the shape of the individual periodic cells. The Q does,

however, increase if there are fewer periods per unit length (for example, fewer disks per wavelength in a disk-loaded structure). But then the amplitudes of the non-synchronous space harmonic components tend also to increase for a given synchronous component amplitude. These trade-offs are explored in detail in Ref. 2, Ch. B.1.1, for the case of the SLAC-type disk-loaded structure.

5.2 Structure Parameters

If $E_a = E_{zn}$ is the accelerating field for the synchronous traveling-wave space harmonic component and w the total stored energy per unit length in the propagating wave with power flow P , then the shunt impedance per unit length and the structure Q are defined by

$$r \equiv \frac{E_a^2}{|dP/dz|} \quad (5.7a)$$

$$Q \equiv \frac{\omega w}{|dP/dz|} \quad (5.7b)$$

$$\frac{r}{Q} = \frac{E_a^2}{\omega w} \quad (5.7c)$$

We can define an energy flow velocity by $v_E = P/w$. In Ref. 22, Sec. 1.5, it is proven that $v_E = v_g$, where v_g was defined as $d\omega/d\beta$. Thus, from the expression for Q ,

$$\frac{dP}{dz} = -\frac{\omega P}{v_g Q} = -2\alpha P \quad (5.8a)$$

$$\frac{dE_a}{dz} = -\alpha E_a \quad (5.8b)$$

$$\alpha = \frac{\omega}{2v_g Q} \quad (5.8c)$$

where α is the attenuation parameter per unit length. The relation between power flow and accelerating field is now obtained as

$$E_a^2 = r |dP/dz| = 2\alpha r P \quad (5.9a)$$

$$\alpha r = \frac{\omega r}{2v_g Q} \quad (5.9b)$$

A structure which has uniform parameters along its length is called a constant impedance structure.* For such a structure, Eqs. (5.8) can be integrated to yield

$$E_a = E_0 e^{-\alpha z} \quad (5.10a)$$

$$P = P_0 e^{-2\alpha z} \quad (5.10b)$$

where E_0 and P_0 are the accelerating field and power flow at the input to the structure. The field and power flow at the end of a structure of length L are then $E_L = E_0 e^{-\tau}$ and $P_L = P_0 e^{-2\tau}$, where

$$\tau = \alpha L = \frac{\omega L}{2v Q} \quad (5.11)$$

is the attenuation parameter for the structure.

Consider now an accelerating mode (no variation with azimuthal angle ϕ) propagating in a disk-loaded structure with disk hole radius a . In the disk hole region, both H_ϕ and E_r are proportional to r near the axis. Thus, if the disk opening is not too large, the power flow per unit area for a given stored energy per unit length is proportional to r^2 . Integrating from $r = a$, the total power flow, and thus the group velocity, will be proportional to a^4 . From Eq. (5.8c), it is therefore possible to change α over a wide range by varying the disk aperture over a relatively small range. Of course, the shunt impedance per unit length will also vary as the disk opening is changed, but its dependence on the disk hole radius is much weaker. From Eq. (5.9a) the possibility now exists, as the power flow along the structure decreases due to dissipation in the structure walls, to keep E_a constant by increasing $\alpha \sim 1/P$. This is the basis for the constant gradient structure.

Let us ignore the weak variation in r along the length of such a structure. Then from Eq. (5.7a) $dP/dz = \text{constant}$, or

$$P = P_0 - (P_0 - P_L)(z/L) \quad (5.12)$$

If the attenuation parameter τ is again defined from the expression $P_L = P_0 e^{-2\tau}$, the above relation gives

$$\frac{P}{P_0} = 1 - (z/L)(1 - e^{-2\tau}) \quad (5.13a)$$

* Note that $\alpha r = E_a^2/2P$ has dimensions of ohms/m². A closely related quantity used in microwave circuit theory, $E_n^2/(2B_n^2 P)$ is called the coupling impedance, or sometimes the interaction impedance for the n th space harmonic component.

$$\frac{dP}{dz} = - \frac{P_o - P_L}{L} = - \frac{P_o}{L} (1 - e^{-2\tau}) \quad (5.13b)$$

From Eqs. (5.8a), (5.8c), (5.13a) and (5.13b) the variation in group velocity with length required to produce a constant gradient is seen to be

$$v_g(z) = \frac{\omega L}{Q} \frac{[1 - (z/L)(1 - e^{-2\tau})]}{1 - e^{-2\tau}} \quad (5.14)$$

Problem 5.1: The filling time for a constant impedance (and hence constant group velocity) structure is simply $T_f = L/v_g$. By integrating $dt = dz/v_g$ from $z = 0$ to $z = L$ using Eq. (5.14), show that for a constant gradient structure

$$T_f = \tau \left(\frac{2Q}{\omega} \right) \quad (5.15)$$

From Eq. (5.11), note that this is exactly the same as the filling time for a constant impedance structure.

5.3 Energy Gain and Beam Loading

By integrating Eq. (5.10a) from $z = 0$ to $z = L$, and substituting for $E_o = (2\alpha r P_o)^{1/2}$ according to Eq. (5.9a), the unloaded energy gain of a constant impedance (CZ) accelerating section is calculated to be

$$CZ: V_o = (rLP_o)^{1/2} \left[(2/\tau)^{1/2} (1 - e^{-\tau}) \right] \quad (5.16)$$

The unloaded energy gain of a constant gradient (CG) section is, using Eq. (5.9a),

$$V_o = E_o L = (rLP_o)^{1/2} (2\alpha L)^{1/2} \quad (5.17)$$

Using Eqs. (5.8a) and (5.13b), the above expression becomes

$$CG: V_o = (rLP_o)^{1/2} (1 - e^{-2\tau})^{1/2} \quad (5.18)$$

As a function of τ , Eq. (5.16) has a broad maximum at $\tau = 1.26$ where $V_o/(rLP_o)^{1/2} = 0.90$. For the case of a constant gradient structure, V_o approaches $(rLP_o)^{1/2}$ for large τ .

We next compute the beam induced field in a traveling-wave structure, assuming that there is no input power from the rf generator. If there is a generator-produced field component, the net accelerating voltage is readily obtained using superposition. From conservation of energy, at any point in the structure

$$\frac{dP}{dz} = I_0 E_b - 2\alpha P \quad , \quad (5.19)$$

where E_b is the peak beam-induced field which opposes the motion of a beam of short bunches with dc current I_0 . Using $E_b^2 = 2\alpha r P$, this becomes

$$\frac{dE_b}{dz} = I_0 \alpha r - \alpha E_b \quad . \quad (5.20)$$

Now assume a constant impedance structure (α independent of z) and integrate to obtain

$$E_b(z) = I_0 r (1 - e^{-\alpha z}) \quad . \quad (5.21)$$

Integrate again to find the energy,

$$V_b = I_0 r L [1 - (1 - e^{-\tau})/\tau] \quad . \quad (5.22)$$

The derivation of the beam loading voltage for the case of a constant gradient structure is given in Appendix A. The result is

$$V_b = I_0 r L \left[\frac{1}{2} - \tau \frac{e^{-2\tau}}{(1 - e^{-2\tau})} \right] \quad (5.22b)$$

The results of Eq. (5.22) and Problem 5.2 can be used, together with superposition, to express the net voltage gain in a beam-loaded structure as

$$V = V_0 \cos\theta - m I_0$$

$$\text{CZ: } m = rL \left[1 - \frac{1 - e^{-\tau}}{\tau} \right] \quad (5.23a)$$

$$\text{CG: } m = rL \left[\frac{1}{2} - \frac{\tau e^{-2\tau}}{1 - e^{-2\tau}} \right] \quad (5.23b)$$

where V_0 is the unloaded energy gain given by Eqs. (5.16) and (5.18), and θ is phase of the current bunches with respect to the crest of the generator-produced wave. If the bunches are not short compared to the rf wave length, the energy gain is reduced by the same bunch form factor computed in Sec. 3.3.

In Fig. 5.2 the energy gain for constant gradient and constant impedance structures is plotted as a function of current for several values of τ . Note the linear load lines, similar to those in Fig. 3.10 for the case of a standing wave structure. Note, in addition, that τ and $1/\beta$ play similar roles in the two types of structures. This can also be seen from the expressions for the filling time,

$$T_f(SW) = \frac{2Q_0}{\omega_o(1+B)} \quad (5.24a)$$

$$T_f(TW) = \frac{2Q\tau}{\omega} \quad (5.24b)$$

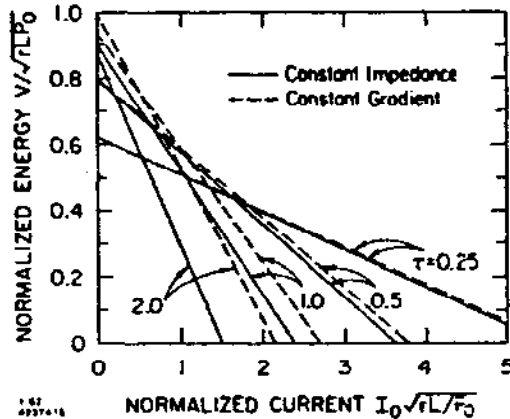


Fig. 5.2. Beam-loaded energy as a function of beam current for constant impedance and constant gradient structures for several values of the attenuation parameter τ .

Multiplying Eq. (5.23) by I_0 , the power transferred to the beam, and hence the conversion efficiency, is seen to be quadratic as a function of beam current. Recall that this was also the case for standing wave structures (see Fig. 3.11). The maximum efficiency is reached when the beam energy is reduced to one-half of its unloaded value at $I_0 = V_0/2m$. The maximum conversion efficiency is then

$$\eta_{max} = \frac{V_0^2}{4 m P_0} \quad (5.25)$$

As an example, η_{max} at $\tau = 1$ is 63% for a constant gradient structure and 54% for a constant impedance structure. These efficiencies increase to 76% and 73% respectively at $\tau = 0.5$, and both increase toward 100% as τ approaches zero according to $\eta_{max} \approx (1 - 2\tau/3)$.

The power flowing into the output termination of a beam-loaded traveling-wave section can be computed by first finding the net field at the load. For example, using Eqs. (5.21), (5.10a) and (5.9a) in the case of a constant impedance structure,

$$E_L = E_0 e^{-\tau} - I_0 r (1 - e^{-\tau}) \quad (5.26)$$

$$P_L = E_L^2 L / 2\tau r$$

The power dissipated in the structure is then obtained as $P_s = P_0 - P_L = I_0 V$.

5.4 Non-Synchronous Operation

If a traveling-wave structure is operated at a frequency different than the synchronous frequency, the bunches will slip in phase with respect to the traveling wave. The total phase slip in length

for an electron with velocity $v_e \approx c$ is described by the parameter

$$\delta = \omega \left(\frac{L}{v_p} - \frac{L}{v_e} \right) \approx \beta_o L \left(1 - \frac{v_p}{c} \right) . \quad (5.27)$$

In a constant gradient structure (or in a constant impedance structure for small τ) without beam loading we expect

$$v = v_o \left[\frac{\sin(\delta/2)}{(\delta/2)} \right] \approx v_o \left(1 - \frac{\delta^2}{24} \right) \quad (5.28)$$

for $\delta \ll 1$. Recall that for a standing-wave cavity,

$$v = v_o \cos\psi \approx v_o \left(1 - \frac{\psi^2}{2} \right) . \quad (5.29)$$

Thus the phase-slip parameter plays a similar role for a traveling-wave structure as the tuning angle does for a standing-wave cavity. This correspondence is evident also from the relation between ψ and δ and the filling times for standing-wave and traveling-wave structures. For a frequency deviation $\Delta\omega = \omega - \omega_o$ and using $\Delta\beta \approx \Delta\omega/v_g$,

$$\begin{aligned} \psi &= \tan^{-1} \left(\frac{2QL}{\omega_o} \Delta\omega \right) \approx T_f(\text{SW}) \cdot \Delta\omega \\ \delta &= L(\beta_o - \beta) = L \Delta\beta \approx T_f(\text{TW}) \cdot \Delta\omega \end{aligned} \quad (5.30)$$

In both cases, the sensitivity to tuning errors is seen to be proportional to the filling time.

A detailed discussion of non-synchronous beam loading in constant impedance structures is given in Ref. 24 and in Appendix B.

6. SINGLE-BUNCH BEAM LOADING

6.1 The Fundamental Theorem of Beam Loading

Consider a point charge crossing a cavity initially empty of energy. After the charge has passed out of the cavity, a beam-induced voltage V_{bn} remains in each mode. What fraction of V_{bn} does the charge itself see? Since the induced voltage for mode n starts at zero as the charge enters the cavity, and ends up at V_{bn} as the charge exits from the cavity, the most naive assumption is to take the average, or $1/2 V_{bn}$, as the effective fraction of the induced voltage acting on the charge. In this section we prove that this factor of one-half is indeed exact for any cavity. The fact that a charge "sees" exactly one-half of its own beam-induced voltage we will call the *fundamental theorem of beam loading*. The theorem provides the key which relates the energy loss by a charge crossing a cavity or passing through a structure to the electromagnetic properties of modes

in the cavity or structure computed in the absence of any charge. By superposition, the beam-induced voltage in a cavity is the same whether or not a generator voltage component is present. Thus the theorem is also basic to the computation of the effective voltage acting on a bunch when both a generator voltage and a beam-induced voltage are present. Following is one of several possible proofs of the theorem.

Let a charge pass through a cavity in which the stored energy is related to the cavity voltage in a given mode by

$$W = \alpha V^2 \quad (6.1)$$

Assume that a fraction f of the beam-induced voltage V_b acts on the particle, or $V_e = fV_b$ where V_e is the effective voltage seen by the charge. Assume further that the beam-induced voltage is not necessarily at such a phase as to maximally oppose the motion of the charge; that is, assume it might lie at an angle ϵ with respect to V_e . Now let the charge be bent back around in a lossless manner, for example by magnetic fields, such that it passes through the cavity a second time. Let the time for the charge to traverse the external path be any multiple n of the rf period, plus a residual time θ/ω_0 where θ is an arbitrary angle and ω_0 is the resonant frequency of the mode. When the particle crosses the cavity reference plane a second time, we have the phasor addition of voltages shown in Fig. 6.1.

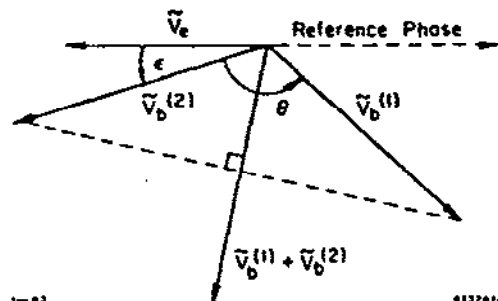


Fig. 6.1. Diagram showing addition of beam-induced voltages for two passes by the same charge through a cavity.

Here $V_b(2)$ is the voltage induced the second pass by the charge, while the voltage induced on the first pass, $V_b(1)$, has rotated with respect to $V_b(2)$ by an angle $2\pi n + \theta$. We can assume the cavity losses are very small so that $V_b(2) = V_b(1)$. Thus the net energy stored in the cavity is

$$W_c = \alpha \left(2 V_b \cos \frac{\theta}{2} \right)^2 \quad (6.2)$$

$$= 2\alpha V_b^2 (1 + \cos\theta)$$

On the other hand, the energy lost by the particle on the two passes is

$$\Delta U = 2qV_e + qV_b \cos(\epsilon + \theta) \quad (6.3)$$

That is, on the first pass the charge experiences a retarding voltage V_e , while on the second pass it sees the sum of V_e plus the component of $V_b(1)$ which lies along the negative real axis in the phasor diagram. By conservation of energy W_c and ΔU must be equal. Letting $V_e = fV_b$ and equating Eqs. (6.2) and (6.3) we have

$$2(qf - \alpha V_b) + (q \cos \epsilon - 2\alpha V_b) \cos \theta - (q \sin \epsilon) \sin \theta = 0 .$$

The left-hand side can only vanish for arbitrary θ if

$$\sin \epsilon = 0, \quad \epsilon = 0 \quad (6.4a)$$

$$V_b = q/2\alpha \quad (6.4b)$$

$$f = \alpha V_b / q = 1/2 \quad (6.4c)$$

Eq. (6.4a) expresses the fact that the beam-induced voltage must have a phase such as to maximally oppose the motion of the inducing charge. (Is $\epsilon = \pi$ a valid solution to Eq. (6.4a)?) Equation (6.4c) tells us that the charge sees exactly one-half of its own beam induced field. Combining Eqs. (6.1) and (6.4b), we obtain

$$W = \alpha V_b^2 = \frac{q^2}{4\alpha} \equiv kq^2 \quad (6.5)$$

for the energy left behind in a cavity by a charge q . The quantity k is called the loss parameter, and, of course, each resonant mode has its own value of k . From Eqs. (6.5) and (6.1) we have

$$\alpha = \frac{1}{4k} \quad (6.6a)$$

$$k = \frac{V_b^2}{4W} \quad (6.6b)$$

Further, from Eqs. (6.4b) and (6.6a),

$$V_b = 2kq \quad (6.7a)$$

$$V_e = \frac{V_b}{2} = kq \quad (6.7b)$$

Thus the loss parameter k relates the beam-induced voltage to the charge, by Eq. (6.7a), and the energy loss by a charge passing through a cavity initially empty of energy, by Eq. (6.5). It is important to note that superposition applies and Eqs. (6.7) are valid even if a voltage is already present in the cavity before the charge arrives. We can therefore construct the basic phasor diagram in Fig. 6.2 for single-bunch beam loading for the accelerating mode ($k = k_0$, $V_b = V_{b0}$), or for any mode with an externally applied generator voltage. Here $\tilde{V}_e = -k_0 q$ is the effective beam loading voltage seen by the charge. The reference phase is taken in the direction $-\tilde{V}_e$. Thus the net accelerating voltage acting on the charge is

$$V_a = V_c \cos \phi = V_g \cos \theta_g - k_0 q \quad (6.8)$$

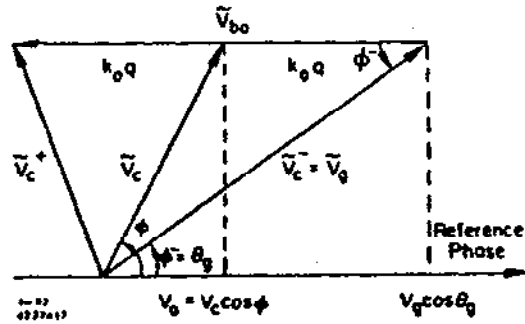


Fig. 6.2. Phasor diagram showing the net single-bunch energy gain for a cavity driven by an external rf source.

where $\phi^- = \theta_g$ is the phase of the generator voltage component just before the charge crosses the cavity reference plane.

Problem 6.1: Prove that relations (6.4), (6.6) and (6.7) are also valid when a generator voltage component is present. Using Fig. 6.2, compute the decrease in cavity stored energy, $\Delta W = \alpha[(V_c^-)^2 - (V_c^+)^2]$. Using conservation of energy, equate this to the energy gained by charge q . Write the result in the form $V_g = f_1(V_b)/f_2(V_b)$ where both f_1 and f_2 must vanish, since V_g cannot depend on V_b .

As a final comment, note that the parameter k_n describes the single-bunch beam loading properties of the n th cavity mode, and that it can be computed in terms of the charge-free properties of the cavity from Eq. (6.6b). As described in Sec. 3.4, the programs LAL and SUPERFISH⁶ compute the quantity $R_a/Q = V_a^2/\omega W$. Then from Eq. (6

$$k = \frac{\omega}{4} (R_a/Q) \quad . \quad (6.9)$$

6.2 Higher-Order Cavity Modes and the Loss Impedance

Consider the energy lost by a charge to all modes in an rf accelerating cavity, assuming the cavity is initially empty of stored energy before the arrival of the charge. Let ΔU_0 be the energy lost to the fundamental (accelerating) mode, and

$$\Delta U_t = B \Delta U_0 \quad (6.10)$$

be the total energy lost to all modes, where B is called the beam loading enhancement factor. The energy lost to higher-order cavity modes only is

$$\Delta U_{hm} = (B - 1) \Delta U_0 \quad . \quad (6.11)$$

After the charge has exited from the cavity, a beam-induced voltage V_{bo} and corresponding stored energy $\Delta U_o = \alpha_o V_{bo}^2$ remain in the fundamental mode. Then From Eqs. (6.11), (6.6a) and (6.7a),

$$\Delta U_{hm} = \alpha_o (B-1) V_{bo}^2 = (B-1) k_o q^2 \quad (6.12)$$

As discussed earlier, $V_{bo} = 2k_o q$ is a voltage which, by superposition, is the same whether or not there is energy stored in the fundamental mode before the arrival of the charge. Equation (6.12) therefore is valid also when the fundamental mode is driven by an external generator.

Consider now a linac or storage ring with equal bunches of charge q spaced apart in time by T_b . If the fields in each cavity mode decay away completely between bunches ($T_b \gg T_{fn}$ for all modes), and using also $q = I_o T_b$ where I_o is the average current, Eq. (6.12) gives

$$P_{hm} = \frac{1}{T_b} \Delta U_{hm} = I_o^2 Z_{hm} = I_o V_{hm} \quad (6.13a)$$

$$V_{hm} = I_o Z_{hm} \quad (6.13b)$$

$$Z_{hm} \equiv (B-1) k_o T_b = T_b \sum_{n>0} k_n \quad (6.13c)$$

In a storage ring the presence of higher-order cavity modes means that, in addition to the synchrotron radiation loss per turn V_s , the rf system must supply an accelerating voltage V_{hm} . There are also losses to other vacuum chamber components outside the rf system. If the sum of all the loss parameters for these components is k_{vc} , and if it is again assumed that the induced fields decay away between bunches, then

$$\begin{aligned} P_{vc} &= I_o^2 Z_{vc} \\ V_{vc} &= I_o Z_{vc} \\ Z_{vc} &= k_{vc} T_b \end{aligned} \quad (6.14)$$

Thus the total accelerating voltage that must be supplied by the rf system to each beam in a storage ring is

$$V_a = V_s + V_{hm} + V_{vc} \quad (6.15)$$

If the beam induced fields do not decay away between bunches for a particular mode, the situation is more complicated. The resonance function, described in Sec. 6.5, is then needed to compute the voltage lost to that mode.

For simplicity, the expressions in this and the preceding section have been written assuming a point bunch. For a bunch of non-zero length, the bunch form factor must be taken into account. For a Gaussian bunch, the loss parameter for each mode must be multiplied by $e^{-\frac{1}{2} \frac{\sigma_z^2}{\lambda^2}}$ (see Sec. 9.4).

6.3 Efficiency for Energy Extraction from a Cavity

In a linac or storage ring rf system, the beam takes energy from the driven fundamental mode, but dumps some of it back into the higher cavity modes. It is of interest to compute the net energy extracted from the cavity. If we apply the law of cosines to the vector triangle $(\tilde{V}_c^+, \tilde{V}_c^-, \tilde{V}_{bo})$ in Fig. 6.2,

$$(\tilde{V}_c^+)^2 = (\tilde{V}_c^-)^2 + V_{bo}^2 - 2\tilde{V}_c^- V_{bo} \cos\phi^- \quad (6.16)$$

By conservation of energy, the energy extracted from the accelerating mode is $\Delta U_o = \alpha_o [(\tilde{V}_c^-)^2 - (\tilde{V}_c^+)^2]$. Using Eq. (6.16),

$$\Delta U_o = \alpha_o (2\tilde{V}_c^- V_{bo} \cos\phi^- - V_{bo}^2) \quad (6.17)$$

To obtain the net energy extracted from the cavity, we subtract off the energy put back into higher-order modes, as given by Eq. (6.12), to obtain

$$\Delta U_{net} = \Delta U_o - \Delta U_{hm} = \alpha_o (2\tilde{V}_c^- V_{bo} \cos\phi^- - B V_{bo}^2) \quad (6.18)$$

The efficiency for net energy extraction is now

$$\eta = \frac{\Delta U_{net}}{\alpha_o (\tilde{V}_c^-)^2} = 2 \left(\frac{V_{bo}}{\tilde{V}_c^-} \right) \cos\phi^- - B \left(\frac{V_{bo}}{\tilde{V}_c^-} \right)^2 \quad (6.19)$$

The maximum efficiency as a function of V_{bo} for a given initial stored energy is readily obtained to be

$$\eta_{max} = \frac{\cos^2 \phi^-}{B} \quad (6.20)$$

at a beam-induced voltage

$$V_{bo} = \frac{\tilde{V}_c^- \cos\phi^-}{B} \quad (6.21)$$

Note that angle ϕ^- in Eq. (6.14) is not the synchronous phase angle for a storage ring. It is the phase angle of the cavity voltage just before the arrival of the bunch. From Fig. 6.2 it is related to the synchronous phase angle by

$$\tan\phi^- = \frac{\tan\phi}{1 + k_0 q/V_a} \quad (6.22)$$

Problem 6.2: A storage ring is often operated with two counter-circulating beams of opposite charge and equal intensity. The rf cavities are located so that the fields induced in the fundamental mode by the q^+ and q^- charges are coherent; that is, the cavities are located at distances from the interaction point which are integral multiples of a half-wavelength at the accelerating mode frequency. On the other hand, it is reasonable to assume that the fields induced in the higher cavity modes are, on the average, incoherent for the two beams (see discussion in Sec. 6.5). Show that for this case the maximum efficiency for energy extraction is

$$\eta_{\max} = \frac{\cos^2\phi^-}{(B+1)/2} \quad (6.23)$$

6.4 Beam Loading by a Bunch Train with $T_b \sim T_f$

We next calculate the build-up of the beam-induced voltage when bunches pass repetitively through a cavity, as in the rf system of a storage ring or for a train of equally-spaced bunches in a linac. A cavity filling time is assumed which is not necessarily short compared to the bunch spacing. The situation is illustrated graphically in Fig. 6.3. Here \tilde{V}_{b0} is the single-pass beam-induced voltage, $e^{-\tau}$ gives the decay of the cavity fields during one turn, δ is the net phase shift per turn (subtracting off multiples of 2π) and \tilde{V}_b^- and \tilde{V}_b^+ are the cavity of voltages for $t =$ just before and just after the passage of a bunch. The decay parameter τ and phase angle δ can be written

$$\tau = \frac{T_b}{T_f} \quad (6.24a)$$

$$\delta = T_b \omega_0 - 2\pi h_b \quad (6.24b)$$

$$= T_b (\omega_0 - \omega)$$

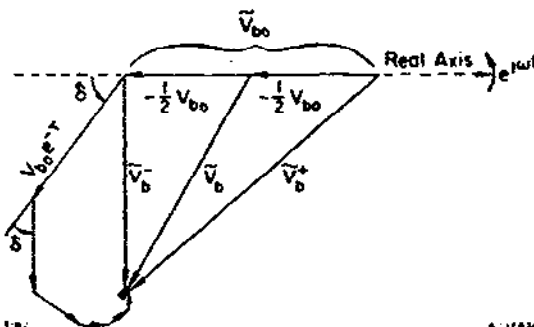


Fig. 6.3. Phasor diagram showing the buildup of the beam-induced voltage by a train of bunches of equal charge.

Here ω_0 is the resonant frequency of the cavity and h_b , an integer, is the harmonic number for a single-bunch machine, or the number of rf wavelengths between bunches for a linac or for a ring with more than one bunch.

In constructing Fig. 6.3, we again consider a reference frame which is rotating at the angular frequency ω of the external rf generator. It is natural to use the external generator as the basic clock for describing field variations in the cavity, since the spacing of bunches in a storage ring is determined by the driving frequency of the generator and not by the cavity resonant frequency.

The final ($t \rightarrow \infty$) voltage just after a bunch passage is now readily obtained as the sum of the geometric series

$$\begin{aligned} \tilde{V}_b^+ &= \tilde{V}_{bo} (1 + e^{-\tau} e^{j\delta} + e^{-2\tau} e^{j2\delta} + \dots) \\ \frac{\tilde{V}_b^+}{\tilde{V}_{bo}} &= \frac{1}{1 - e^{-\tau} e^{j\delta}} \end{aligned} \quad (6.25e)$$

To obtain the effective beam-loading field \tilde{V}_b in the limit $t \rightarrow \infty$, we take the field \tilde{V}_b^+ induced by all the previous bunch passages at a time just before the arrival of a bunch at the cavity reference plane and add to it a phasor $\tilde{V}_e = -1/2 V_{bo}$ to account for the effective self-field seen by the bunch in question to obtain

$$\tilde{V}_b = \tilde{V}_b^+ - \frac{1}{2} V_{bo} = \tilde{V}_b^+ + \frac{1}{2} V_{bo} \quad (6.25f)$$

Using this expression together with Eq. (6.25a) and the fact that $\tilde{V}_{bo} = -V_{bo}$,

$$\frac{\tilde{V}_b}{(-V_{bo})} = \frac{1}{1 - e^{-\tau} e^{j\delta}} - \frac{1}{2} = F_R(\tau, \delta) + jF_I(\tau, \delta) \quad (6.26a)$$

$$F_R(\tau, \delta) = \frac{1 - e^{-2\tau}}{2(1 - 2e^{-\tau} \cos\delta + e^{-2\tau})} \quad (6.26b)$$

$$F_I(\tau, \delta) = \frac{2e^{-\tau} \sin\delta}{2(1 - 2e^{-\tau} \cos\delta + e^{-2\tau})} \quad (6.26c)$$

These expressions give the real and imaginary parts of the enhancement of the single-bunch beam loading voltage due to resonant build-up.

The quantities τ , δ and V_{bo} in Eqs. (6.26) can be expressed in terms of more usual cavity parameters. The voltage decay parameter per turn is

$$\tau = \tau_o (1 + \beta), \quad \tau_o = T_b / T_{fo} \quad (6.27)$$

where $T_{fo} = 2Q_o / \omega_o$. From the definition of the tuning angle, $\tan\psi = (\omega_o - \omega) / \omega_o = T_f(\omega_o - \omega)$ and Eq. (6.24b), we have

$$\delta = \tau \tan\psi \quad (6.28)$$

The single-bunch beam loading voltage can also be written as

$$V_{bo} = 2k_o q = \frac{\omega_o}{2} \left(\frac{R_a}{Q} \right) q = \frac{I_o R_a}{1+\beta} \tau = I_o R_a \tau_o \quad (6.29)$$

where I_o is dc current (assuming short bunches) or the total circulating current for both beams in a storage ring. Equation (6.26a) can now be written in the form

$$\tilde{V}_b = -I_o R_a \tau_o [F_R(\tau_o, \beta, \psi) + jF_I(\tau_o, \beta, \psi)] \quad (6.30)$$

In a storage ring the desired net cavity voltage, including the effect of beam loading, is usually specified; that is, a certain accelerating voltage $V_c \cos\phi$ and synchronous phase angle ϕ are required. If the beam current and cavity parameters are specified, then the generator voltage can be obtained from the phasor relation

$$\tilde{V}_g = \tilde{V}_c - \tilde{V}_b \quad (6.31)$$

This is illustrated in Fig. 6.4, in which a constant generator voltage has been added to the beam-induced voltages shown in Fig. 6.3.

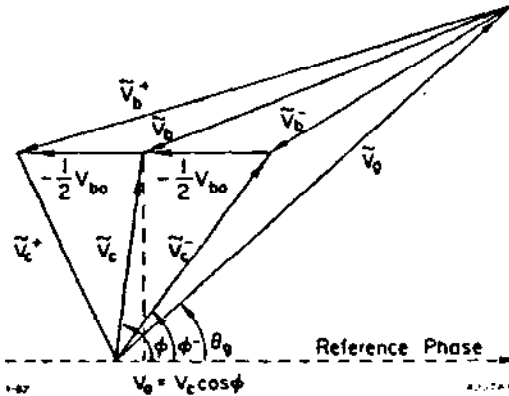


Fig. 6.4. Vector sum of voltages in a beam-loaded cavity driven by an external generator.

Let us now compute the required generator power for a linac or storage ring rf system with beam loading under the condition $T_b \sim I_f$. Taking the real and imaginary components of the preceding phasor relation and using also the notation in Fig. 6.4, together with Eq. (6.26a), we obtain

$$V_g \cos \theta_g = V_c \cos \phi + V_{bo} F_R(\tau, \delta) \quad (6.32a)$$

$$V_g \sin \theta_g = V_c \sin \phi + V_{bo} F_I(\tau, \delta) \quad (6.32b)$$

Squaring and adding these two expressions to eliminate θ_g , then using Eqs. (3.35a) and (3.42a) to express V_g^2 in terms of P_g , we have

$$P_g = \frac{V_c^2}{R_a \cos^2 \psi} \cdot \frac{(1+\beta)^2}{4\beta} \cdot \left\{ \left[\cos \phi + \frac{I_o R_a \tau_o}{V_c} F_R(\tau_o, \beta, \psi) \right]^2 + \left[\sin \phi + \frac{I_o R_a \tau_o}{V_c} F_I(\tau_o, \beta, \psi) \right]^2 \right\} \quad (6.33)$$

Problem 6.3: Show that, in the limit $\tau_o \rightarrow 0$, the result in Eq. (6.33) approaches that in Eq. (4.2).

The phase angle of the generator voltage is obtained by dividing Eq. (6.32b) by Eq. (6.32a),

$$\tan \theta_g = \frac{V_c \sin \phi + V_{bo} F_I(\tau_o, \beta, \psi)}{V_c \cos \phi + V_{bo} F_R(\tau_o, \beta, \psi)} \quad (6.34)$$

For a given τ_o , the generator power in Eq. (6.33) can be minimized by varying β and ψ , although it is not possible to obtain simple analytic expressions as was the case for the minimization of Eq. (4.2) for $\tau \ll 1$. However, the minimum value of Eq. (6.33), and the corresponding values of β and ψ , are easily found numerically. It is found that the transient nature of the beam loading between bunches increases the minimum generator power by a few percent for typical cavity parameters for τ_o up to about 0.5. For $\tau_o > 1$ the generator power increases rapidly, and for large τ_o , where the time between bunches becomes large compared to the cavity filling time, it is clear that some sort of pulsed rf system is desirable. In such a system, power is applied to the cavities for about a filling time preceding the arrival of the bunch. For most of the period between bunches there is no stored energy in the rf cavities and hence no power dissipation. A discussion of pulsed rf systems for large storage rings is given in Ref. 25.

6.5 The Resonance Function

From Fig. 6.4 and Eq. (6.32a), the net accelerating voltage acting on a charge passing through an rf cavity is

$$V_a = V_c \cos \phi = V_g \cos \theta_g - k_o q [2F_R(\tau, \delta)] \quad (6.35)$$

Since k_{0q} is the effective beam loading voltage seen by a charge making a single passage through a cavity initially empty of energy, the factor $2F_R(\tau, \delta)$ takes into account the resonant build-up of fields due to successive bunch passages, either for a storage ring or for a train of bunches in a linac. For large τ , $2F_R$ is seen to approach unity, as expected. For small τ , Eq. (6.35) can be rewritten in a form which is more natural for a nearly continuous beam,

$$V_a = V_g \cos \theta_g - \frac{1}{1+\beta} \frac{R}{\omega} [\tau F_R(\tau, \delta)]$$

In Problem 6.3 it was shown that τF_R approaches $\cos^2 \psi$ in the limit $\tau \rightarrow 0$. This can be compared with the result of Eq. (4.1a), noting that $\theta_g = \theta + \psi$ (see Fig. 3.13).

In Fig. 6.5, the resonance function

$$2F_R(\tau, \delta) = \frac{1 - e^{-2\tau}}{1 - 2e^{-\tau} \cos \delta + e^{-2\tau}}$$

is plotted as a function of δ for two values of τ . Note that the maximum amplitude at resonance ($\delta = 0$) is given by

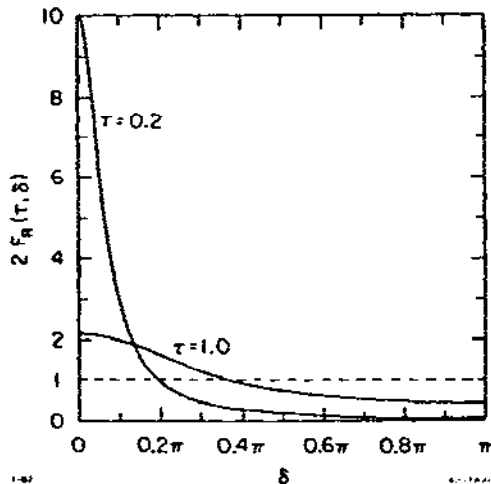


Fig. 6.5. The resonance function $2F_R(\tau, \delta)$ as δ for two values of the decay parameter τ .

$$2F_R(\tau, 0) = \frac{1 + e^{-\tau}}{1 - e^{-\tau}} \quad (6.37)$$

$$2F_R(\tau, 0) \approx \frac{2}{\tau} \quad \tau \ll 1$$

At anti-resonance ($\delta = \pi$),

$$2F_R(\tau, \pi) = \frac{1 - e^{-\tau}}{1 + e^{-\tau}} \quad (6.38)$$

$$2F_R(\tau, \pi) \approx \frac{\tau}{2} \quad \tau \ll 1$$

The phase angle which divides resonance and anti-resonance, that is, the value of δ at which $2F_R(\tau, \delta_1) = 1$, is seen to be

$$\cos \delta_1 = e^{-\tau} \quad (6.39)$$

$$\delta_1 \approx (2\tau)^{1/2} \quad \tau \ll 1$$

An important property of the resonance function has been pointed out by Sands.²⁶ The average value of the resonance function is computed to be

$$\langle 2F_R \rangle = \frac{1}{\pi} \int_0^{\pi} 2F_R(\tau, \delta) d\delta = 1 \quad (6.40)$$

Thus, if the phase shift δ is chosen at random, the expectation value of the resonance function is unity. For small τ , the maximum value of the resonance function is indeed very large, but the chance of finding $\delta < \delta_1$ is very small. In a storage ring, therefore, since the exact frequencies of the higher modes and hence the values of δ are never precisely known, it is reasonable to compute the higher-mode losses in the single-pass limit as $\Delta U_n = k_n q^2$, even though the factors I_b/I_{fn} might be small compared to unity. On the average, the single-pass limit ($2F_R = 1$) will be correct, although in any particular machine there is always the possibility of hitting a high resonance with a consequent large enhancement of the beam loading voltage for that particular mode.

The condition (6.40) also has an important implication for the higher-mode losses in the rf cavities in a storage ring with two counter-rotating beams. The cavities are placed an appropriate distance from the interaction points so that the q^+ and q^- bunches pass through the cavities (in opposite directions) with a time difference that is an integral multiple of the rf period for the accelerating mode. The higher-mode frequencies, however, are in general not rational multiples of the fundamental mode frequency. Thus the angle δ_n for the passage time between the counter-circulating bunches is effectively random for any particular higher-order cavity mode. In other words, the voltages induced in the higher-order modes do not coherently. The induced voltage and power loss for the higher-order modes can therefore be computed for each beam separately, ignoring the presence of the other beam. Thus the total power lost to both higher-order cavity modes and to parasitic modes in the vacuum chamber components if there are two beams with circulating currents I_0^+ and I_0^- is

$$P_{hm} + P_{vc} = \left[(I_0^+)^2 + (I_0^-)^2 \right] (Z_{hm} + Z_{vc}) \quad (6.4)$$

where Z_{hm} and Z_{vc} are defined by Eqs. (6.13c) and (6.14) and we assume that the k_n 's contain the factor $e^{-\omega_n^2 \sigma_z^2}$. However, in computing the required generator power for the fundamental accelerating mode using Eq. (6.33), I_0 must be replaced by $(I_0^+ + I_0^-)$.

7. TRANSIENT BEAM LOADING

7.1 Transient Response of a Resonant Cavity

We want first to compute the response of a resonant cavity to a step change in driving voltage. This result will be used to find the transient variation in the voltage and reflected power between bunches for a cavity loaded by a periodic bunch train. The response of a resonant circuit to a step change in driving voltage can, of course,

be obtained by applying standard mathematical techniques to solve an appropriate differential equation. Here, however, let us use our phasor approach to find the answer in a very simple way.

Consider first an undriven cavity with resonant frequency ω_0 and damping time T_f . Suppose the cavity is initially charged to voltage $V_d(0)$, and that this voltage then decays as e^{-t/T_f} for $t > 0$ while viewed in a reference frame rotating at angular frequency ω (the rf driving frequency). The time variation of the cavity voltage is

$$\tilde{V}_d(t) = \tilde{V}_d(0) e^{-t/T_f} e^{jt\Delta\omega} \quad (7.1)$$

where $\Delta\omega = \omega_0 - \omega$. The time variation of $V_d(t)$ [the reason for the subscript will become clear shortly] is illustrated in Fig. 7.1.

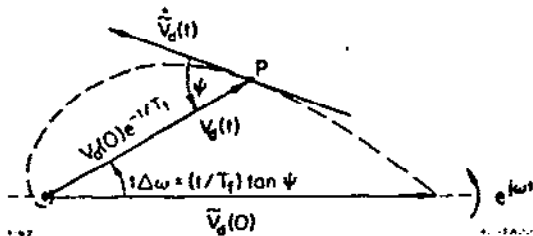


Fig. 7.1. Discharge of a cavity resonant at frequency ω_0 viewed in a coordinate frame rotating at frequency ω .

plus an undriven discharge toward this voltage, which occurs at the natural cavity resonant frequency ω_0 . Thus, by adding a final steady-state vector $\tilde{V}(\infty)$ to the diagram in Fig. 7.1, we obtain the general transient variation of the cavity voltage $\tilde{V}(t)$, as shown in Fig. 7.2. Equation (7.1) now gives the time variation of the "difference vector," $V_d(t)$, where

$$\tilde{V}_d(t) = \tilde{V}(t) - \tilde{V}(\infty) \quad (7.2a)$$

$$\tilde{V}_d(0) = \tilde{V}(0) - \tilde{V}(\infty) \quad (7.2b)$$

Using the definition of the tuning angle, $\tan\psi = T_f\Delta\omega$, Eq. (7.1) becomes

$$\tilde{V}_d(t) = \tilde{V}_d(0) e^{-(t/T_f)(1 - j \tan\psi)} \quad (7.3)$$

Substituting for $\tilde{V}_d(t)$ and $\tilde{V}_d(0)$ in this expression using Eqs. (7.2), we obtain

The relevance of this seemingly simple physical picture may not be obvious at first glance. In a storage ring or linac we are dealing with driven rf cavities, and the bunch repetition frequency is also a sub-harmonic of the driving frequency ω . Thus all steady-state driven voltages are phasors viewed in a coordinate system rotating at the driving frequency ω . Transient variations can, however, be viewed as the superposition of a final steady-state voltage

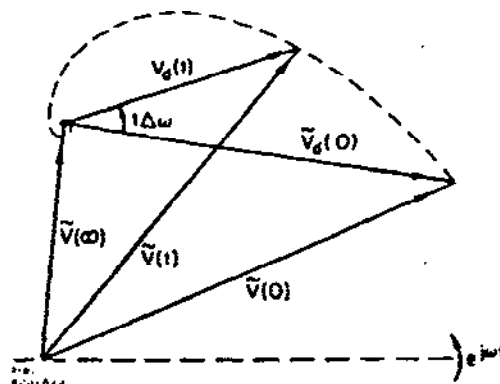


Fig. 7.2. Transient response of a resonant cavity to a step change in driving voltage $\Delta\tilde{V} = -\tilde{V}_d(0)$ applied at $t = 0$.

$$\tilde{V}(t) = \tilde{V}(\infty) + [\tilde{V}(0) - \tilde{V}(\infty)] e^{-(t/T_f)(1-j \tan\psi)} \quad (7.4)$$

This expression can also be considered as giving the transient response of a resonant cavity to a step change in driving voltage $\Delta\tilde{V} = \tilde{V}(\infty) - \tilde{V}(0) = -\tilde{V}_d(0)$, applied at time $t = 0$.

It is interesting to show that Eq. (7.3) represents an equiangular spiral; that is, the tangent to the curve at any point P in Fig. 7.1 makes a constant angle with respect to the difference vector joining point P to the origin. The derivative $\dot{\tilde{V}} = d\tilde{V}/dt$ is tangent to the curve $\tilde{V}(t)$. From Eq. (7.3),

$$\dot{\tilde{V}}_d(t) = -\tilde{V}_d(t)(1-j \tan\psi)/T_f$$

Since

$$e^{-j\psi} = (1-j \tan\psi) \cos\psi$$

we have

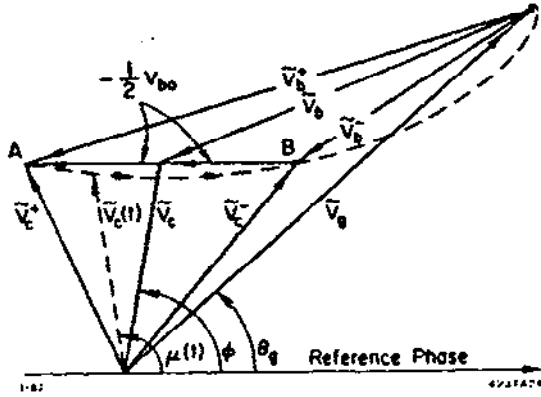
$$\dot{\tilde{V}}_d(t) = -\tilde{V}_d(t) \frac{e^{-j\psi}}{T_f \cos\psi} \quad (7.5)$$

Thus if $\dot{\tilde{V}}_d(t)$ is rotated by angle $+\psi$, it will lie along the direction of $-\tilde{V}_d(t)$ as shown in Fig. 7.1.

7.2 Transient Variation of Cavity Voltage and Reflected Power Between Bunches

Let us now apply Eq. (7.4) to find the transient variation of the cavity voltage between bunches for the case of a bunch train in which the time between bunches is not necessarily small compared to

the cavity filling time. We start with the vector diagram in Fig. 6.4, showing the cavity and beam loading voltages just before and just after the passage of a single bunch through a cavity driven by a generator voltage \tilde{V}_g . These voltages are redrawn in Fig. 7.3.



When the bunch crosses the cavity reference plane, the cavity voltage changes instantaneously (in our model) from \tilde{V}_c^- to \tilde{V}_c^+ . The magnitude of the change is $-V_{bo}$. The voltage then begins to charge toward \tilde{V}_g along the spiral path shown. At the precise moment the voltage once again reaches \tilde{V}_c^+ , another bunch comes by to repeat the cycle. We can now make the following correspondences between the voltages in Eq. (7.4) and those in Fig. 7.3:

Fig. 7.3. Transient response of a driven cavity to a train of equal bunches.

$$\begin{aligned} \tilde{V}(t) &\sim \tilde{V}_c(t) \\ \tilde{V}(0) &\sim \tilde{V}_c^+ \\ \tilde{V}(\infty) &\sim \tilde{V}_g \end{aligned} \quad (7.6)$$

We have therefore

$$\tilde{V}_c(t) = \tilde{V}_g + (\tilde{V}_c^+ - \tilde{V}_g) e^{-(t/T_f)(1-j \tan\psi)} \quad (7.7)$$

But from the diagram in Fig. 7.3,

$$\begin{aligned} \tilde{V}_c^+ - \tilde{V}_g &= \tilde{V}_b^+ \\ \tilde{V}_g &= \tilde{V}_c^- - \tilde{V}_b^+ - \frac{1}{2} V_{bo} \end{aligned} \quad (7.8)$$

Therefore

$$\tilde{V}_c(t) = \tilde{V}_c^- + \tilde{V}_b^+ \left[e^{-(t/T_f)(1-j \tan\psi)} - 1 \right] - \frac{1}{2} V_{bo} \quad (7.9)$$

To simplify the notation, we introduce a normalized time $x = t/T_b$, such that $x = 1$ when t is equal to the arrival time of the next bunch. Recall also that $\tan\psi = \delta/\tau$. Substituting for \tilde{V}_b^+ from Eq. (6.25), again taking into account that $\tilde{V}_{bo} = -V_{bo}$, we find

$$\tilde{V}_c(x) = \tilde{V}_c^- - \frac{V_{bo} \left[e^{-x\tau} e^{jx\delta} - 1 \right]}{1 - e^{-\tau} e^{j\delta}} - \frac{V_{bo}}{2} \quad (7.10)$$

Separating this expression into real and imaginary components with the aid of Fig. 7.3,

$$V_c(x) \cos \nu = V_c \cos \phi + V_{bo} F_A(x) \quad (7.11a)$$

$$V_c(x) \sin \nu = V_c \sin \phi + V_{bo} F_B(x) \quad (7.11b)$$

where

$$F_A(x) = [1 - e^{-2\tau} - 2e^{-x\tau} \cos x\delta + 2e^{-(1+x)\tau} \cos \delta(1-x)] / 2D \quad (7.12a)$$

$$F_B(x) = [e^{-\tau} \sin \delta - e^{-x\tau} \sin x\delta - e^{-(1+x)\tau} \sin \delta(1-x)] / D \quad (7.12b)$$

$$D = 1 - 2e^{-\tau} \cos \delta + e^{-2\tau}$$

Squaring and adding Eqs. (7.11a) and (7.11b), using also $V_{bo} = i_o R \tau_o$

$$\frac{V_c^2(x)}{V_c^2} = \left[\cos \phi + \frac{i_o R \tau_o}{V_c} F_A(x) \right]^2 + \left[\sin \phi + \frac{i_o R \tau_o}{V_c} F_B(x) \right]^2 \quad (7.13)$$

For a fixed τ_o , the optimum values of β and ψ can be obtained by minimizing the generator power as given by Eq. (6.33). Equation (7.13) together with the definitions of F_A and F_B given by Eqs. (7.12), determines the transient variation between bunches in the amplitude of the cavity voltage. The transient variation in the phase of the cavity voltage is obtained by taking the ratio of Eqs. (7.11b) and (7.11a).

$$\tan \nu(x) = \frac{V_c \sin \phi + V_{bo} F_B(x)}{V_c \cos \phi + V_{bo} F_A(x)} \quad (7.14)$$

The reflected power P_r can now be computed using conservation of energy:

$$P_r = P_g - P_c - dW/dt \quad (7.15)$$

where P_g is the incident generator power, $P_c = V_c^2(t)/R_g$ is the instantaneous cavity dissipated power and W is the stored energy given by

$$W(t) = \frac{V_c^2(t)}{\omega_o (R_g/Q)} = \frac{1}{2} T_{fo} P_c(t)$$

Here $T_{fo} = 2Q_0/\omega_0$ is again the unloaded filling time. Equation (7.15) now becomes

$$P_r(t) = P_g - P_c(t) - \frac{1}{2} T_{fo} \frac{d}{dt} [P_c(t)] \quad (7.16)$$

If a normalized cavity voltage $v(t) = V_c(t)/V_c$ is introduced, the above expression can be written in normalized form, again using $x = t/T_b$ and $\tau_0 = T_b/T_{fo}$, as

$$P_r(x) = P_g - \frac{v^2}{R_a} \left\{ v^2(x) + \frac{1}{2\tau_0} \frac{d}{dx} [v^2(x)] \right\} \quad (7.17)$$

The function $v^2(x)$ is just that given by Eq. (7.13).

The above derivation does not give the phase of the reflected voltage wave in the input transmission line to the cavity, which may sometimes be of interest. An alternative derivation, which solves for both the magnitude and the phase of the reflected wave, is given in Ref. 27.

7.3 Transient Beam Loading in Traveling-Wave Linacs

The concepts introduced in Ch. 6 to deal with single-bunch beam loading in standing-wave structures can also serve as the starting point for an analysis of transient beam loading in traveling-wave structures. Assume an element of charge dq passes through a traveling-wave structure at a velocity $v_q \approx c$. Assume also that the group velocity is low, $v_g \ll c$, so that the induced wave of amplitude dE_b travels a negligible distance during the time $\Delta t = L/c$ it takes for dq to transit through the structure. By analogy to Eq. (6.7a), the induced wave will have amplitude

$$dE_b = 2 k_1 dq \quad (7.18)$$

where k_1 is the traveling-wave loss parameter per unit length given by

$$k_1 = (\omega/4)(r/Q) = \frac{1}{2} \alpha r v_g \quad (7.19)$$

Here r is the shunt impedance per unit length for a synchronous wave as defined by Eq. (5.7a), α is the attenuation parameter per unit length, and Eq. (5.8c) has been used to eliminate ω/Q .

Assume now a constant impedance structure in which v_g does not vary with length. The analysis for the case of a constant gradient structure would diverge at this point. For a constant impedance structure of length L , the voltage induced by dq is, using Eq. (7.18)

$$dV_b = L(dE_b) = 2 k_1 L dq \quad (7.20)$$

Using Eq. (7.19) for k_1 in this expression, together with $dq = \bar{I}_0 dt$, $T_f = L/v_g$, $\tau \equiv \alpha L$ and $x \equiv t/T_f$, we obtain

$$dV_b = I_0 \tau v_g (dt) = I_0 \tau L \tau (dx) \quad (7.21)$$

As time proceeds, this induced field element propagates downstream through the structure and slips out of the downstream end into the terminating load. If dE_b is induced at $t = 0$, then at time $t = xT_f$ the above voltage element dV_b is reduced by a factor $(1-x)$ due to this downstream propagation. In addition, the voltage element will also decay by a factor $\exp(-\omega t/2Q) = \exp(-\tau x)$ because of wall losses. The preceding expression for dV_b thus becomes at time x ,

$$dV_b(x) = I_0 \tau L \tau (1-x) e^{-\tau x} dx \quad (7.22)$$

Integrating to add up all the induced voltage elements from $t = 0$ to $t = x$, we obtain

$$V_b(x) = I_0 \tau L \left[\left(1 - \frac{1}{\tau}\right) (1 - e^{-\tau x}) + x e^{-\tau x} \right] \quad (7.23)$$

For $\tau \ll 1$, this reduces to

$$V_b(x) \approx I_0 \tau L \tau (x - x^2/2) \quad (7.24)$$

In this limit the beam-loading voltage increases parabolically with time. In general, the beam loading voltage starts off linearly for $x \ll 1$ with slope $dV_b/dt \approx I_0 \tau v_g \tau$ and approaches the steady-state limit

$$V_b = I_0 \tau L [1 - (1 - e^{-\tau})/\tau] \quad (7.25)$$

with slope $I_0 \tau v_g \tau^2$ at $t = T_f$.

The transient energy gain from the generator voltage component can be obtained by integrating Eq. (5.10a) from $z = 0$ to $z = xL$. The result is, assuming V_g is turned on at time $t' = 0$,

$$V_g(x') = (rLP_0)^{1/2} [(2/\tau)^{1/2} (1 - e^{-x'\tau})] \quad (7.26)$$

When a generator-produced wave and beam-induced wave are both present the net energy gain as a function of time can be obtained by a superposition of Eqs. (7.23) and (7.26). The two voltage components can, of course, be turned on at different times. There may be a phase difference also, which can be taken into account by multiplying V_g by $\cos\theta$ where again θ is the phase angle of \tilde{V}_g with respect to a reference phase taken in the direction $-\tilde{V}_b$.

As a final comment, note that by setting $dq = I_0 dt$ we have implicitly assumed a train of bunches, each of which is short compared to an rf wavelength, and which are spaced closely compared to the filling time. If this is not the case, then from Eq. (7.22) the net

voltage at time t can be obtained by summing the beam induced voltages

$$V_{bn}(t) = r v_g \tau (1 - x_n) e^{-\tau x_n} q_n \quad (7.27)$$

due to charges q_n passing through the structure at times t_n , where $x_n = (t - t_n)/T_f$ and $V_{bn} = 0$ for $x_n > 1$.

8. BEAM BREAKUP

Both the theoretical and experimental aspects of beam breakup in electron linacs are discussed in detail in Refs. 1 and 2, and we will not attempt to duplicate this coverage here. However, since we have set ourselves the task in these notes of reviewing the main features of the beam-structure interaction problem, a brief summary follows giving a few of the important analytic results of beam breakup theory.

8.1 Regenerative Beam Breakup

Regenerative beam breakup is an oscillation within a single accelerating section due to the interaction of the beam with a dipole (deflecting) mode. In these modes the E_z field component varies linearly with distance r from the axis, and as $\cos\phi$ in the azimuthal direction (see Sec. 5.1). Regions of transverse magnetic deflecting fields lie displaced from the region of maximum E_z by $\pm\lambda/4$ in a synchronous wave moving at velocity c . The field pattern for such a "TM₁₁-like," or HEM hybrid mode, is sketched in Fig. 8.1. In the usual disk-loaded structure, these deflecting modes are often of the backward wave type; that is, the phase velocity and the group velocity are in opposite directions. The interaction between a synchronous particle and a deflection mode can be characterized by the transverse shunt impedance per unit length, defined by

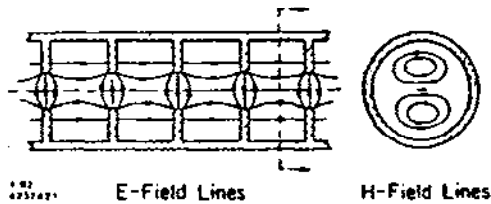


Fig. 8.1. Approximate electric and magnetic field lines for the TM₁₁-like deflection mode in a disk-loaded structure with π -phase shift per cavity. Maximum H-field occurs a quarter-cycle after maximum E-field at the cross-section shown.

$$r_i = \frac{(1/k^2) (\partial E_z^+ / \partial r)^2}{dP_g/dz} \quad (8.1)$$

Here $k = \omega/c$ and E_z^+ is the synchronous forward-wave field component. For a standing-wave mode,

dP_g/dz is the average power dissipated in the structure walls per unit length. For a typical disk-loaded structure, the relation

$$\frac{r_i}{Q} \approx \frac{100 \text{ ohms}}{\lambda} \quad (8.2)$$

can be used to get a rough estimate of the transverse shunt impedance of the lowest-order deflection mode. In a typical structure the frequency of this mode is 40-50% higher than the accelerating mode frequency. Therefore, the Q can be expected to be somewhat lower (70-80%) compared to the Q for the accelerating mode.

Consider now a traveling-wave structure with fields proportional to an amplitude factor A_1 , and assume a continuous electron beam entering the structure on axis. The particles in the region of transverse magnetic field will experience a deflecting force, and the transverse displacement of these particles will tend to increase as the square of the distance along the structure. Since the sign of the deflecting field alternates every half wavelength, the beam viewed from the side will look like a wave of growing amplitude, something like the wiggles in a stream of water from a hose nozzle which is shaken sideways. The mechanism for energy interchange depends upon the beam velocity being slightly non-synchronous with respect to the wave. If the electrons in the regions of maximum displacement (maximum deflecting B field) begin to slip ahead of the wave, they enter a region of the wave having a decelerating E_z electric field component. We would, consequently, expect maximum energy to be extracted from the beam if the electrons slip ahead by about a half a wavelength in the length of the structure. A detailed calculation shows that the phase slip parameter defined in Eq. (5.27) is $\delta = 2.65$ for maximum energy extraction. The power extracted from the beam is proportional to the beam current. This power propagates toward the upstream end of the section, since we are dealing with a backward wave, where it produces a field with an amplitude factor A_2 . The condition for an oscillation is that A_2 be equal to the assumed initial field amplitude A_1 . Detailed calculations²⁶ give a starting current

$$I_s (\text{TW}) = \frac{\pi v_0 \lambda^2 (v/c)^2}{8 g_2(\delta) L^3 (r_1/Q)} \quad (8.3a)$$

Here eV_0 is the energy of the beam in electron volts, and $g_2(\delta)$ is a function of the phase slip parameter. This function has a maximum value of 1.04 at $\delta = 2.65$, giving the minimum starting current. This expression was derived assuming a constant electron energy in the section. However, the first section in a linac is most likely to oscillate since the energy is lowest, and the energy is far from constant over the length of this section. If V_i and V_f are the input and output energies for such a section, and if $V_f \gg V_i$, then it can be shown that the starting current is reduced by a factor of 3 below that in Eq. (8.3) when $V_f = V_0$, giving

$$I_s (\text{TW}) = \frac{V_f \lambda^2 (v/c)^2}{8 L^3 (r_1/Q)} \quad V_f \gg V_i \quad (8.3b)$$

Attenuation in the section was not taken into account in deriving these expressions. Thus, measured threshold currents tend to exceed

the computed thresholds by perhaps 50%. It is also assumed that the phase slip condition is accurately maintained over the entire length of the section, which may not be the case if the group velocity is very small.

The above relations were derived for a traveling-wave section in which it was assumed that the backward-wave deflecting mode is not reflected at the input coupler (upstream end) of the structure. If the structure is short with bad reflections, or if we are considering deflecting mode fields trapped within a short region of a constant gradient structure, then a standing-wave analysis is more appropriate. In such an analysis, the condition for oscillation is that the power extracted from the beam be equal to the power dissipated in the structure walls. This leads to a starting current

$$I_s(\text{SW}) = \frac{\pi^2 v_o \lambda}{4 g_2 r_1 L^2} \quad (8.4)$$

Again, $g_2(\text{max}) = 1.04$, and if the energy gain in the section is large compared to the input energy the starting current is expected to be lower. By using r_1/Q from Eq. (8.2) in Eq. (8.4), and setting g_2 equal to $g_2(\text{max})$, we have

$$I_s(\text{SW}) \approx .025 \frac{v_o \lambda^2}{QL^2} \quad (8.5)$$

Note that $I_s(\text{TW})$ varies as $(\lambda/L)^3$ since $r_1/Q \sim 1/\lambda$, and that $I_s(\text{SW})$ varies as $(\lambda/L)^2$ for a given Q .

The above starting currents were derived assuming a continuous beam. For a beam pulse of finite length t_p , the starting current is increased by the ratio²⁸

$$\frac{I_s(t_p)}{I_s(\infty)} = 1 + \frac{F_e T_f}{t_p} \quad (8.6)$$

Here $T_f = 2Q/\omega$ is the filling time and e^{F_e} is the amplification factor from noise required to produce breakup. Experimental data indicate that F_e is in the range 10-20.

8.2 Cumulative Beam Breakup

The mechanism for cumulative beam breakup is quite different. In a multi-section accelerator, each section acts like an amplifier which provides a small increase in the amplitude of the transverse displacement wave. Even though the "gain" per stage is close to unity, $(1+\epsilon)$ say, the total gain in an accelerator such as SLAC with many sections can be very large. Thus for the SLAC accelerator $(1+\epsilon)^N = \exp(F_e)$, where $N \approx 960$. F_e (the e-folding factor) ≈ 20 and $(1+\epsilon) \approx 1.02$ at the threshold for breakup. Assume that the

deflecting mode occupies a length l in a structure of total length L . The total transverse shunt impedance per section is then $R_1 = r_1$, where, for the particular case of the SLAC constant gradient structure $l \approx 25$ cm, $L = 3$ m and R_1/Q has been measured to be 400 ohms.

Details of the beam-cavity interaction are relatively easy to calculate from first principles in the steady-state limit (cw beam). At each amplifying cavity (regions in the structure) there is a transverse displacement modulation and a transverse momentum modulation on the beam. The transverse displacement modulation excites the cavity through the interaction with the off-axis E_z field component, and the resulting H_y field component provides an additional momentum kick to the beam. In the drift space between cavities, the transverse momentum is converted into additional displacement. For maximum gain, it can be shown²⁹ that the momentum "wave" lags the displacement wave by 30° . Furthermore, the frequency of the modulation for maximum gain is such as to drive the cavities off resonance with a tuning angle $\psi = 30^\circ$. For an accelerator with a uniform accelerating gradient $V' = dV/dz$, the e-folding factor in the asymptotic limit ($F_e \gg 1$) can be shown to be^{28,29}

$$F_e(\text{CW}) = (3)^{3/4} \cdot \left[\frac{\pi I_o z R_1}{2 V' \lambda L} \right]^{1/2} \quad (8.7)$$

For the transient case (pulse length t_p less than or comparable to the filling time), the analysis is more complex. For times which are not too long ($t_p < F_e T_f$), the e-folding factor can be written²⁸

$$F_e(t) = \frac{(3)^{3/2}}{2} \cdot \left[\frac{\pi^2 I_o z c t (R_1/Q)}{V' \lambda^2 L} \right]^{1/3} \quad (8.8)$$

The preceding expressions were all derived assuming no focusing. If the focusing is not too strong, the e-folding factor can be modified²⁸ to take focusing into account. For the case of an accelerating gradient and a focusing strength which are constant along the accelerator,

$$F'_e = F_e \left[1 - C k_\beta^2 z^2 / F_e^2 \right] \quad (8.9)$$

Here k_β is the betatron wave number of the focusing system and the constant C has the values for the steady-state and transient cases

$$C_{ss} = 1/2$$

$$C_t = 3/4$$

In Ref. 30 an analysis is given for cumulative beam breakup in the presence of solenoidal focusing. An asymptotic expression (z must be sufficiently large) is developed which is valid for strong focusing and arbitrary pulse length compared to the cavity filling time.

9. IMPEDANCES AND WAKES*

9.1 Longitudinal Impedance Function and Wake Potential

If a sinusoidal current at frequency ω having a peak value $I(\omega)$ induces a voltage with peak value $V(\omega)$ in a component or chain of components, then the impedance is defined as

$$Z(\omega) = V(\omega)/I(\omega) \quad .$$

The impedance is complex, since $V(\omega)$ can be out of phase with $I(\omega)$. The chain of components can be, in particular, the components in one complete turn for a storage ring. Similarly, if a unit point charge passes through a component or chain of components, the wake potential $w(\tau)$ is defined as the potential experienced by a test particle following a distance ct behind the unit charge. In the following discussion we assume high-energy electrons or positrons traveling close to the speed of light, such that space charge forces between particles can be neglected. Both the impedance function and wake potential are therefore identically zero for a beam of particles in free space. As we will see, either $Z(\omega)$ or $w(\tau)$ is sufficient to completely characterize the longitudinal effects produced by the beam environment.

The concepts of an impedance function and a wake potential apply both to particles and currents passing through vacuum chamber components and to currents and charges in lumped equivalent circuits. In the case of an equivalent circuit, the wake potential is the voltage across the circuit as a function of time following the application of a unit current impulse $I(t) = \delta(t)$. The response of a component to a unit current step is also useful in certain calculations. If $s(\tau)$ is the response to a unit current step applied at $\tau = 0$, then the relation between the step and impulse response functions is

$$s(\tau) = \int_0^\tau w(\tau') d\tau' \quad .$$

Note that $w(\tau)$ is in units of volts per coulomb or ohms per second, while $s(\tau)$ is in ohms. The forms for $w(\tau)$ and $s(\tau)$ for several common circuit elements are shown in Fig. 9.1. A resistive (or decelerating) wake is taken to be positive.

9.2 Transform Relations

Problems in accelerator theory can often be viewed within the conceptual framework provided by either the frequency or the time domains. Sometimes the framework provided by one domain or the other is more useful for viewing or solving a particular problem. In the past, there may have been some preference for the frequency domain as being the more fundamental. In these notes, however, problems have been approached wherever possible in a time-domain framework, with phasors providing a graphic aid in describing the physics of such processes as, for example, beam loading by bunch trains. It is

* See Refs. 50 and 51 for a more extensive treatment of wake potentials and their applications.

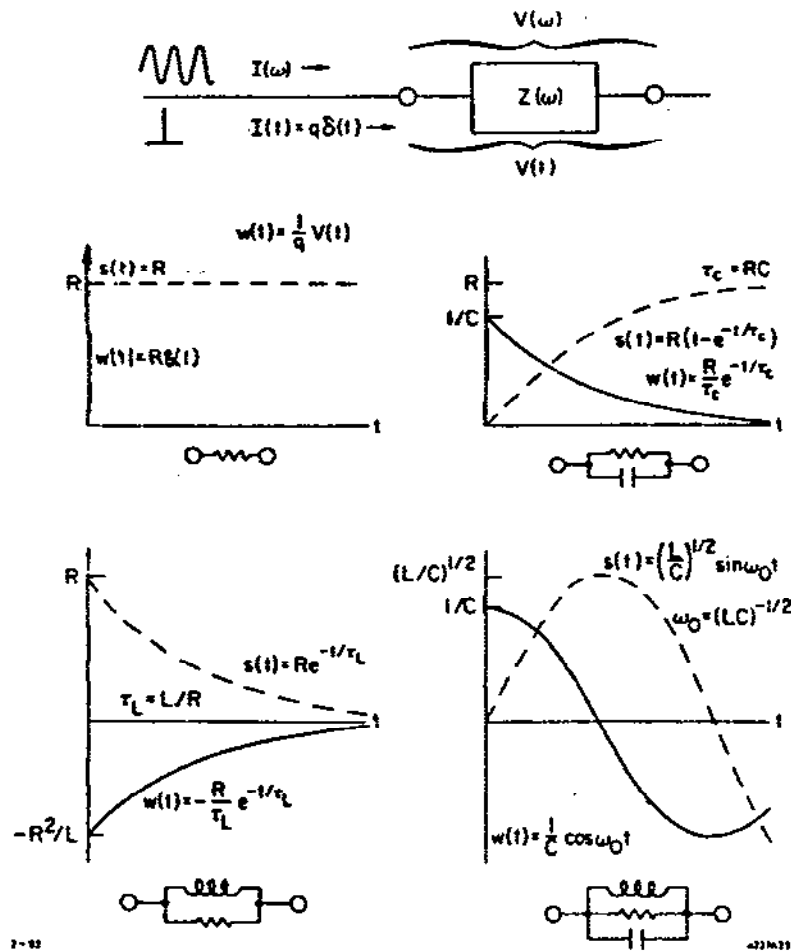


Fig. 9.1. Impulse and step response function for four circuit elements.

clearly desirable to be able to view a problem in either domain, and to transform physical quantities back and forth between these two worlds.

Consider the Fourier expansion for a periodic time-domain function, such as the current $I(t)$ for a bunch train with period Δt :

$$I(t) = \sum_{-\infty}^{\infty} \alpha_n e^{jn\omega_0 t} = I_0 + \sum_1^{\infty} I_m(\omega_0 t) \quad (9.1)$$

where $\omega > 0$ and

$$\alpha_n = \frac{\omega_0}{2\pi} \int_{-\Delta t/2}^{\Delta t/2} I(t) e^{-jn\omega_0 t} dt$$

$$\begin{aligned}
 I_m &= a_m \cos \omega_m t + b_m \sin \omega_m t ; I_o = \alpha_o \\
 \omega_m &= m\omega_o = 2\pi m / \Delta t ; m > 0 \\
 a_m &= (\alpha_n + \alpha_{-n}) , b_m = j(\alpha_n - \alpha_{-n})
 \end{aligned}$$

If $I(t)$ is physically measurable function of time (beam current for example), then it is a real function. Furthermore, it can be expanded in terms of positive (physically measurable) frequency components ω_m . Then the relation between the coefficients a_m, b_m and α_n depends on the symmetry of $I(t)$. If $I(t)$ is symmetric, then from Eq. (9.1)

$$\begin{aligned}
 \alpha_n &= \alpha_{-n} = \text{Real} , \\
 a_m &= 2\alpha_n ; b_m = 0
 \end{aligned}$$

If $I(t)$ is antisymmetric

$$\begin{aligned}
 \alpha_n &= -\alpha_{-n} = \text{Imaginary} \\
 b_m &= 2j\alpha_n = \text{Real} ; a_m = 0
 \end{aligned}$$

Now consider the limit $\Delta t \rightarrow \infty, \omega_o \rightarrow 0$. Set $n\omega_o = \omega$ and $\omega_o = d\omega$, and let $I(\omega) = (2\pi/\omega_o)\alpha_n$ be the density at frequency ω of the Fourier components in the expansion of $I(t)$ as ω_o approaches 0. We then obtain the Fourier transform relations for the general function $f(t)$:

$$\mathcal{F}(t) = \frac{1}{2\pi} \int_{-\infty}^{\infty} F(\omega) e^{j\omega t} d\omega \equiv \overline{F(\omega)} \quad (9.2a)$$

$$F(\omega) = \int_{-\infty}^{\infty} f(t) e^{-j\omega t} dt \equiv \overline{\mathcal{F}(t)} . \quad (9.2b)$$

For the particular case of a Gaussian bunch with charge q and bunch length σ_t ,

$$I(t) = \frac{q}{\sqrt{2\pi}\sigma_t} \exp(-t^2/2\sigma_t^2) \quad (9.3a)$$

$$I(\omega) = q \exp(-\omega^2\sigma_t^2/2) \quad (9.3b)$$

For a repetitive train of Gaussian bunches, using $I_o = (\omega_o/2\pi)q$,

$$a_m = \frac{\omega_o}{2\pi} [I(\omega) + I(-\omega)] = 2I_o \exp(-m^2\omega_o^2\sigma_t^2/2) \quad (9.4)$$

Let us now apply these transform relations to a bunch with current distribution $I(t)$. The wake function $w(\tau)$, sometimes called the delta-function wake potential, gives the potential a distance $c\tau$ behind a unit point charge. The contribution $dV_b(t)$ to the potential at position ct due to an element of charge dq a distance $c(t-t')$ ahead in the bunch is then

$$dV_b(t) = w(t-t')dq = w(t-t')I(t')dt'.$$

Summing the contributions to the potential produced by all charge elements in the bunch ahead of position ct ,

$$V_b(t) = \int_{-\infty}^t w(t-t')I(t')dt' = \int_0^{\infty} w(\tau)I(t-\tau)d\tau \quad (9.5)$$

The total energy loss by charge q , in terms of the loss parameter k introduced in Eq. (6.5), is $\Delta U = kq^2$. Thus

$$k = \frac{1}{q^2} \int_{-\infty}^{\infty} v_b(t) I(t) dt \quad . \quad (9.6)$$

Now take the transform of Eq. (9.5) to obtain

$$\overline{v_b(t)} = \int_{-\infty}^{\infty} e^{-j\omega t} dt \int_0^{\infty} w(\tau) I(t-\tau) d\tau \quad . \quad (9.7)$$

Reverse the order of integration, let $t = \tau + t'$ and find

$$V(\omega) \equiv \overline{v_b(t)} = I(\omega) \overline{w(\tau)} \quad . \quad (9.8)$$

Since $Z(\omega) \equiv V(\omega)/I(\omega)$, we have

$$Z(\omega) = \overline{w(\tau)} \quad (9.9a)$$

$$V(\omega) = \overline{v_b(t)} \quad (9.9b)$$

$$I(\omega) = \overline{I(t)} \quad . \quad (9.9c)$$

9.3 Properties of the Impedance Function

We define the wake function to be a real function of time. This then imposes a condition on the impedance function, $Z(\omega) = Z_R(\omega) + j Z_I(\omega)$. Thus

$$\begin{aligned} w(t) = \overline{Z(\omega)} &= \frac{1}{2\pi} \int_{-\infty}^{\infty} Z(\omega) e^{j\omega t} d\omega \\ &= \frac{1}{2\pi} \int_{-\infty}^{\infty} [Z_R(\omega) \cos\omega t - Z_I(\omega) \sin\omega t] d\omega \quad (9.10) \\ &+ \frac{1}{2\pi} \int_{-\infty}^{\infty} [Z_R(\omega) \sin\omega t + Z_I(\omega) \cos\omega t] d\omega \quad . \end{aligned}$$

If the imaginary part is to vanish for arbitrary $Z(\omega)$, it is necessary for $Z_R(\omega)$ to be an even function of frequency and for $Z_I(\omega)$ to be an odd function of frequency. We can confine ourselves to positive frequencies only, to obtain

$$w(t) = \frac{1}{\pi} \int_0^{\infty} [Z_R(\omega) \cos \omega t - Z_I(\omega) \sin \omega t] d\omega \quad (9.11)$$

In addition, the wake potential must be causal; that is, $w(t) \equiv 0$ for $t < 0$. Therefore

$$w(-t) = \frac{1}{\pi} \int_0^{\infty} [Z_R(\omega) \cos \omega t + Z_I(\omega) \sin \omega t] d\omega \equiv 0 \quad (9.12)$$

leading to

$$\int_0^{\infty} Z_R(\omega) \cos \omega t d\omega \equiv - \int_0^{\infty} Z_I(\omega) \sin \omega t d\omega \quad (9.13)$$

Substituting Eq. (9.13) in Eq. (9.11),

$$w(\tau) = \frac{2}{\pi} \int_0^{\infty} Z_R(\omega) \cos \omega \tau d\omega \quad (9.14)$$

Problem 9.1: Show that Eq. (9.13) is equivalent to the Hilbert transform,

$$Z_I(\omega) = \frac{1}{\pi} \int_{-\infty}^{\infty} \frac{Z_R(\omega')}{\omega' - \omega} d\omega' \quad (9.15)$$

Hint: Rewrite Eq. (9.13) with limits of integration between $-\infty$ and ∞ . Substitute for $Z_I(\omega)$ using Eq. (9.15), then reverse the order of integration. $Z_R(\omega)$ is obtained from $Z_I(\omega)$ by the inverse transform (above transform multiplied by -1).

Thus, if either the real or the imaginary component of the impedance function is specified, the other component is also determined as a consequence of the causality condition.

The preceding relations can be visualized using phasor concepts. Consider a unit point charge interacting with an impedance $Z(\omega)$. By Eq. (9.3b), the spectral density of the current in the frequency domain is $I(\omega) = 1/\pi$ at all frequencies. At time $t = 0$, due to the interaction of the charge with the real component of the impedance, beam-induced voltage elements

$$d\tilde{V}_R^+(0) = Z_R(\omega) I(\omega) d\omega = \frac{1}{\pi} Z_R^+(\omega) d\omega \quad (9.16)$$

$$d\tilde{V}_R^-(0) = \frac{1}{\pi} Z_R^-(-\omega) d\omega = \frac{1}{\pi} Z_R^+(\omega) d\omega$$

are produced in the frequency interval $d\omega$ at $i\omega$. A positive real impedance component indicates that the induced voltage elements oppose the motion of the charge and extract energy from it. At $t = 0$, imaginary beam-induced voltage components

$$\begin{aligned} d\tilde{V}_I^+(0) &= \frac{1}{\pi} Z_I^+(\omega) d\omega = -j \left[-\frac{1}{\pi} Z_I^+(\omega) d\omega \right] \\ d\tilde{V}_I^-(0) &= \frac{1}{\pi} Z_I^-(-\omega) d\omega = +j \left[-\frac{1}{\pi} Z_I^+(\omega) d\omega \right] \end{aligned} \quad (9.17)$$

are also produced which are at right angles to the real components and hence play no part in the energy interchange with the charge. These real and imaginary voltage elements are shown schematically by the solid phasors in Fig. 9.2. The total self-voltage acting on the charge is obtained by integrating the real components over all frequency at $t = 0$,

$$V_S = \frac{1}{2} \int_{-\infty}^{\infty} d\omega \left[dV_R^+(0) + dV_R^-(0) \right] = \frac{1}{\pi} \int_0^{\infty} Z_R^+(\omega) d\omega \quad (9.18)$$

At some later time t , the phasor voltage elements will have rotated to the positions shown by the dashed phasors in Fig. 9.2. The total wake voltage, including the contribution from the imaginary (at $t = 0$) components, is obtained by integrating over frequency,

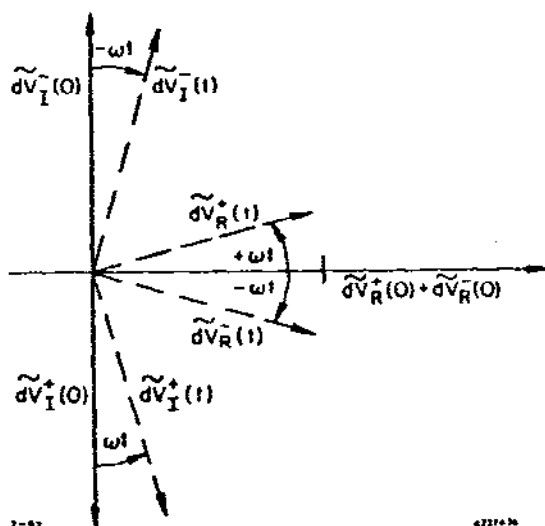


Fig. 9.2. Diagram showing how imaginary voltage elements induced by a point charge at $t = 0$ in the frequency interval $d\omega$ rotate to produce a causal wake.

$$\begin{aligned}
 w(t > 0) &= \int_0^{\infty} \left[dV_R^+ \cos \omega t + dV_I^+ \sin \omega t \right] d\omega \\
 &= \frac{1}{\pi} \int_0^{\infty} \left[Z_R^+(\omega) \cos \omega t - Z_I^+(\omega) \sin \omega t \right] d\omega .
 \end{aligned} \tag{9.19}$$

For $t < 0$, the four phasors rotate in the opposite sense, and

$$w(t < 0) = \frac{1}{\pi} \int_0^{\infty} \left[Z_R^+(\omega) \cos \omega t + Z_I^+(\omega) \sin \omega t \right] d\omega \equiv 0 . \tag{9.20}$$

This last relation is equivalent to the causality condition (9.13), and together with the preceding relation leads again to Eq. (9.14).

Thus, to satisfy causality, the imaginary voltage components induced at $t = 0$ in a frequency interval $d\omega$ rotate and always add up for $t < 0$ so as to cancel the wake produced by the sum of the real components induced at $t = 0$ when integrated over all frequencies. For $t > 0$, the imaginary components rotate so as to produce a total real wake which is exactly double that due to the sum of all real components. Note that by extrapolating Eq. (9.14) to $t = 0$, we obtain

$$w(0) = 2w_s . \tag{9.21}$$

The factor of two in this expression is essentially the same as that in Eq. (6.7b), which was obtained by applying conservation of energy and superposition to resonant modes in a cavity. To see this more clearly, let us calculate the total loss parameter k , using Eq. (9.6)

$$k = \frac{1}{2} \int_{-\infty}^{\infty} V_b(t) I(t) dt = \frac{1}{2\pi q} \int_{-\infty}^{\infty} V_b(t) dt \int_{-\infty}^{\infty} I^*(\omega) e^{-j\omega t} d\omega . \tag{9.22}$$

Reversing the order of integration,

$$k = \frac{1}{2} \int_{-\infty}^{\infty} I^*(\omega) V(\omega) d\omega = \frac{1}{2\pi q} \int_{-\infty}^{\infty} I^2(\omega) Z(\omega) d\omega . \tag{9.23}$$

Since $I(t)$ is a real function of time, we have by the same argument that lead to Eq. (9.11) that the real and imaginary part of $I(\omega)$ are symmetric and anti-symmetric respectively. Thus $I^2(\omega)$ is symmetric, and

$$k = \frac{1}{\pi q} \int_0^{\infty} I^2(\omega) Z_R(\omega) d\omega . \tag{9.24}$$

For a Gaussian bunch, using Eq. (9.3b),

$$k = \frac{1}{\pi} \int_0^{\infty} Z_R(\omega) e^{-\omega^2 \sigma^2 \tau} d\omega \quad (9.25)$$

For a point charge this agrees with the self-wake derived in Eq. (9.18).

9.4 Application to Resonant Modes

Let us now compute the wake potential and loss parameter for a single resonant mode. The impedance for such a mode is given by Eq. (3.39),

$$Z(\omega) = Z_R(\omega) + jZ_I(\omega) = \frac{R_o}{1 + j\xi} \quad (9.26)$$

$$Z_R(\omega) = \frac{R_o}{1 + \xi^2} \quad Z_I(\omega) = \frac{-R_o \xi}{1 + \xi^2}$$

where, as before, $\xi = (\omega - \omega_o)T_f$ and $T_f = 2Q_L/\omega_o$.

Problem 9.2: Show that $Z_R(\omega)$ and $Z_I(\omega)$ above obey the causality condition in Eq. (9.13), assuming $\omega_o T_f = 2Q_L \gg 1$.

Applying Eq. (9.14), assuming a high Q mode so that $\cos \omega t \approx \cos \omega_o t$ over the range of ω where $Z_R(\omega)$ is appreciable, we obtain

$$w(\tau) \approx \cos \omega_o \tau \cdot \frac{2R_o}{\pi T_f} \int_{-\infty}^{\infty} \frac{d\xi}{1 + \xi^2} = \frac{\omega_o R_o}{Q_L} \cos \omega_o \tau \quad (9.27)$$

Using $R_o = [G_c(1 + \beta)]^{-1}$, $Q_o = (1 + \beta)Q_L$ and the fact that the accelerator shunt impedance is $R_a = 2/G_c$, we have

$$w(\tau) = \frac{\omega_o}{2} \left(\frac{R_a}{Q} \right) \cos \omega_o \tau \quad (9.28)$$

for the wake function for a mode resonant at frequency ω_o . The total loss parameter for a Gaussian bunch is obtained in a similar fashion using Eq. (9.25),

$$k(\sigma_t) = \frac{\omega_o}{4} \left(\frac{R_a}{Q} \right) e^{-\omega_o^2 \sigma_t^2} \quad (9.29)$$

Note that for a point bunch $w(0) = 2k_o$, where $k_o = (\omega_o/4)(R_a/Q)$. This gives

$$w(\tau) = 2k_o \cos \omega_o \tau \quad (9.30a)$$

$$k(\sigma_t) = k_0 e^{-\frac{\omega_0^2 \sigma^2}{2}} \quad (9.30b)$$

These results are readily extended to find the total wake function and total loss parameter by summing over all modes (assumed non-overlapping) in a resonant cavity or traveling-wave structure:

$$w(\tau) = 2 \sum_n k_n \cos \omega_n \tau \quad (9.31a)$$

$$k(\sigma_t) = \sum_n k_n e^{-\frac{\omega_n^2 \sigma^2}{2}} \quad (9.31b)$$

For the case of a resonant cavity, using Eq. (6.6b),

$$k_n = \frac{\omega_n}{4} \left(\frac{R}{Q} \right)_n = \frac{V_n^2}{4W_n} \quad (9.32)$$

where V_n is the maximum voltage gain for the n th mode for a velocity of light test particle when the stored energy in the mode is W_n . Similar concepts apply to traveling-wave modes in a periodic structure. Using Eq. (5.7c),

$$k_n = \frac{\omega_n}{4} \left(\frac{r}{Q} \right)_n = \frac{E_n^2}{4w_n} \quad (9.33)$$

where E_n is the amplitude of the synchronous space harmonic component of the axial electric field for the n th mode, and w_n is the stored energy per unit length summed over all space harmonic components for that mode.

In order to compute the wake potential using Eq. (9.31a), values for ω_n and k_n are needed for as many modes as possible, either resonant modes in the case of a cavity or traveling-wave modes for a periodic accelerating structure. Values of ω_n and k_n are obtained solving the boundary value problem for a charge-free cavity or structure. Two computer programs are generally available at the present time which accomplish this purpose. The program KN7C³¹ solves for traveling-wave modes in a round pipe loaded by disks with flat, parallel faces. This structure is described by four parameters: radius of the beam aperture in the disk, the inside radius of the pipe, the length of a period, and the length of the pipe between d faces. The program SUPERFISH⁶ solves for resonant modes in an axisymmetric cavity having an arbitrary boundary as a function of the axial coordinate z ; that is, on the boundary $r(\phi)$ is constant but $r(z)$ is an arbitrary function.

As frequency increases, the number of modes per unit frequency interval also increases. Since there is a limit on the total number

of modes that can be calculated with reasonable computer time, there is a corresponding maximum frequency for the sums in Eqs. (9.31). If this frequency is ω_m , details in the wake will not be accurate for time intervals $\Delta t \lesssim \omega_m^{-1}$, and the loss parameter will not be accurate for bunch lengths $\sigma_t \lesssim \omega_m^{-1}$. For high frequencies where the mode density is large, it is only the statistical properties of the modes that are important.

Problem 9.3: For a pillbox cavity of radius b and length L , show that the density of modes approaches $dn/d\omega = \omega b L / 2\pi c^2$.

In the case of a disk-loaded structure, loss by a point charge into high frequency traveling-wave modes can be considered as a diffraction loss by an equivalent plane wave having the same power spectrum and Poynting vector at the disk radius as the actual field due to the charge. This is the so-called optical resonator model³² for the energy loss by a point charge passing through a periodic sequence of thin plates with circular holes. In the limit of high-energy ($\gamma \gg \omega a/c$ where a is the hole radius), the loss parameter per unit frequency interval predicted by this model is³²

$$\frac{dk}{d\omega} = \frac{1}{\pi} Z_R(\omega) = \frac{A_0}{\omega^{3/2}} \quad (9.34)$$

The wake potential due to this "analytic extension" for loss at all frequencies $\omega > \omega_m$ is then

$$\begin{aligned} w_a(\tau) &= 2A_0 \int_{\omega_m}^{\infty} \frac{\cos \omega \tau}{\omega^{3/2}} d\omega \\ &= \frac{4A_0}{\omega_m^{1/2}} \left\{ \cos x - \sqrt{\frac{\pi x}{2}} \left[1 - 2S\left(\sqrt{\frac{2x}{\pi}}\right) \right] \right\}_{x=\omega_m \tau} \end{aligned} \quad (9.35)$$

where S is the Fresnel integral. The constant A_0 can, in principle, be specified analytically, at least for a structure with thin disks. In practice, it is better to obtain A_0 for a particular structure by making a fit of Eq. (9.34) to a log-log plot of computed modes for $\omega < \omega_m$.

The preceding concepts have been applied to compute the wake for the SLAC disk-loaded structure having a periodic length $\lambda/3 = 3.50$ cm. The disk thickness is 0.58 cm, the radius of the outer wall is 4.13 cm and the disk hole radius is 1.16 cm for an average cell near the center of each constant gradient structure of 3 m length. The wake for the first 10 ps is shown in Fig. 9.3. The dashed curve gives the wake due to 416 computed modes, using Eq. (9.31a). The total wake is obtained by adding an analytic extension given by Eq. (9.35). Note that, because of the analytic extension, the total wake has a vertical tangent at $\tau = 0$ but a finite value of $w(0) = 8$ V/pC/period. The wake due to the excitation of the fundamental accelerating mode

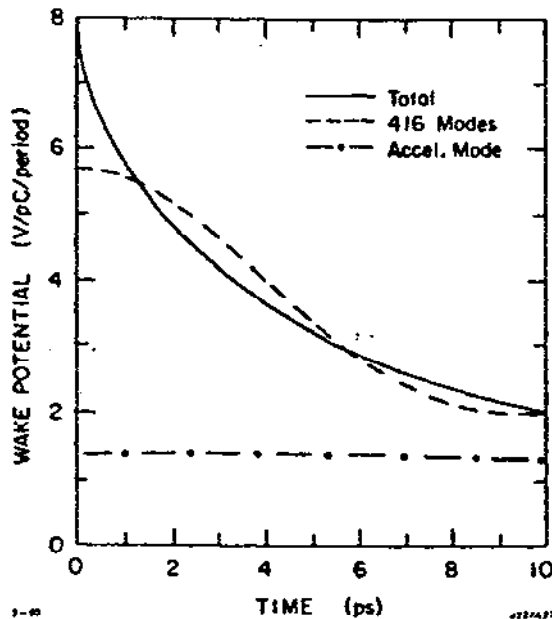


Fig. 9.3. Longitudinal wake per cell for the SLAC disk-loaded structure (0-10 ps). Cell length = 3.5 cm; beam aperture radius = 1.163 cm.

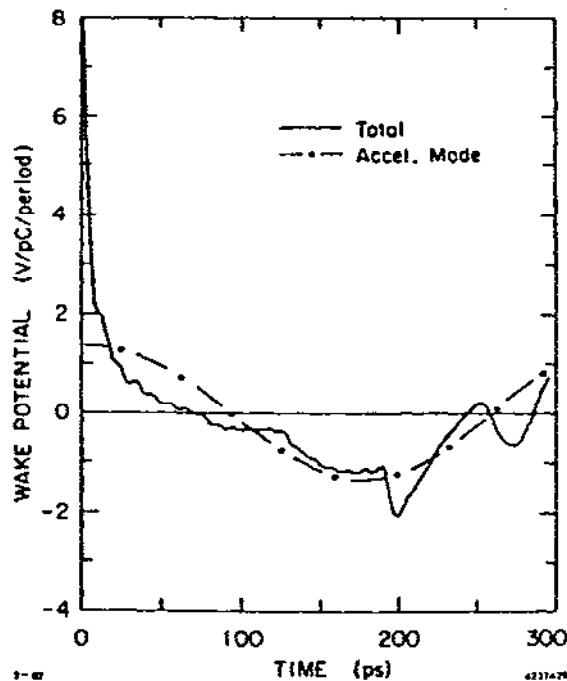


Fig. 9.4. Longitudinal wake per cell for the SLAC disk-loaded structure (0-300 ps).

only, is shown for comparison. Note that on this scale it is almost constant (the period is 350 ps), with an amplitude of about one-sixth of $w(0)$.

Figure 9.4 shows the longitudinal wake for the SLAC structure out to 300 ps. The large negative (accelerating) spike at 200 ps is the first reflection from the outer wall arriving at the structure axis. Shown again is the wake due to the fundamental mode, which undergoes almost a full period of oscillation. After 5 to 10 periods, it will be the dominant term in the wake, the higher modes having almost entirely decohered. On the time scale of interest, damping of the modes has also been ignored. Damping could be taken into account by multiplying each term in Eq. (9.31a) by $\exp(-\alpha_n \tau)$, where α_n is the damping constant for the n th mode.

For a number of years there was a controversy as to whether the modal analysis leading to Eq. (9.31a) was giving the complete wake. It was thought that this modal approach might be neglecting terms in the wake due to the scalar potential of the charge. Bane³³ has recently shown analytically that the modal analysis gives a wake which agrees with that derived from the vector and scalar potentials for a charge with $v = c$. Weiland and Zotter³⁴ have shown that the modal wake is in agreement with that obtained by direct integration of Maxwell's equations, using the program BCI, for a bunch moving through a cavity.

9.5 The Transverse Wake

In this section we work out the transverse wake for the specific case of an axisymmetric disk-loaded structure. For such a structure, the synchronous space harmonic component of the n th traveling-wave mode has an axial electric field variation described by²³

$$E_{zn} = E_{on} \left(\frac{r}{a}\right)^m \cos m\phi \cos \omega_n (t - z/c) \quad . \quad (9.36)$$

where E_{on} is the field strength at the radius of the disk opening. For each mode a loss parameter

$$k_n \equiv \frac{E_{on}^2}{4w_n} \quad (9.37)$$

can again be defined in terms of the "cold" (no charge present) electromagnetic properties of the structure. Using the same formalism developed for the case of longitudinal modes, k_n will also describe the interaction of a point charge with the mode in question. Specifically, the beam-induced energy deposited per unit length in the n th mode by a charge q traveling parallel to the axis at radius $r = r_q$ is

$$w_n = k_n \left(\frac{r_q}{a}\right)^{2m} q^2 \quad . \quad (9.38)$$

Eliminating w_n using the preceding two expressions,

$$E_{on} = -2 \left(\frac{r_q}{a}\right)^m k_n q \quad . \quad (9.39)$$

The minus sign indicates that the induced field is such as to oppose the motion of the charge. Substituting Eq. (9.39) in Eq. (9.36), the induced field at position r , azimuth ϕ (assuming the driving charge q is at $\phi = 0$) and position $\Delta z = cr$ behind a charge q at radius r_q is

$$E_{zn} = -2k_n q \left(\frac{r}{a}\right)^m \left(\frac{r_q}{a}\right)^m \cos m\phi \cos \omega_n \tau \quad . \quad (9.40)$$

For $m = 0$, we see that the longitudinal wake potential per unit length is recovered.

Now define the transverse (deflecting) wake per unit length of structure by

$$\vec{w}_t(\tau) = (c/e) d\vec{p}_t/dz = (\vec{E}_t + c\vec{B}_t) \quad (\text{cmf}) \quad (9.41)$$

where $d\vec{p}_t/dz$ is the transverse momentum kick experienced per unit length of structure by a particle following at distance cr behind a unit driving charge. The superscript indicates as before that the

transverse fields are to be evaluated in a reference frame which is co-moving with the particle. In a theorem due to Panofsky and Wenzel,³⁵ it is shown that the momentum kick in such a co-moving frame can be expressed in terms of the E_z field component only:

$$(\vec{E}_t + c\vec{B}_t)^{(cmf)} = j(c/\omega)\vec{v}_t E_z^{(cmf)} \quad (9.42)$$

Problem 9.4: Prove the Panofsky-Wenzel theorem.

Hint: Express \vec{E}_t and $(\vec{c} \times \vec{B})_t$ in terms of the vector potential \vec{A} . Expand $\vec{c} \times \vec{v} \times \vec{A}$, find the total derivative $d\vec{A}/dt$, and set this equal to zero for a synchronous wave.

For a synchronous wave, putting Eq. (9.40) in the form $E_{zn} = -|E_{zn}|e^{j\omega_n \tau}$ and using the preceding theorem, the transverse wake becomes

$$\vec{w}_{tn} = (c/\omega) \sin\omega\tau \left(\hat{r} \frac{\partial |E_{zn}|}{\partial r} + \hat{\phi} \frac{1}{r} \frac{\partial |E_{zn}|}{\partial \phi} \right) \quad (9.43)$$

where \hat{r} and $\hat{\phi}$ are unit vectors. Evaluating these two components,

$$\hat{r}: w_{tn}(r, \phi, \tau) = 2m \left(\frac{k_n c}{\omega_n a} \right) \left(\frac{r}{a} \right)^{m-1} \left(\frac{r_q}{a} \right)^m \cos m\phi \sin\omega_n \tau \quad (9.44a)$$

$$\hat{\phi}: w_{tn}(r, \phi, \tau) = -2m \left(\frac{k_n c}{\omega_n a} \right) \left(\frac{r}{a} \right)^{m-1} \left(\frac{r_q}{a} \right)^m \sin m\phi \sin\omega_n \tau \quad (9.44b)$$

The \hat{r} component of the dipole ($m=1$) wake at $\phi = 0$ is of most interest

$$w_{dn}(\tau) = 2 \left(\frac{k_n c}{\omega_n a} \right) \left(\frac{r_q}{a} \right) \sin\omega_n \tau \quad (9.45)$$

Note that the amplitude of the dipole wake depends on the transverse coordinate r_q of the exciting unit charge, but that behind r_q the wake itself is independent of r . Again, for a sum of modes

$$w_{dn}(\tau) = 2 \left(\frac{r_q}{a} \right) \sum_n \frac{k_n c}{\omega_n a} \sin\omega_n \tau \quad (9.46)$$

Assuming $dk_n/d\omega = A_1/\omega^{3/2}$, we can compute an analytic extension to the above sum over modes following the same procedure as that which led to Eq. (9.35). The result to be added to a sum over modes up to a maximum frequency ω_m is

$$w_{da}(\tau) = \left(\frac{\tau_0}{a}\right) \left(\frac{4 A_1 c}{\omega_m^{3/2} a}\right) \left\{ \frac{x}{3} \left[2 \cos x + \frac{\sin x}{x} - \sqrt{2\pi x} \left(1 - 2S\left(\sqrt{\frac{2x}{\pi}}\right) \right) \right] \right\}_{x = \omega_m \tau} \quad (9.47)$$

Again, S is the Fresnel integral and the constant A_1 is obtained by fit to modal results for $\omega < \omega_m$.

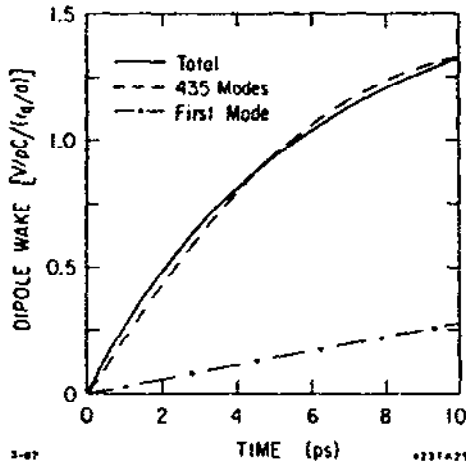


Fig. 9.5. Dipole wake per cell for the SLAC disk-loaded structure (0-10 ps).

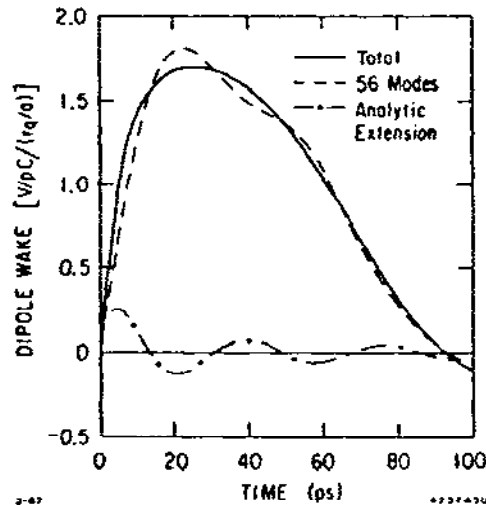


Fig. 9.6. Dipole wake per cell for the SLAC disk-loaded structure (0-100 ps).

Values for ω_m and k_{dn} can be computed for an axisymmetric disk-loaded structure using the program TRANSVERS.³⁶ The resulting transverse wake per period for the SLAC structure is shown in Figs. 9.5 to 9.7. Note in Fig. 9.5 that for very short times the total wake increases almost linearly at the rate of 0.25 V/pC/ps per period. This is about 10 times the slope due to the lowest frequency mode, which is responsible for beam-breakup in SLAC. In Fig. 9.6, note how the analytic extension combines with the modal contribution to produce a smooth total wake. If more modes are used, together with a contribution from the analytic extension which is consequently smaller, essentially the same total wake is obtained. The long-range wake is shown in Fig. 9.7. The high frequency modes, all of which add coherently at $\tau = 0$, have nearly decohered on this time scale. The main contribution to the wake is the lowest frequency mode, which has a period of 235 ps and an amplitude of 1.0 V/pC.

It is sometimes useful to define a dipole transverse impedance per unit length of structure by

$$Z_d(\omega) = -j \frac{(E_t + cB_t)}{I_0 \Delta r} \quad (9.48)$$

where E_t and B_t are the transverse deflecting field components produced by a current filament of strength I_0 having a sinusoidal

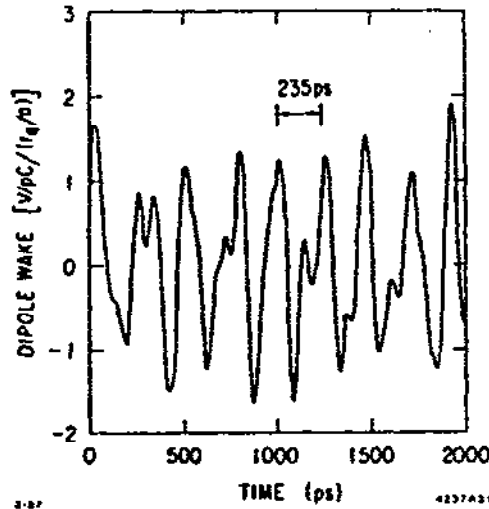


Fig. 9.7. Dipole wake per cell for the SLAC disk-loaded structure (0-2000 ps).

transverse modulation of amplitude Δr at frequency ω . For a component or for a storage ring of circumference L , the transverse impedance is $Z_d(\omega) = V_t(\omega)/I_d(\omega)$ where $V_t(\omega) = \int_0^L (\vec{E} + \vec{c} \times \vec{B})_t dz$ and $I_d(\omega) = q\Delta r$

Problem 9.5: Show that, for a resonant mode,

$$\frac{Z_d}{Q} = \frac{2c k_d}{\omega^2 a^2} \quad (9.49)$$

Hint: Multiply Eq. (9.45) by $e^{-\omega t/2Q}$, then take the transform using Eq. (9.2b) to find $V_t(\omega)$, noting also that $I_d(\omega) = q r_q$ for a point charge.

For typical dipole and longitudinal modes having the same E_z at the disk radius in a disk-loaded structure, we expect $k_d \approx 4 k_l$. However, the density of transverse modes per unit frequency interval is twice as large, since both TE- and TM-like modes can be excited.³⁷ Using also the fact that $k_l = (\omega/2)(Z_l/Q)$ for a longitudinal mode (setting $R_d = 2Z_l$ in Eq. (6.9)), we obtain

$$Z_d = \frac{2c}{\omega a^2} Z_l \quad (9.50)$$

This expression is often used to estimate the broadband dipole impedance if the longitudinal impedance is known.

9.6 The Quadrupole Wake

Evaluating the expression for the \hat{r} component of $w_{tn}(r, \phi, \tau)$ in Eq. (9.44a) for $m = 2$, we obtain the quadrupole wake potential

$$w_{qn}(\tau) = 4 \left(\frac{r_q}{a}\right)^2 \left(\frac{r}{a}\right) \sum_n \frac{k_n c}{\omega_n a} \sin \omega_n \tau \quad (9.51)$$

The wake varies with azimuthal angle as $\cos 2\phi$, where again it is assumed that $\phi = 0$ is the azimuth of the exciting charge at radius r_q . The expression for the analytic extension is that given by Eq. (9.25) multiplied by $2(r_q/a)(r/a)$. The quadrupole wake computed for the SLAC disk-loaded structure is shown in Figs. 9.8 and 9.9. The wake is again normalized to the disk hole radius $a = 1.163$ cm and to the periodic length $p = 3.50$ cm. To convert to a wake per unit length of structure, $w_q(\tau)/r_q^2 r$ in units of $V/C/m^4$, the ordinate must be multiplied by $10^{12}/a^3 p = 1.82 \times 10^{19}$. (To obtain the dipole wake $w_d(\tau)/r_q$ in units of $V/C/m^2$, the corresponding factor is $10^{12}/ap = 2.45 \times 10^{15}$.)

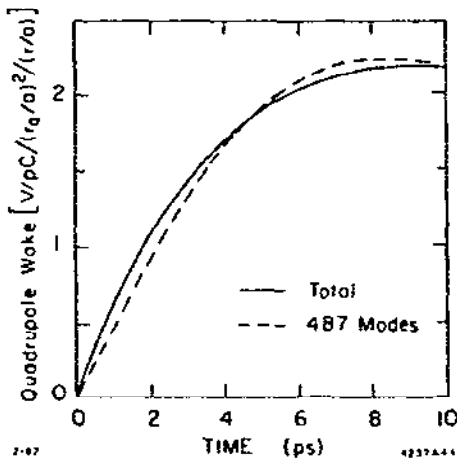


Fig. 9.8. Quadrupole wake per cell for the SLAC structure (0-10 ps).

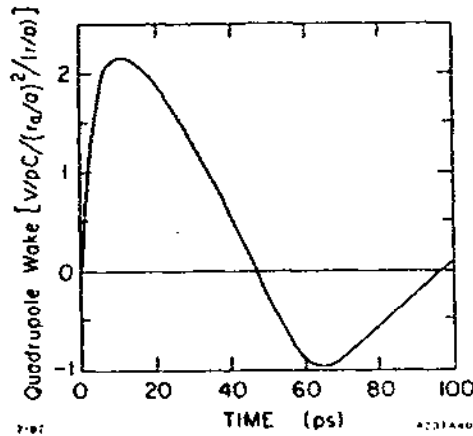


Fig. 9.9. Quadrupole wake per cell for the SLAC structure (0-100 ps).

It can be argued that effects due to the quadrupole wake will be small, since its strength is smaller than the strength of the dipole wake by roughly a factor $r_q r/a^2$. Note, however, that the quadrupole wake sets a fundamental limit on emittance growth in a linac with alternating gradient focusing. In such a machine the beam cannot always be round. Even if the beam is exactly on axis and there are no misalignments, there will still be an emittance growth due to the quadrupole wake because the beam will necessarily have a quadrupole moment. In a recent calculation, Chao and Cooper³⁸ have found such a situation in which effects due to the quadrupole wake can be

significant. In the first sector of the SLAC accelerator, there is non-negligible emittance growth for an injected bunch of 5×10^{10} particles with $\sigma_{x,y,z} \approx 1 \text{ mm}$.

9.7 Scaling of the Wake With Frequency and Structure Parameters

The scaling with frequency of the amplitude of the wake potential for a resonant mode, or the magnitude of some characteristic feature such as the intercept at $\tau = 0$ for the longitudinal wake or the value of the first maximum for the deflection wake, is per unit of structure,

$$\begin{aligned} w(\text{longitudinal}) &\sim \omega^2 \\ w(\text{dipole}) &\sim \omega^3 \\ w(\text{quadrupole}) &\sim \omega^5 \end{aligned} \quad (9.52)$$

The time at which some characteristic feature occurs, such as the first zero crossing of the longitudinal wake or the first maximum of the deflection wake, scales of course as ω^{-1} . The magnitude of the impedance for a resonant mode, again per unit length of structure, then scales as

$$\begin{aligned} \frac{Z}{Q}(\text{longitudinal}) &\sim \omega \\ \frac{Z}{Q} \frac{dn}{dn}(\text{dipole}) &\sim \omega^2 \\ \frac{Z}{Q} \frac{qn}{qn}(\text{quadrupole}) &\sim \omega^4 \end{aligned} \quad (9.53)$$

The amplitude of the so-called broad-band impedance function scales with the same frequency dependence. The impedance or the wake for specific vacuum chamber component (as opposed to the impedance or w per unit length of structure) scales as one power of frequency less than given above.

The dependence of both the longitudinal and transverse wakes on beam aperture has been investigated by K. Bane³⁹ for the SLAC disk-loaded structure. The intercept at $\tau = 0$ of the longitudinal wake was found to vary as

$$w_L(0) \sim a^{-1.68} \quad (9.54)$$

over the range in aperture radii for the SLAC structure. The time which the longitudinal wake falls to one-half its value at $\tau = 0$ is

$$\tau_{1/2} \approx 0.09 a/c \quad (9.54)$$

The amplitude of the first maximum of the dipole wake was computed to vary as

$$w_d(\tau_m) \sim a^{-2.25} \quad (9.55a)$$

However, the time at which the wake reaches its maximum value also varies with the beam aperture radius as

$$\tau_m \approx 0.64 a/c \quad (9.55b)$$

Thus the initial slope of the wake was found to vary more strongly with a than the value of the first maximum:

$$\frac{dw_d}{d\tau} \sim a^{-3.48} \quad \tau \rightarrow 0 \quad (9.55c)$$

These scaling relations would not be expected to hold when extrapolating to beam apertures significantly different from $a = 1.163$ cm, which is the aperture radius for an average cavity in the SLAC constant gradient structure. If the scaling law is written in the form a^{-n} , then the value n is larger than given above when scaling to larger values of a , and smaller when scaling to smaller a .

A structure filling factor can be defined by $f \equiv (p-t)/p$, where p is the periodic length and t is the disk thickness. For the SLAC structure, $p = 3.5$ cm and $f = 0.83$. When scaling to a structure with a different filling factor, computations indicate that the amplitude of the wake scales roughly in direct proportion to f .

10. SOME APPLICATIONS OF WAKE POTENTIALS

10.1 Single Bunch Acceleration

In this section we consider the acceleration of single bunches in traveling-wave linac structures. As will be discussed later, traveling-wave structures are to be preferred over standing-wave structures for single-bunch acceleration because the stored energy per unit length required to produce a given accelerating gradient is in general lower.

Using the notation in Ch. 5, the average accelerating gradient \bar{E}_a for a structure of length L with input power P and unloaded energy gain V_0 can be written in the form

$$\bar{E}_a^2 = \left(\frac{V_0}{L} \right)^2 = \frac{P \tau}{L} f(\tau) \quad (10.1)$$

For constant impedance (CZ) and constant gradient (CG) structures,

$$\text{CZ: } f(\tau) = (2/\tau)(1 - e^{-\tau})^2 \approx 2\tau(1 - \tau + \tau^2/2 \dots) \quad (10.2a)$$

$$\text{CG: } f(\tau) = (1 - e^{-2\tau}) \approx 2\tau(1 - \tau + 2\tau^2/3 \dots) \quad (10.2b)$$

For single-bunch acceleration it is also of interest to relate the energy stored per unit length of structure, w_s , to the energy gradient. The loss parameter k introduced previously and defined in Eq. (9.33) provides the desired relation:

$$k_1 = \frac{\bar{E}_a^2}{4w_s} = \frac{\omega}{4} \left(\frac{r}{Q} \right)^2 \sim \omega^2,$$

where the subscript emphasizes that k_1 is per unit length of structure. The average gradient for a structure of length L can now be written as

$$\bar{E}_s^2 = 4 k_1 w_o \eta_s = 4 k_1 T_f P_1 \eta_s \quad (10.3)$$

where $w_o = P_o T_f / L$ is the input energy per unit length, $P_1 = P_o / L$ is the input power per unit length, and η_s is a structure efficiency, given by

$$\text{CZ: } \eta_s = (1 - e^{-\tau})^2 / \tau^2 \quad (10.4a)$$

$$\text{CG: } \eta_s = (1 - e^{-2\tau}) / 2\tau \quad (10.4b)$$

Problem 10.1: Derive the expressions for η_s in Eqs. (10.4).
Hint: Recall that the filling time for both constant impedance and constant gradient structures is given by $T_f = \tau(2Q/\omega)$.

The structure efficiency η_s and normalized power $P_n = P_o / (\bar{E}_s^2 L / \tau)$ $1/f(\tau)$ are plotted in Fig. 10.1 as a function of the attenuation parameter τ for a constant impedance structure. Note that a high structure efficiency and the lowest peak power requirement are mutually exclusive. The best compromise for both high η_s and low P_n is reached for a τ on the order of 0.3-0.5.

The structure parameter k_1 is a strong function of the beam aperture radius a . The dependence of k_1 on beam aperture is shown in Fig. 10.2 for the SLAC disk-loaded structure at 2856 MHz. The solid curve can be approximated analytically by the expression

$$k_1 \approx \frac{27 \text{ V/pC/m}}{1 + 30.5(a/\lambda)^2} \quad (10.5)$$

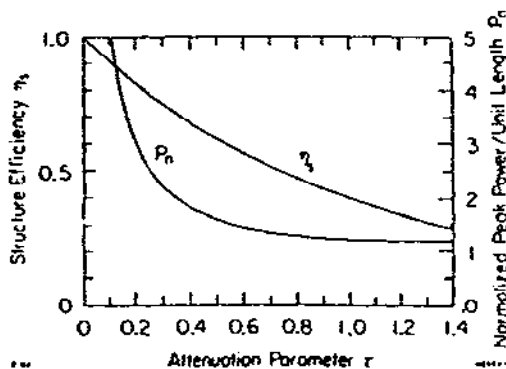


Fig. 10.1. Structure efficiency and normalized peak power per unit length as a function of the attenuation parameter τ .

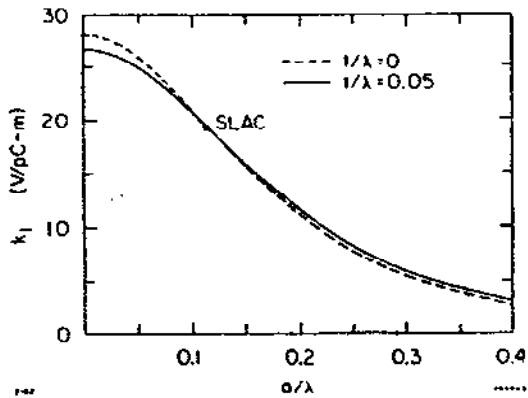


Fig. 10.2. Structure parameter k_1 as a function of beam aperture radius for the SLAC disk-loaded structure for two values of disk thickness t ($t/\lambda = 0.056$, $\lambda = 10.5$ cm for the SLAC structure).

0.10 for the $\pi/3$ mode. Table 10.1 compares the jungle gym and disk-loaded structures at three frequencies that might be of interest for a high-energy linear collider. Values of r , k_1 , Q and v_g/c for the $\pi/2$ -mode jungle gym are scaled from values measured⁴⁰ at 714 MHz for a structure used for several years as an rf cavity in the Cornell University electron synchrotron. Values for the $\pi/3$ -mode jungle gym are estimated from some old measurements⁴¹ made at the Stanford University Microwave Laboratory. The k_1 value for the disk-loaded structure with a wider beam aperture, $a = 1.50$, is obtained from Fig. 10.2; v_g/c is scaled as a^4 . From Eq. (9.55c), the slope of transverse wake for this structure for $t \rightarrow 0$ should be lower by a factor of about 2.5 compared to a structure with $a = 1.16$ cm. Finally, values for the standing-wave disk-and-washer structure, described in Sec. 3.4, are given for comparison. Note that although the Q and shunt impedance for this structure are very high, the value of k_1 is low compared to both the jungle gym and disk-loaded structures.

Other structures might be expected to have a similar dependence of k_1 on a/λ .

The familiar disk-loaded structure does not necessarily have the highest value of k_1 at a given frequency and beam aperture. An alternative structure is the jungle gym structure, shown in Fig. 10.3. The group velocity of the accelerating mode in the jungle gym structure tends to be considerably higher than is the case for the disk-loaded structure.

In addition, the jungle gym is a backward wave structure (phase velocity and group velocity have opposite signs for the accelerating mode). Typically, $v_g/c \approx 0.20$ for the $\pi/2$ mode ($\pi/2$ phase shift between adjacent bar), and $v_g/c \approx$

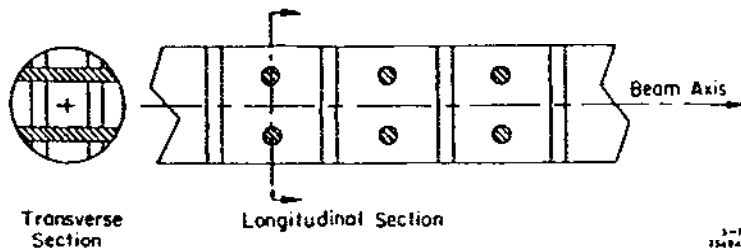


Fig. 10.3. The jungle gym bar-loaded accelerating structure.

Table 10.1 Comparison of Accelerating Structures

	τ (M Ω /m)	k_1 (V/pC/m)	Q	v_g/c	L (m)	T _f (μ s)
<u>2856 MHz</u>						
Disk-Loaded (a = 1.16 cm)	56	19	13,300	.012	3	.83
Disk-Loaded (a = 1.50 cm)	46	16	13,000	.035	6	.57
Disk and Washer (a = 1.16 cm)	85	10	40,000	--	--	--
Jungle Gym ($\pi/2$) (1/2 diag. = 0.84 cm)	51	25	9,000	.22	6	.09
Jungle Gym ($\pi/3$) (1/2 diag. = 0.90 cm)	60	30	9,000	.10	6	.20
<u>4040 MHz</u>						
Jungle Gym ($\pi/2$)	61	50	7,500	.22	6	.09
Jungle Gym ($\pi/3$)	71	60	7,500	.10	6	.20
<u>5712 MHz</u>						
Jungle Gym ($\pi/2$)	72	100	6,500	.22	6	.09
Jungle Gym ($\pi/3$)	85	120	6,500	.10	6	.20

10.2 Single Bunch Beam Loading for a Gaussian Bunch

Equation (9.5) gives the beam loading potential within a bunch in terms of the wake potential $w(\tau)$. As a specific illustration, consider the disk-loaded structure for the SLAC linac. The computation of the wake potential for this structure was described in the last chapter; the resulting wake is shown again in Fig. 10.4 for range 0-20 ps. For this time range, the wake is described quite closely by the expression

$$w(\tau) = A \exp[-(\tau/B)^n] \quad (10.)$$

where

$$A = 226 \text{ V/pC/m} \sim \omega^2$$

$$B = 6.13 \text{ ps} \sim \omega^{-1}$$

$$n = 0.605$$

For a Gaussian bunch, Eq. (9.5) can be written in the form

$$E_b(t) = \frac{ecAN_b}{\sqrt{2\pi}\sigma_z} \int_{-\infty}^t \exp\left[-\left(\frac{t-t'}{B}\right)^n\right] \exp\left[-t'^2 c^2 / 2\sigma_z^2\right] dt' \quad (10.7)$$

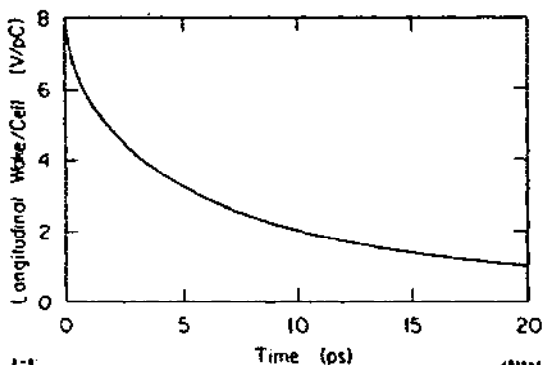


Fig. 10.4. Longitudinal wake potential per period, $p = 3.50$ cm, for the SLAC structure.

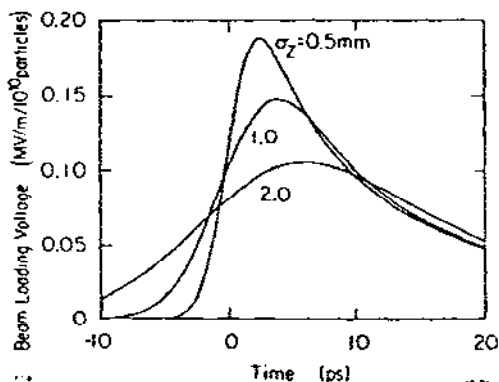


Fig. 10.5. Beam loading voltage within a Gaussian bunch for the SLAC structure for three values of bunch length.

Results for the SLAC structure at 2856 MHz for several values of σ_z are shown in Fig. 10.5.

The total energy gain per unit length by a particle at time t in the bunch can be obtained by adding the external accelerating voltage to the beam loading voltage,

$$E(t) = \bar{E}_a \cos(\omega t - \theta) - E_b(t) \quad (10.8)$$

Here θ is the phase angle by which the bunch center leads the crest of the accelerating wave produced by the external rf source. By adjusting this phase angle, the rising slope of the accelerating voltage waveform can be made to cancel, at least in part, the negative-going beam loading waveform, resulting in a reduction in the energy spread of the particles in the bunch below the energy spread for the case $\theta = 0$. This is shown schematically in Fig. 10.6. Note, however, that the decrease in energy spread is achieved at the expense of a reduction in the average energy gain per unit length per particle, given by

$$\bar{E} = \frac{1}{q} \int_{-\infty}^{\infty} E(t) I(t) dt \quad (10.9)$$

As an example, consider the case of the SLAC structure operating at $\bar{E}_a = 17$ MV/m ($V_0 = 50$ GeV total energy) to accelerate a single bunch of particles with $N_b = 5 \times 10^{10}$ and $\sigma_z = 1.0$ mm. The energy spread $\Delta V/V_0$ which contains 90% of the particles, and the average particle

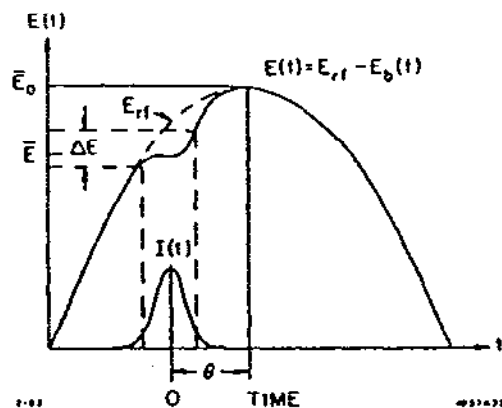


Fig. 10.6. Diagram showing how the single-bunch beam loading gradient $E_b(t)$ subtracts from the rf accelerating wave $E_{rf} = \bar{E}_a \cos(\omega t - \theta)$ to give the net gradient $E(t)$.

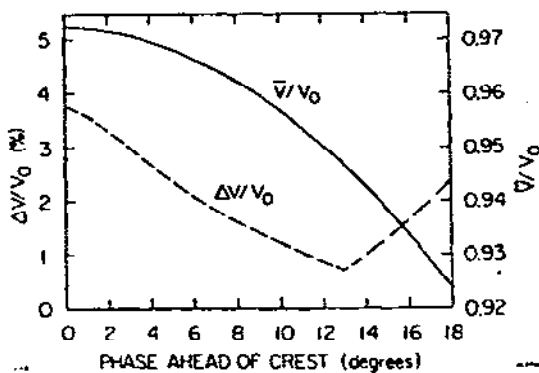


Fig. 10.7. Energy spread and average gain per particle for the SLAC structure with $\bar{E}_a = 17$ MV/m, $N_b = 5 \times 10^{10}$ and $\sigma_z = 1.0$ mm.

in the SLAC linac are given in Ref. 42 for various values of the phase offset parameter θ . Agreement between the measured and computed distribution functions is very good, indicating that the functional form of the wake as shown in Fig. 10.4 has a basis in physical reality. The measurements indicate, however, that the amplitude of the computed wake may be about 30% low.*

The efficiency for transfer of stored energy in the structure into beam energy is also of interest:

$$\eta_b \equiv q \bar{E} / \bar{w}_s \quad (10.1)$$

where $\bar{w}_s = \bar{E}_a^2 / 4k_1$ is defined as the effective stored energy per unit length in the structure. Thus

energy \bar{V}/V_0 , are plotted as a function of the phase offset θ in Fig. 10.7. In this example the energy spread at $\theta = 13^\circ$ is reduced by a factor of four below the spread at $\theta = 0$, but at the expense of an additional 2-1/2% loss in average energy per particle.

The detailed energy distribution function for the particles within the bunch may sometimes be of interest. The charge dq in the energy range dV is given by

$$\frac{dq}{dV} = \sum_n \frac{I(t_n)}{(dV/dt)_{t=t_n}} \quad (10.)$$

The sum is necessary because, as can be seen from Fig. 10.6 there may be up to four values of time $t = t_n$ giving the same energy $V(t_n)$. The energy spectrum actually observed in a linac is modified further because of the finite energy range accepted by the energy defining slits. This effect can be taken into account by convolving the above distribution function with an appropriate slit function. This removes the infinite spikes at energies where the derivative dV/dt vanishes, resulting in a smoothed distribution function. Examples of energy spectra for beam loading by single bunches

* Recent measurements (1991) on the SLC are in very good agreement with predictions based on the calculated longitudinal wake.⁴³

$$\eta_b = \frac{4 e N_b k_1 \bar{E}}{\bar{E}_a^2} \sim \frac{\omega^2 N_b}{\bar{E}_a} \left(\frac{\bar{E}}{\bar{E}_a} \right) \quad (10.12)$$

Note that, from Eqs. (10.3) and (10.11),

$$q \bar{E} = \eta_b \eta_s \omega_0 \quad (10.13)$$

Thus, the product of the beam efficiency and the structure efficiency gives the net efficiency for the conversion of the applied input energy per unit length from the rf sources into beam energy.

It is informative to introduce the beam loading enhancement factor B, defined in Sec. 6.2 for a point bunch, into the expressions for average energy gain per particle and beam efficiency. By definition,

$$\bar{E} = \bar{E}_a F_1 \cos\theta - \Delta E_b \equiv \bar{E}_a - \Delta E \quad (10.14a)$$

$$\Delta E_b = k_1 q B(\sigma) \quad (10.14b)$$

In Eq. (10.14b) we note explicitly that B is a function of bunch length. The bunch form factor for the accelerating mode, F_1 , is also introduced in Eq. (10.14a), although usually it will be quite close to unity (see Sec. 3.3). If a given relative energy reduction per particle $\Delta E/\bar{E}_a$ is specified, the number of particles that can be accelerated is, from Eqs. (10.14),

$$N_b = \frac{\bar{E}_a}{e B k_1} \left[\frac{\Delta E}{\bar{E}_a} - (1 - F_1 \cos\theta) \right] \quad (10.15)$$

For $F_1 \cos\theta \approx 1$, note that N_b scales as $\bar{E}_a/B\omega^2$. The beam efficiency, Eq. (10.12), can also be written in terms of B, using Eqs. (10.14), as

$$\eta_b = \frac{4}{B} \left(1 - \frac{\Delta E}{\bar{E}_a} \right) \left[\frac{\Delta E}{\bar{E}_a} - (1 - F_1 \cos\theta) \right] \quad (10.16)$$

The maximum possible efficiency as a function of $\Delta E/\bar{E}_a$ is

$$\eta_b(\text{max}) = \frac{F_1^2 \cos^2\theta}{B} \quad (10.17)$$

at $\Delta E/\bar{E}_a = 1 - (F_1 \cos\theta)/2$.

The enhancement factor can be computed using

$$B(\sigma) = \frac{1}{F_1^2 k_1 q} \int_{-\infty}^{\infty} E_b(t) I(t) dt \quad (10.18)$$

where F_1 is the bunch form factor for the accelerating mode (normally $F_1 \approx 1$). The enhancement factor is shown as a function of bunch length in Fig. 10.8 for the SLAC disk-loaded structure ($\lambda = 10.5$ cm, $k_1 = 19$ V/pC/m). As an example, consider a 1 mm bunch with $B = 3.1$. For $\Delta E/\bar{E}_a = 0.1$, $F_1 \cos = 1$ and $\bar{E}_a = 100$ MV/m, the number of particles that can be accelerated is, from Eq. (10.15), $N_b = 1.1 \times 10^{12}$. Using Eq. (10.16), the beam efficiency is 12%.

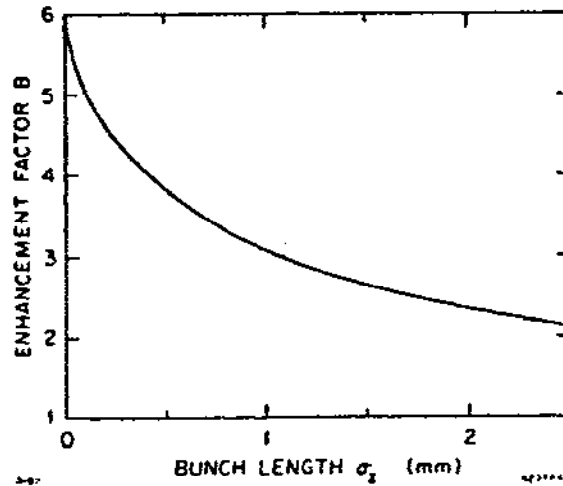


Fig. 10.8. Beam loading enhancement factor as a function of bunch length for the SLAC structure.

For a Gaussian bunch, $B(\sigma)$ can be written directly in terms of the values k_n and ω_n for the structure modes as

$$B(\sigma) = \left(k_1 e^{-\omega_1^2 \sigma^2 / t} \right)^{-1} \sum_{\text{all } n} k_n e^{-\omega_n^2 \sigma^2 / t} \quad (10.19)$$

It was shown earlier that, for a single bunch of 5×10^{10} particles in the SLAC linac operating at 17 MeV/m, the single bunch energy spread due to the longitudinal potential was minimized by running the bunch about 13° ahead of crest (see Fig. 10.7). Figure 10.9 shows this optimum phase as a function of the number of particles per bunch for the case of a linear collider using the SLAC accelerating structure at a gradient of 100 MV/m. Results are given for several bunch lengths at 2856 MHz and 5712 MHz. Figure 10.10 shows the minimum energy spread at the optimum phase, while Fig. 10.11 shows the average energy per particle in the bunch. Figure 10.12 gives the beam energy extraction efficiency as defined in Eq. 10.11.

In Fig. 10.10 it is seen that the minimum energy spread is divided into two regimes. At low bunch charge the spread is dominated by the curvature of the rf wave near the crest, and is given by

$$\left(\frac{\Delta V}{V}\right)_{90\%} \approx 50 \left(\frac{\sigma_z}{\lambda}\right)^2 \quad (10.20a)$$

At large values of bunch charge, the energy spread is dominated by the bunch wake, and is given roughly by

$$\left(\frac{\Delta V}{V}\right)_{90\%} \approx 0.3 \frac{\eta_b}{\cos^2 \theta_m} = 1.2 \frac{k_1 q}{E_a \cos \theta_m}, \quad (10.20b)$$

where θ_m is the phase for minimum energy spread.

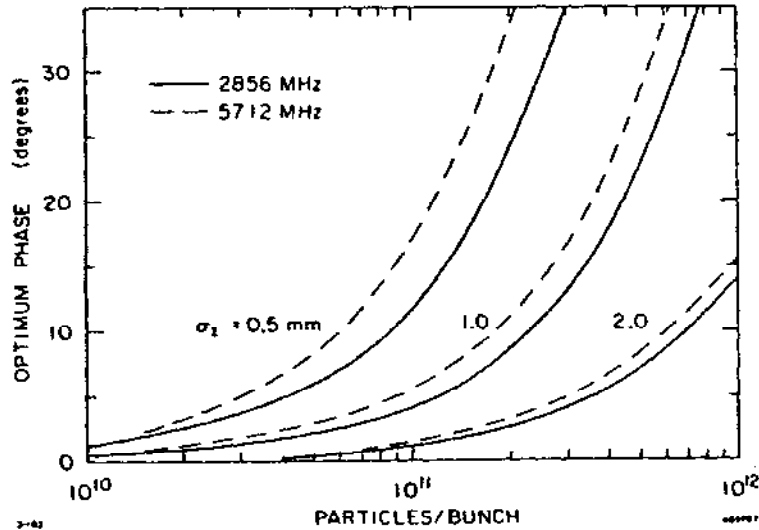


Fig. 10.9. Phase angle ahead of crest which minimizes the single-bunch beam loading energy spread as a function of number of particles per bunch for the SLAC disk-loaded structure at a gradient of 100 MV/m.

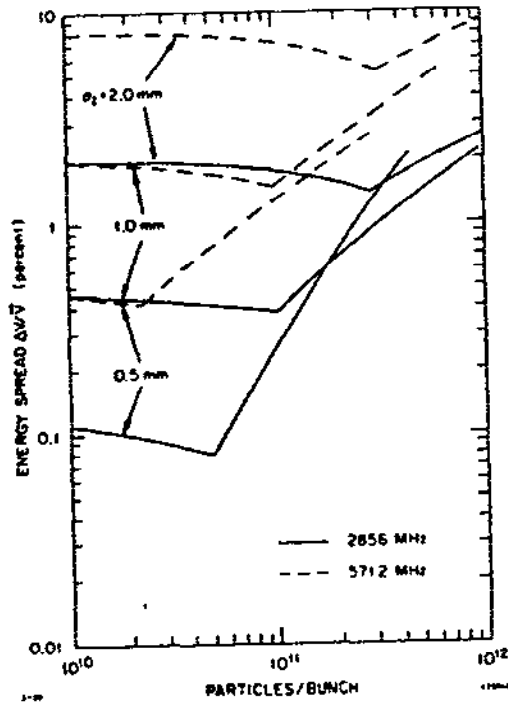


Fig. 10.10. Minimum energy spread as a function of number of particles per bunch.

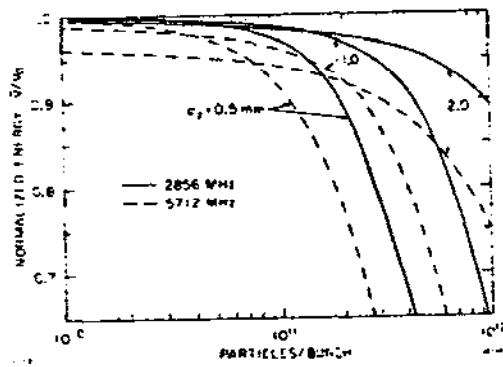


Fig. 10.11. Average energy per particle at minimum energy spread.

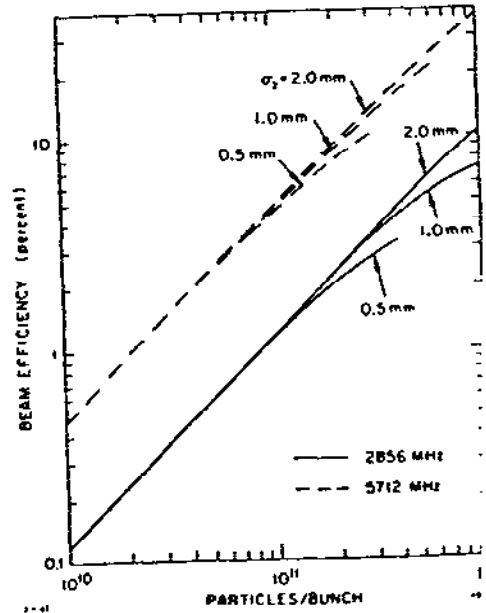


Fig. 10.12. Beam efficiency at minimum energy spread.

10.3 Two-Particle Model for Transverse Emittance Growth

In a continuous distribution of charge, each particle is affected by the transverse wakes from all other particles in the bunch which are ahead of the particle in question. To solve the transverse equation of motion for the case of an arbitrary charge distribution, also taking into account acceleration and external focusing, is a formidable task. Chao *et al.*,⁴⁴ give a solution for the case of a linear wake and a rectangular charge distribution, but the result is too complex to be cast in a form permitting simple scaling. The simplest model that still contains the essentials of the physical situation is a two-particle model for the bunch. Consider a model for a Gaussian bunch of total charge q in which a head charge $q/2$ is located at $z' = +\sigma_z$ and a tail charge $q/2$ is located at $z' = -\sigma_z$, where z' is the coordinate relative to the bunch center. Assume a uniform external focusing field of strength k_β , such that the head particle moves on an orbit described by $x_0 \cos k_\beta z$ as a function of distance z along the accelerator. The transverse force acting on the tail particle due to the dipole wake is then

$$F_1 = \frac{1}{2} e q x_0 w_d(2\sigma_z) \cos k_\beta z \quad ,$$

where $w_d(2\sigma_z)$ is the dipole wake evaluated at $2\sigma_z$. The displacement x_1 for the tail particle obeys the transverse equation of motion

$$\frac{d}{dz} \left[v(z) \frac{dx_1}{dz} \right] + v(z) k_\beta^2 x_1 = F_1(z)/e \quad , \quad (10.21)$$

where $eV(z)$ is the energy. For the case of constant energy eV_0 , Eq. (10.21) simplifies to

$$x_1'' + k_\beta^2 x_1 = C \cos k_\beta z \quad , \quad (10.22)$$

where $x_1' \equiv dx_1/dz$, $x_1'' \equiv d^2x_1/dz^2$ and

$$C = \frac{q x_0 w_d(2\sigma_z)}{2 V_0} \quad . \quad (10.23)$$

Equation (10.22) is the equation for the amplitude of a lossless harmonic oscillator driven at resonance. Assuming $x_1 = x_1' = 0$ at $z = 0$, the solution is

$$x_1 = \frac{C}{2k_\beta} (z \sin k_\beta z) \quad (10.24a)$$

$$x_1' = \frac{C}{2k_\beta} (\sin k_\beta z + k_\beta z \cos k_\beta z) \quad . \quad (10.24b)$$

Two limits are of special interest. For $k_\beta = 0$ we obtain

$$x_1 = Cz^2/2 \quad (10.25a)$$

$$x_1' = Cz \quad (10.25b)$$

$$\epsilon = \pi x_1 x_1' = \pi \left(\frac{C^2}{2}\right) z^3 \quad (10.25c)$$

In the limit of strong focusing, $k_\beta z \gg 1$,

$$x_1 = \left(\frac{Cz}{2k_\beta}\right) \sin k_\beta z \quad (10.26a)$$

$$x_1' = \left(\frac{Cz}{2}\right) \cos k_\beta z \quad (10.26b)$$

$$\epsilon \approx \pi |x_1| |x_1'| = \pi \left(\frac{C^2}{4k_\beta}\right) z^2 \quad (10.26c)$$

Thus, the ratio of the maximum displacement with strong focusing to the displacement with no focusing is

$$\frac{|x_1|(\text{focusing})}{x_1(\text{no focusing})} = \frac{1}{k_\beta z} = \frac{1}{2\pi N_\beta} \quad (10.27)$$

where $N_\beta = z/\lambda_\beta$ is the number of betatron wavelengths. The corresponding ratio of emittances is $1/(4\pi N_\beta)$.

Note that the motion of the tail particle is 90° out of phase with respect to the motion of the head particle. In phasor notation Eq. (11.24a) gives

$$\tilde{x}_1(z) = \tilde{x}_1(0) - jA\tilde{x}_0 \quad (10.28)$$

where

$$A = \frac{Cz}{2k_\beta x_0} = \frac{q z w_t(2\sigma_z)}{4 V_0 k_\beta} \quad (10.29)$$

As an example, consider the SLAC linac ($z = 3 \times 10^3$ m), with $\lambda_\beta = 100$ m and a bunch with 5×10^{10} particles ($q = 8 \times 10^{-9}$ C). Assume a bunch length $\sigma_z = 1$ mm, or $\sigma_t = 3.3$ ps (these are parameters for the proposed SLAC Linear Collider). From Fig. 9.5 the transverse wake at 6.6 ps is 1.0×10^{14} V/C-m/period, recalling that the dimension a of the disk opening is 1.163×10^{-2} m. Since the length of cell is 3.5×10^{-2} m, the wake $w_t(2\sigma_z) = 2.8 \times 10^{15}$ V/C-m². Let us approximate acceleration to 50 GeV (again, the energy for the SLAC Linear Collider) by a constant energy of 25 GeV. Putting these numbers in Eq. (10.29) we obtain $A = 10$, or $|x_1| = 10|x_0|$, for the amplitude of the oscillation of the tail charge as driven by the head charge. The solution obtained by Chao *et al.*,⁴⁴ for these same

parameters, but assuming a continuous rectangular charge distribution and uniform acceleration from 1.2 to 50 GeV, is $A = 6$. Thus, Eq. (10.29) provides a simple but reasonably accurate expression for estimating the single-bunch emittance growth due to the transverse wake in a linac with focusing.

Problem 10.2: Write the equation of transverse motion, Eq. (10.21), for the case of a linac with uniform acceleration, $V(z) = V_0 + V'z$. Let the strength of the focusing force scale with beam energy so that k_β remains constant, independent of z . Can you find an asymptotic expression analogous to Eq. (10.29) for the growth ratio A ?

If there is an energy spread for the particles within the bunch, there will also be spread in betatron frequencies, since $k_\beta^2 \sim 1/\gamma$ for a given focusing strength. This corresponds, in the two-particle model, to a head particle with frequency (wave number) $k_{\beta 0}$ driving a tail particle with frequency $k_{\beta 1} = k_{\beta 0} + \delta k$. The tail particle is now a harmonic oscillator being driven off-resonance, and we might expect a reduction in the growth of the amplitude of the oscillation compared to that given in Eq. (10.26a).

The equation of motion for this case and its solutions, assuming $x_1 = x_1' = 0$ at $z = 0$, is

$$x_1'' + k_{\beta 1}^2 x_1 = C \cos k_{\beta 0} z \quad (10.30a)$$

$$x_1 = \frac{C}{k_{\beta 1}^2 - k_{\beta 0}^2} (\cos k_{\beta 0} z - \cos k_{\beta 1} z) \quad (10.30b)$$

$$= \frac{2C}{k_{\beta 1}^2 - k_{\beta 0}^2} \left\{ \left[\sin \frac{1}{2} (k_{\beta 1} + k_{\beta 0}) z \right] \left[\sin \frac{1}{2} (k_{\beta 1} - k_{\beta 0}) z \right] \right\}$$

$$x_1' = \frac{C}{k_{\beta 1}^2 - k_{\beta 0}^2} (k_{\beta 1} \sin k_{\beta 1} z - k_{\beta 0} \sin k_{\beta 0} z) \quad (10.30c)$$

The maximum amplitudes of x and x' , assuming $\delta k/k_\beta$ is small, are

$$|x_1| = \frac{C}{k_\beta \delta k} \quad (10.31a)$$

$$|x_1'| = \frac{C}{\delta k} \quad (10.31b)$$

$$\epsilon = \pi \left[\frac{C^2}{k_\beta (\delta k)^2} \right] \quad (10.31c)$$

By comparing Eq. (10.31a) with Eq. (10.26a) the reduction in $|x_1|$ due to the head-tail frequency difference is

$$\frac{|x_1|(\text{with } \delta k)}{|x_1|(\delta k = 0)} = \frac{2}{z \delta k} \quad (10.32)$$

The emittance is reduced by the square of this factor.

10.4 Strong Head-Tail Instability in a Storage Ring

In a storage ring, the head and the tail of the bunch change places periodically due to synchrotron oscillations. The head first drives the tail for half a synchrotron period, and on the next half-period the tail moves forward to drive the former head, which has now become the new tail. Thus a feedback mechanism exists which can lead to a possible instability. Let us assume that the transverse deflection wake is confined to the rf structure only, of length L_{rf} . There will certainly be transverse wakes associated with other vacuum chamber components in the ring, but the rf structure is often the major impedance source. In one-half synchrotron period the bunch will pass through the rf structure $f_r/2f_s$ times, where f_r is the revolution frequency and f_s is the synchrotron frequency. Since the current per bunch is $I_b = q f_r$, the growth factor A in Eq. (10.29) is, after one-half synchrotron period,

$$A = \frac{I_b L_{rf} \bar{w} \beta_{rf}}{8 V_0 f_s} \quad (10.33)$$

Here we have introduced the beta function, $\beta_{rf} = 1/k_\beta$, which is normal in storage ring nomenclature. The wake function in Eq. (10.33) must also be averaged from $\tau = 0$ to $\tau_m = 2\sigma_z$, where $\tau = \tau_m \sin \omega_s t$.

Problem 10.3: Show that the average wake seen by the tail particle during one-half period of synchrotron oscillation is

$$\bar{w} = \frac{2}{\pi} \int_0^{\tau_m} \frac{w(\tau) d\tau}{(\tau_m^2 - \tau^2)^{1/2}} \quad (10.34)$$

The phasor diagram in Fig. 10.13 illustrates how the phasors representing the betatron oscillations of the head and the tail particles change during each half synchrotron period. Let $\tilde{x}_o^{(1)}$ and $\tilde{x}_1^{(1)}$ be the head and tail particles during the first half-period. If $\tilde{x}_1^{(1)} = \tilde{x}_o^{(1)} e^{j\alpha}$ at the beginning of the half-period, then it will be driven to $\tilde{x}_1^{(1)} e^{-j\alpha}$ at the end of the half-period, where (see Fig. 10.

$$\sin \alpha = \frac{A}{2} \quad (10.35)$$

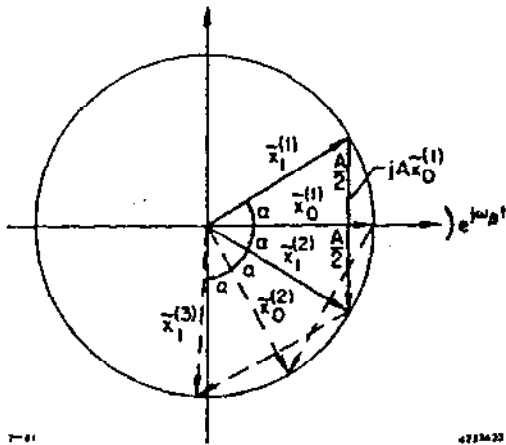


Fig. 10.13. Diagram showing the eigenvectors on successive half periods of synchrotron oscillation for the motion of two particles driven by the transverse wake in a storage ring.

From the geometry of Fig. 10.13 it is also seen that $A = 2$, $\alpha = \pi/2$ is a limit for stable amplitudes of oscillation for the two particles. This limit on stability using the two-particle model was first derived by Kohaupt.⁴⁵ The threshold current for the instability can be found by setting $A = 2$ in Eq. (10.33),

$$I_b(\text{threshold}) = \frac{16 V_o f_s}{\bar{w} L_{rf} \beta_{rf}} \quad (10.37)$$

Measurements of threshold currents for the single-bunch transverse instability observed in PEP, PETRA and SPEAR are in reasonable agreement with Eq. (10.37).

10.5 The Long-Range Wake and Multibunch Acceleration

See Ref. 50 (SLAC-PUB-5062) and Ref. 53.

Thus $\tilde{x}_0(1)$ and $\tilde{x}_1(1)$, when chosen in this manner, are eigenvectors which differ from one turn to the next by a real phase shift only. During the next half period the roles of the particles are reversed, and particle \tilde{x}_0 is changed according to $\tilde{x}_0(2) = \tilde{x}_1(2) e^{-j\alpha} = \tilde{x}_0(1) e^{-j2\alpha}$.

Equation (10.35) has two important consequences. First, if $(A/2) \leq 1$, it corresponds to a real shift in betatron frequency given by

$$\Delta\omega = -\left(\frac{\alpha}{\pi}\right)\omega_s = -\left(\frac{1}{\pi} \sin^{-1} \frac{A}{2}\right)\omega_s \quad (10.36)$$

Secondly, for $A > 2$ the frequency shift becomes imaginary, indicating unstable growth.

ACKNOWLEDGEMENTS

In developing the material presented in these lectures, I have profited through interactions with many colleagues over a period of years. While it is not possible to acknowledge the many relevant discussions in detail, I would like to single out a few contributions which have been especially helpful. The proof of the fundamental theorem of beam loading outlined in Problem 6.1 was suggested by Klaus Halbach. Karl Bane has been involved in all aspects of the theory and computation of the wake potentials, and in particular was responsible for computing the wake potentials shown in Figs. 9.3 through 9.9. Discussions with Alex Chao and Phil Morton have been helpful in clarifying various aspects of the impedance-wake potential formalism presented in Ch. 9. The two-particle model for transverse emittance growth in a linac, as given in Sec. 11.1, is largely based on an analysis suggested by Alex Chao and Phil Morton. The analysis in Sec. 11.2 of the strong head-tail instability in storage rings is the result of a collaboration with Alex Chao, Phil Morton, John Rees and Matthew Sands. ~~A paper with a more formal derivation of the theory, together with a comparison with experimental results in PEP, will be published.~~ Finally, I would like to thank Ronald Ruth for his effort in editing the manuscript for these lectures, and for his numerous helpful comments and suggestions.

REFERENCES

1. R. B. Neal, ed. The Stanford Two-Mile Accelerator, (W. A. Benjamin, New York, 1968).
2. P. Lapostolle and A. Septier, eds. Linear Accelerators (North Holland, Amsterdam, 1970). See Chapters B.1.1, Accelerating Structures; B.1.2, Particle Dynamics; B.1.3, Beam Loading and Transient Behavior; B.1.4 Beam Breakup.
3. Marvin Chodorow and Charles Susskind, Fundamentals of Microwave Electronics (McGraw-Hill, New York, 1964).
4. A. Staprans, E. W. McCune and J. A. Ruetz, "High Power Linear Beam Tubes," Proc. IEEE 61, 299 (1973).
5. H. C. Hoyt, D. D. Simmonds and W. F. Rich, Rev. Sci. Instrum. 37 755 (1966).
6. K. Halbach and R. Holsinger, Particle Accel. 7, 213 (1976).
7. R. L. Gluckstern, K. Halbach, R. F. Holsinger and G. N. Minerbo, 1981 Linear Accelerator Conference (Santa Fe, New Mexico, October 19-23, 1981). To be published.
8. D. E. Nagle, E. A. Knapp and B. C. Knapp, Rev. Sci. Instrum. 38, 1583 (1967).
9. E. A. Knapp, Ch. C.1.1c in Linear Accelerators, P. Lapostolle and A. Septier, eds. (North Holland, Amsterdam, 1970).
10. J. R. Rees, "A Perturbation Approach to Calculating the Behavior of Multi-cell Radiofrequency Accelerating Structures" PEP-255, Stanford Linear Accelerator Center (1976).
11. P. B. Wilson, IEEE Trans. Nucl. Sci. NS-16, No. 3, 1092 (1969).

12. J. J. Manca, E. A. Knapp and D. A. Swenson, IEEE Trans. Nucl. Sci. NS-24, No. 3, 1087 (1977).
13. S. O. Schriber, Proc. 1979 Linear Accelerator Conference (BNL-51134, Brookhaven National Laboratory, 1979), p. 164.
14. H. Henke, "The LEP Accelerating Cavity," LEP Note 143, CERN (1979).
15. C. G. Montgomery, R. H. Dicke and E. M. Purcell, eds. Principles of Microwave Circuits. Radiation Laboratory Series Vol. 8 (McGraw-Hill, New York, 1948), Ch. 7.
16. M. Lee and L. Smith, PEP-Note-222, Stanford Linear Accelerator Center (1977).
- 16a. P. B. Wilson, Ref. 2, Ch. E.2.
17. M. Sands, "The Physics of Electron Storage Rings: An Introduction," in Physics with Intersecting Storage Rings, B. Touschek, ed. (Academic Press, New York, 1971); p. 257f. Also available as SLAC-121, Stanford Linear Accelerator Center (November 1970).
18. K. W. Robinson, "Stability of Beam in Radiofrequency System." Cambridge Electron Accelerator Report CEAL-1010 (February 1964).
19. A. Hofmann in Theoretical Aspects of the Behavior of Beams in Accelerators and Storage Rings. (CERN 77-13, July 1977), pp. 163-165.
20. P. B. Wilson, Proc. 9th Int. Conf. on High Energy Accelerators (Stanford Linear Accelerator Center, 1974), p. 60.
21. P. H. Ceperly, IEEE Trans. Nucl. Sci. NS-19, No. 2, 217 (1972).
22. D. A. Watkins, Topics in Electromagnetic Theory (John Wiley, New York, 1958), Ch. 1.
23. B. Zotter and K. Bane, "Transverse Resonances of Periodically Widened Cylindrical Tubes with Circular Cross Section." PEP-Note 308, Stanford Linear Accelerator Center (September 1979).
24. G. A. Loew, "Non-Synchronous Beam Loading in Linear Electron Accelerators," Microwave Laboratory Report No. 740, Hansen Laboratories, Stanford University (August 1960).
25. P. B. Wilson, IEEE Trans. Nucl. Sci. NS-26, No. 3, 3255 (1979).
26. M. Sands, PEP-Note-90, Stanford Linear Accelerator Center (July 1974).
27. P. B. Wilson, "Transient Beam Loading in Electron-Positron Storage Rings," PEP-Note-276, Stanford Linear Accelerator Center (December 1978).
28. R. H. Helm and G. A. Loew, Ref. 2, Ch. B.1.4.
29. P. B. Wilson, "A Simple Analysis of Cumulative Beam Breakup for the Steady State Case." HEPL-TN-67-8, High Energy Physics Laboratory, Stanford University (September 1967).
30. V. K. Neil, L. S. Hall and R. K. Cooper, Part. Accel. 9, 213 (1979).
31. E. Keil, Nucl. Instrum. Methods 100, 419 (1972).
32. See, for example, Sec. 4.3 in Ref. 31.
33. K. Bane, "Constructing the Wake Potentials from the Empty Cavity Solutions of Maxwell's Equations." CERN/ISR-TH/80-47 (November 1980).
34. T. Weiland and B. Zotter, "Wakefield of a Relativistic Current in a Cavity." CERN/ISR-TH/80-36 (July 1980).
35. W.K.H. Panofsky and W. A. Wenzel, Rev. Sci. Instrum. 27, 967 (1956).

36. K. Bane and B. Zotter, *11th International Conf. on High Energy Accelerators* (Birkhäuser Verlag, Basel, Switzerland, 1980), p. 581.
37. K. Bane, "Transverse Cavity Impedance in LEP," CERN/ISR-TII/80-48 (November 1980).
38. A. W. Chao and R. K. Cooper, "Beam Breakup Due to Quadrupole Wake Field for Sector 1." International Note CN-142, Stanford Linear Accelerator Center (January 1982).
39. K. Bane, private communication.
40. M. Tigner, IEEE Trans. Nucl. Sci. NS-18, No. 3, 249 (1971).
41. See, for example, Microwave Laboratory Reports ML-416, ML-432, ML-520, ML-557, and ML-581, Stanford University (April 1957- February 1959).
42. R. F. Koontz, G. A. Loew, R. H. Miller and P. B. Wilson, IEEE Trans. Nucl. Sci. NS-24, No. 3, 1493 (1977).
43. K. Bane, private communication (1991).
44. A. W. Chao, B. Richter and C. Y. Yao, *11th International Conf. on High Energy Accelerators* (Birkhäuser Verlag, Basel, Switzerland, 1980), p. 597.
45. R. D. Kohaupt, "Simplified Presentation of Head-Tail Turbulence". DESY Internal Report M-80/19 (October 1980).
46. G. Caryotakis, "Multimegawatt RF Power Sources for Linear Colliders", *Proceedings of the 1991 Particle Accelerator Conference, San Francisco, CA, May 6-9, 1991* (to be published). Also SLAC-PUB-5508 (April 1991).
47. Z. D. Farkas, H. A. Hogg, G. A. Loew and P. B. Wilson, *Proceedings of the 9th International Conference on High Energy Accelerators, SLAC, Stanford, May 1974*; pp. 576-583. Also SLAC-PUB-1453.
48. Z. D. Farkas, IEEE Trans. MTT-34, 1036 (1986). Also SLAC-PUB-3694 (1986).
49. P. B. Wilson, Z. D. Farkas and R. D. Ruth, *Proceedings of the 1990 Linear Accelerator Conference, Albuquerque, NM, September 1990* (LANL Report LA-12004-C, Los Alamos, NM, March 1991) pp. 204-206. Also SLAC-PUB 5330 (September 1990).
- 50 ~~46~~. K. L. F. Bane, P. B. Wilson and T. Weiland, "Wakefields and Wakefield Acceleration", in *Physics of High Energy Particle Accelerators*, AIP Conference Proceedings No. 127, M. Month, P. Dahl and M. Dienes, eds. (American Inst. Physics, New York, 1985), pp. 875-928. Also SLAC-PUB-3528.
- 51 ~~47~~. P. B. Wilson, "Introduction to Wakefields and Wake Potentials", in *Physics of Particle Accelerators*, AIP Conference Proceedings 184, M. Month and M.

- Dienes, eds. (American Inst. Physics, New York, 1989), pp 525-564. Also SLAC-PUB-4547 (1989).
- 52 ~~52~~ D.U.L.Y. Yu and P. B. Wilson, *Proceedings of the 14th International Conference on High Energy Accelerators*, in *Particle Accelerators* **30**, 65 (1990). Also SLAC-PUB-5062, (September 1989).
- 53 ~~53~~ Ronald D. Ruth, "Multi-bunch Energy Compensation", SLAC-PUB-4541 (February 1988).

LIST OF SYMBOLS

Symbols are listed by chapter, in order of first use. The equation number in which, or immediately following which, the symbol is first defined or used is given in parentheses after each definition. Symbols are omitted when they have a clear, conventional meaning (e.g., t, q, γ), or when they are used a single time only without possibility of confusion. Note that several symbols have different meanings in different chapters.

Chapter 2

ω	Angular frequency of rf generator (2.1)
\tilde{V}, \tilde{V}_c	Complex (phasor) cavity voltage (2.1)(2.3)
\tilde{V}_g	Generator voltage component in a cavity (2.3)
\tilde{V}_b	Beam loading voltage component in a cavity (2.3)
W_c, W	Stored energy in a cavity or in a given cavity mode (2.4)(2.5)
$f(z)$	Function relating cavity field to stored energy (2.6)
ω_o	Resonant frequency for a particular cavity mode (2.7)
V_o	Voltage induced in a cavity by a point charge (2.8)
σ, σ_t	RMS bunch length in time (2.9)

Chapter 3

$E_z(\text{cmf})$	Axial field in a co-moving frame (3.3)
k	Free-space propagation constant $k \equiv \omega/c = 2\pi/\lambda$ (3.3)
C, S	Cosine and sine integrals for cavity voltage (3.5)
R_a	Cavity shunt impedance (accelerator definition)(3.9)
P	Cavity power dissipation (3.10)
R_s	Surface impedance (3.11)
Z_o	Impedance of free space (3.11)
R_u	Uncorrected shunt impedance (3.12a)
V_u	Uncorrected cavity voltage (3.12b)
T	Transit-time factor (3.13a)
L	Length of cavity or gap (3.14)
θ	Transit angle, $\theta = kL$ (3.14)
\tilde{V}_a	Average voltage gain per particle; accelerating voltage (3.21)
C', S'	Cosine and sine integrals for bunch form factor (3.22)
F	Bunch form factor (3.24)
t_b	Total length in time of a rectangular bunch (3.25b)
b	Radius of a pillbox cavity (3.27)
Q, Q_o	Unloaded cavity Q (3.28a)
r	Shunt impedance per unit length (3.28c)
λ	Free space rf wavelength (3.28b)

G_1, G_2	Geometry constants for a pillbox cavity (3.29a,b)
N	Number of cells, coupled resonator model (3.30)
m	Mode number, coupled resonator model (3.30)
B	Bandwidth, coupled resonator model (3.30)
ω_0	Center frequency of passband, coupled resonator model (3.30)
n	Cell number, coupled resonator model (3.31)
$f(n)$	Field flatness function, coupled resonator model (3.32)
β	Cavity coupling coefficient (3.34')
G_c	Cavity shunt conductance, equivalent circuit model (3.34')
P_c	Cavity power dissipation, equivalent circuit model (3.34')
i_b	Peak value of rf current (3.34')
I_0	DC current (3.34')
i_g	RF Generator current, equivalent circuit model (3.35)
P_g	Generator power, equivalent circuit model (3.35a)
V_{gr}	Generator voltage component at resonance (3.35a)
V_{br}	Beam loading voltage component at resonance (3.35b)
K	Beam loading parameter, $K \equiv (I_0/2)(R_a/P_g)^{1/2}$ (3.36a)
η	Beam conversion efficiency (3.36b)
P_r	Reflected power
Y_c	Unloaded cavity admittance for a resonant mode (3.37)
δ	Tuning parameter, $\delta \equiv (\omega - \omega_0)/\omega_0$ (3.38)
Z_L, \tilde{Y}_L	Loaded cavity impedance, admittance (3.39)
R_0	Loaded impedance at resonance, $R_0 \equiv [G_c(1 + \beta)]^{-1}$ (3.39)
Q_L	Loaded Q, $Q_L \equiv Q_0/(1 + \beta)$ (3.39)
ψ	Tuning angle, $\psi \equiv \tan^{-1}[-2Q_L\delta]$ (3.40)
T_f	Loaded filling time, $T_f \equiv 2Q_L/\omega_0$ (3.43)

Chapter 4

θ	Phase of V_{gr} with respect to $-\tilde{i}_b$ (see Fig. 3.13) (4.1a)
ϕ	Phase of V_c with respect to $-\tilde{i}_b$ (synchronous phase angle) (4.1a)
P_b	Power transferred to beam, $P_b = I_0 V_a$ (4.6a)
β_0	Cavity coupling for zero reflected power (4.6a)
P_{g0}	Generator power at optimum tuning and coupling (4.6)
ψ_0	Tuning angle at optimum tuning and coupling (4.7)
ω_s	Synchrotron frequency (4.8)
ξ	Tuning parameter, $\xi \equiv (\omega - \omega_0)T_f$ (4.13)
η	Filling-time parameter, $\eta \equiv \omega_s T_f$ (4.13)
V_0, \tilde{i}_0	Equilibrium beam loading voltage and current (4.13)
$\delta W, \bar{P}$	Stored energy and average power transfer for a phase oscillation (4.14)

Chapter 5

ϕ	Azimuthal angle, cylindrical coordinates (5.1)
γ	Complex propagation constant per unit length (5.1)
β	Propagation constant per unit length (5.2)
α	Attenuation parameter per unit length (5.2)
p	Periodic length (5.3)
β_0	Propagation constant for the fundamental space harmonic (5.3)
β_n	Propagation constant for the nth space harmonic (5.3)
v_p	Phase velocity, $v_p \equiv \omega/\beta$ (5.4)
E_a	Accelerating field in a traveling-wave structure (5.7a)
P	Power flow in a traveling-wave structure (5.7a)
r	Traveling-wave shunt impedance per unit length (5.7a)
w	Stored energy per unit length (5.7b)
v_g	Group velocity, $v_g \equiv d\omega/d\beta$ (5.8a)
E_0, E_L	Field at $z = 0$ and $z = L$ in a traveling-wave structure (5.10a)
P_0, P_L	Power flow at $z = 0$ and $z = L$ (5.10b)
τ	Attenuation parameter, $\tau \equiv \alpha L$, for structure of length L (5.11)
T_f	Filling time for a traveling-wave structure (5.15)
V_0	Unloaded energy gain for a structure of length L (5.16)
E_b	Beam-induced field in a traveling-wave structure (5.20)
V_b	Beam-induced voltage in a structure of length L (5.22)
m	Beam-loading coefficients for a traveling-wave structure (5.23)
δ	Phase slip parameter (5.27)

Chapter 6

α	Parameter relating stored energy and voltage, $\alpha \equiv W/V^2$ (6.1)
θ, ϵ	Angles in the proof of the fundamental theorem of beam loading (see Fig. 6.1) (6.2)(6.3)
V_b	Single-pass beam induced voltage (6.2)
V_e	Effective voltage seen by a point charge (5.3)
f	Self-voltage factor, $f \equiv V_e/V_b$ (6.4c)
k	Energy loss parameter, $k \equiv w/q^2$ (6.5)
θ_g	Phase of the generator voltage component (see Fig. 6.2) (6.8)
k_0	Loss parameter for the accelerating mode (6.8)
B	Beam-loading enhancement factor (6.10)
$\Delta U_0, \Delta U_{hm}$	Energy loss to the fundamental and to higher-order modes (6.11)
α_0	Parameter α for the fundamental (accelerating) mode (6.12)
V_{b0}	Single-pass beam induced voltage for the fundamental mode (6.12)
Z_{hm}, V_{hm}	Higher-order mode loss impedance and voltage (6.13a)
k_n	Loss parameter for the nth mode (6.13c)

T_b	Time between bunches (6.13c)
V_s	Synchrotron radiation loss (in volts) per turn (6.15)
V_c^-, V_c^+	Cavity voltage just before and just after arrival of bunch (see Fig. 6.2) (6.16)
ϕ^-	Phase of cavity voltage just before arrival of bunch (6.16)
τ	Decay parameter, $\tau \equiv T_b/T_f$ (6.24a)
δ	Phase shift between bunches, $\delta \equiv T_b(\omega_0 - \omega)$ (6.24b)
V_b^-, V_b^+	Beam-induced voltage component just before and just after arrival of bunch (see Fig. 6.3) (6.25a)
\tilde{V}_b	Effective beam-induced voltage (see Fig. 6.3) (6.25b)
F_R, F_I	Real and imaginary components of \tilde{V}_b (6.26)
T_{fo}	Unloaded filling time, $T_{fo} \equiv 2Q_0/\omega_0$ (6.27)
τ_0	Unloaded decay parameter, $\tau_0 \equiv T_b/T_{fo}$ (6.27)

Chapter 7

$\tilde{V}_d(t)$	Transient difference vector (see Fig. 7.1) (7.1)
$\tilde{V}(t), V_c(t)$	Transient cavity voltage (see Fig. 7.2) (7.2a) (7.6)
x	Normalized time, $x \equiv t/T_b$ (Sec. 7.2) (7.10)
τ	Decay parameter, $\tau \equiv T_b/T_f$ (Sec. 7.2) (7.10)
$\mu(t)$	Transient phase angle of cavity voltage (7.11)
F_A, F_B	Real and imaginary components of the transient part of $V_c(x)$ (7.11)
k_1	Loss parameter per unit length for the accelerating mode in a traveling-wave structure (7.19)
x	Normalized time, $x \equiv t/T_f$ (Sec. 7.3) (7.21)
τ	Traveling-wave attenuation parameter (Sec. 7.3) (7.21)

Chapter 8

r_1	Transverse shunt impedance per unit length (8.1)
eV_0	Beam energy in electron volts (8.3)
F_e	e-folding factor (8.6)
t_p	Beam pulse length (8.6)
V'	Energy gradient, dV/dz (8.7)
k_B	Focusing strength (betatron wave-number) (8.9)

Chapter 9

$Z(\omega)$	Complex impedance function (longitudinal) (Sec. 9.1)
$w(\tau)$	Time domain wake potential (Sec. 9.1)
$s(\tau)$	Step response function (Sec. 9.1)
τ	Time following a unit point charge (Sec. 9.1)
$V_b(t)$	Beam-induced voltage within a bunch (9.5)
w_s	Self-wake seen by a point charge (9.18)
k_n, ω_n	Loss parameter and frequency for the nth mode (9.31)
$S(\sqrt{2x/\pi})$	Fresnel integral, with $x = \omega_m \tau$ (9.35)
ω_m	Maximum frequency for sum over modes (9.35)
a	Disk-hole radius (9.36)
m	Azimuthal mode index (9.36)

k_n	Transverse loss parameter (Sec. 9.5) (9.37)
E_{on}	Field at disk-hole radius (9.37)
r_q	Radius at location of wake-producing charge (9.38)
$w_t(\tau)$	Transverse wake (any $m > 1$) (9.41)
$w_d(\tau)$	Dipole wake potential ($m = 1$) (9.45)
$Z_d(\omega)$	Transverse impedance ($m = 1$) (9.48)
k_d	Dipole loss parameter (9.49)
$w_q(\tau)$	Quadrupole wake potential ($m = 2$) (9.51)

Chapter 10

\bar{E}_a	Unloaded accelerating gradient averaged over structure length (10.1)
η_s	Structure efficiency (10.3)
N_b	Particles per bunch (10.7)
σ_z	RMS bunch length, $\sigma_z = c\sigma_\tau$ (10.7)
θ	Phase angle ahead of crest (10.8)
\bar{E}	Average energy gain per particle (10.9)
\bar{w}_s	Effective stored energy per unit length (10.11)
η_b	Beam efficiency (10.11)
w_o	Energy from rf source per unit length (10.13)
θ_m	Phase for minimum energy spread (10.20b)
k_β	Wave number for focusing field, $k_\beta = 2\pi/\lambda_\beta$ (10.21)
A	Amplitude growth factor, $A = x_1(z)/x_0$ (10.29)
f_s	Synchrotron frequency, $f_s = \omega_s/2\pi$ (10.33)
f_r	Revolution frequency (10.33)
I_b	Current per bunch, $I_b = qf_r$ (10.33)
β_{rf}	Beta-function in rf system, $\beta = 1/k_\beta$ (10.33)
2α	Phase shift per half synchrotron period (10.35)